EVALUATION OF LOW-COST MULTI-HOLE PROBES FOR ATMOSPHERIC BOUNDARY LAYER INVESTIGATION

By

SOLMOZ KATHLEEN AZARTASH-NAMIN

Bachelor of Science in Mechanical Engineering
Oklahoma State University
Stillwater, Oklahoma
2014

Bachelor of Science in Aerospace Engineering
Oklahoma State University
Stillwater, Oklahoma
2014

Submitted to the Faculty of the
Graduate College of the
Oklahoma State University
in partial fulfillment of
the requirements for
the Degree of
MASTER OF SCIENCE
July 2017

EVALUATION OF LOW-COST MULTI-HOLE PROBES

FOR ATMOSPHERIC BOUNDARY LAYER

INVESTIGATION

Thesis Approved:

DR. JAMEY JACOB

Thesis adviser

DR. BRIAN ELBING

DR. JOE CONNER

Name: Solmoz Kathleen Azartash-Namin

Date of Degree: JULY 2017

Title of Study: EVALUATION OF LOW-COST MULTI-HOLE PROBES FOR ATMOSPHERIC BOUNDARY LAYER INVESTIGATION

Major Field: MECHANICAL & AEROSPACE ENGINEERING

ABSTRACT:

This work presents the development of evaluating low-cost multi-hole probes (MHPs) for atmospheric boundary layer (ABL) studies. This concept is an integral part of CLOUD MAP, a National Science Foundation (NSF) funded grant led by multiple universities. CLOUD MAP stands for the Collaboration Leading Operational UAS Development for Meteorology and Atmospheric Physics and is focused on the development and implementation of unmanned aircraft systems and their integration with sensors for atmospheric measurements on Earth with the emphasis on Meteorology and Atmospheric Physics (MAP). MHPs are multi-dimensional mean-velocity measurement devices that measure pressure along a set of ports on the probe tip. MHPs are used in studies of from turbomachinery characterization, wake surveys, turbulence, ABL wind vectoring to determining the updrafts in smoke plumes. The accurate detection of sideslip angle in wind gusting is desired with MHPs. The current commercially available MHPs with sensor packages can run thousands of dollars indicating a need for highly accurate low-cost alternatives. Probes are designed using rapid prototyping methods through 3D printing and are evaluated through calibration testing. Probe tip geometry and internal tube dimensions give each probe different performance characteristics as no probe can be perfectly manufactured identically, and must all be calibrated once their lifespan in known testing flow regimes. This study addresses the development of testing platforms with a low turbulence subsonic wind tunnel as well as flight test sensor package development. Each probe is tested and validated through flight testing and comparisons with calibration curves. Standard non-nulling calibration and data reduction methods were used showing performance characteristics of each probe. Two geometries, hemispherical and pyramid, of multiple sizes are evaluated. Of the two geometry types, the hemisphere 5HPs produced the best quality pressure coefficient calibration curves with normal angular linear range between -25 to +25 degrees. Symmetry of these curves and the velocity curves indicate symmetry with the probes. A custom weather data sensor package has been developed for flight testing in ABL studies during the CLOUD MAP flight campaign. Further studies to determine print quality consistency, optimized probe designs, and furthering sensor development were examined and will improve overall accuracy and performance of these probes.

ACKNOWLEDGEMENTS

I would like to acknowledge all of my research colleagues, peers, and professors for the support, advice and guidance throughout my undergraduate and graduate studies at Oklahoma State University. A personal acknowledgment to Dr. Jamey Jacob for his mentorship and guidance throughout the entirety of my education and this thesis research. Because of you I own two copies of Abbott's "Theory of Wing Sections", for I am a "real" aerospace engineer. Dane Johnson and Taylor Mitchell were instrumental in the integration of the sensor package system and probes, respectively. I would like to thank Kristen McKinney for her hard work and dedication to this project in doing even the simplest of things well. I have to give a big "Thank You" to my brother, fellow engineer, and personal therapist for your efforts in helping me get through all of the late nights, study sessions, and all of the inspirational memes and cat videos. Without them I would have survived, but it would not have been nearly as manageable nor funny. I want to acknowledge my parents, Nancy and Hossein, for them instilling a drive to be ambitious, take education serious, and reach for the stars. Lastly, I would like to thank the efforts on part of CLOUD-MAP and the National Science Foundation for their part in bringing together this research and funding in furthering the sciences associated with this project.

Per aspera ad astra

Acknowledgements reflect the views of the author and are not endorsed by committee members or Oklahoma State University.

TABLE OF CONTENTS

LIST OF TABLES

LIST OF FIGURES

NOMENCLATURE

$\bar{x}$	Mean value of data
Δp	Differential pressure
μ	Dynamic viscosity
5HP	5-hole probe
7HP	7-hole probe
A/D	Analog to digital
ABL	Atmospheric boundary layer
B_{acq}	Error associated with data acquisition in bias
B_{cal}	Calibration bias error
B_{red}	Data reduction bias error
B_x	Bias error
c	Speed of sound
CFD	Computational fluid dynamics
CLOUD-MAP	Collaboration leading operational UAS development for meteorology and atmospheric physics
Cp	Coefficient of pressure
$Cp\theta$	Coefficient of pressure (pitching axis)
$Cp\phi$	Coefficient of pressure (yaw axis)
D, d	Probe diameters for large and small, respectively
f	Frequency of the pressure signal
f_n	Natural frequency
g	Gravitational acceleration
h	Height

HWA	Hotwire anemometer
ID	Inner diameter
L	Length of the pressure tube
LDV	Laser Doppler velocimetry
Ma	Mach number
MHP	Multi-
N	Number of samples
NCAR	National Center for Atmospheric Research
OD	Outer diameter
P_0	Total or stagnation pressure
p_∞	Freestream pressure
P_a	Average pressure measured
p_i	Pressure measured in ith probe port
PIV	Particle-image velocimetry
p_s	Static pressure
q	Dynamic pressure
r	Radius
Re	Reynolds number
S_x	Standard deviation
u, v, w	Cartesian velocity vector components
U_∞ *or* U	Freestream velocity
UAS	Unmanned aerial system
U_x	Uncertainty
V	Sensor volume
x_i	Measurements taken for uncertainty analysis

θ	Pitch angle
ξ	Damping ratio
ρ	Density
ϕ	Yaw angle

CHAPTER I

1. INTRODUCTION

1.1 Motivation

Flow fields with complex behavior and characteristics due to weather, flow interactions, and fluid properties are features scientific communities across multiple fields are interested in studying. It is only natural that an interest in studying these phenomena are catalyzed by the use of varying aircraft platforms, particularly in unmanned aerial systems (UAS); as measuring devices and hardware become miniaturized over time it is becoming more accessible to take measurements by way of hardware versatility and reducing overall costs. Manned and unmanned aircraft are an essential platform utilized for atmospheric boundary layer (ABL) research. A big advantage of aircraft systems in measuring ABL conditions is the capability to measure horizontal tracks and vertical probing by slant profiles [1]. Traversing flow fields in this way makes fixed-wing aircraft, in particular, acutely beneficial as measurement taking inertial platforms. As such, the multi-hole pressure probe has proven to be a significant tool in determining steady state, three-dimensional velocity vectors as well as fluid properties like density in unknown flow fields [2].

Multi-hole probes (MHP) have been used in the studies of everything from turbomachinery characterization, vortical flows, wake surveys, turbulence, ABL wind vectoring to skin friction characterization in turbulent flows as well as giving highly accurate aircraft attitude awareness. The MHP is derived from the same principles of flow velocity measurements as standard Pitot-static probes, but unlike a typical Pitot-static probe it has the unique ability to take pressure measurements from the pitching and yawing axes to extract velocity components in magnitude and direction.

Furthermore, MHPs have gone beyond the conventional 5-hole probes to utilizing 7-hole and even up to 19-hole probes. The velocity vector can be accurately determined with a properly calibrated probe through calibration in a known flow field to acquire port pressures and develop calibration curves. The probe is then placed in an unknown flow field to collect the same data to compare with the calibration set [2]. Through this procedure MHPs have the ability to provide the local value of three velocity components, and static and dynamic pressures, as well as total and static temperature, and local composition of the fluid if properly instrumented [3].

The importance of proper calibration becomes essential to retain high accuracies in the measurements, and with careful calibration a probe will only need to be calibrated once in its lifetime unless the tip geometry is changed in some way such as minor damage or purposeful adjustments. Manufacturing defects are unavoidable and also requires probe calibration as each set of data curves will be unique to that specific probe. Although calibration and data reduction methods can be cumbersome and extensive it is a necessity for the probe measurements as there are not any good analytical models for MHPs yet.

Moreover, MHPs have shown to be robust and with good repeatability in measurements. Other velocity measurement tools like Laser Doppler Velocimetry (LDV) and Particle-Image Velocimetry (PIV) have disadvantages to MHPs as both LDV and PIV are costly in comparison. These devices also require complex methods of laser and optical equipment to acquire the same data a much cheaper MHP can take. Hot-wire Anemometry (HWA) is another well-known method to collect velocity data, but is sensitive to flow particulates more so than a MHP typically is [3]. MHPs are very useful robust devices, but commercially available probes typically come at a high price. Thus, there is an interest for cost effective manufacturing processes to cut the high costs of commercial probes while retaining the same measurement qualities as higher end probes. Rapid prototyping is made possible with 3D printing by giving flexibility and nearly endless possibilities in optimal design while loosening time constraints that handmade probes might incur. Each probe can be designed and printed for much less than handmade probes, and can be done at much faster

rates by printing multiple at a time without the use of a specialized technician. MHP manufacturers, such as Aeroprobe, make highly accurate and professionally designed probes, but at a steep cost as compared to printed probes. Ranging between $5,000 and $7,000, Aeroprobe probes come at a cost that once the air data sensor package is added can increase to $12-$15,000 depending on how many probe holes and which sensor package is added. It is of high interest in the scientific community using MHPs to find robust, low-cost alternatives for taking measurements. Proving the validity of 3D printed probe accuracy in taking data would be a positive change giving more access to researchers needing data for their prospective science.

Figure 1-1 : Commercially manufactured and calibrated Aeroprobe 5-hole probe [4].

This concept is an integral part of CLOUD-MAP, Collaboration Leading Operational UAS Development for Meteorology and Atmospheric Physics, a National Science Foundation (NSF) funded grant led by the Oklahoma State University (OSU), the University of Oklahoma, the University of Kentucky, and the University of Nebraska Lincoln. CLOUD-MAP is focused on the development and implementation of unmanned aircraft systems and their integration with sensors for atmospheric measurements on Earth with the emphasis on Meteorology and Atmospheric Physics (MAP). CLOUD-MAP has objectives to create and demonstrate UAS capabilities needed to support UAS operating in the extreme conditions typical in atmospheric observations, including the sensors, navigation planning, learning, control, and communications technologies as well as develop and demonstrate coordinated control and collaboration between autonomous air vehicles

during MAP missions. The motivation for this work is rooted within the advancement of three-dimensional forecasting, but its impact will contribute to a much larger UAS movement.

1.2 Goals & Objectives

The purpose of this research is to evaluate the performance of low-cost MHPs constructed with rapid prototyping methods and compare their performance to high-cost commercially available probes, primarily for ABL applications though the systems can be used in many other areas of interest. Determining whether high quality low-cost probes can be developed through 3D printing techniques and validated through standard calibration, flight testing, and data reduction methods is the primary goal. This can be validated by utilizing several calibration techniques, those namely derived from two main methods: nulling method and non-nulling method. Since the non-nulling method requires less space and calibration complexity as the nulling method (albeit still an exhaustive method itself), it is the method chosen for this research. More detail into this method will be described in later chapters of this paper. ABL research is a driving force behind this project in application and in situ measurements. A goal to accurately obtain the wind vector in boundary layer research via properly calibrated probes, quality sensors and computing is important to reach as the interest and use of MHPs continues to grow in this field of research. The wind vector is an important parameter in ABL; however, it is still a complex variable to obtain accurately. Miniaturization of sensors and hardware, overall, have provided a means to make more robust and versatile sensor packages that can be accompanied with the probe on lighter aircraft such as UAS. With the help of CLOUD-MAP, a goal to develop a sensor package for weather data and, thus, accurately extracting the three-dimensional wind vector component is also part of this study.

This research must take into consideration the effectiveness of 3D printing MHPs with varying geometries and size to determine the probes' design characteristics. This will be done through wind tunnel testing and comparisons with other probes. Previous work done in this area of probe design has given a good strategy in initial probe design trade studies. Primary objectives for

evaluating the probes naturally fall into these main categories: calibration, data reduction, and flight testing. For calibration using the non-nulling method, the design of a testing rig to automate and reduce calibration time for probes while also reducing human error is necessary for acquiring accurate data curves. The probes will be calibrated over a range of Reynolds while traversing a range of angles for pitch and yaw. Once data is acquired, analyzing it using common data reduction methods by finding the pressure coefficients and velocities compared to the angular displacements along the pitching and yawing axes, a set of reference calibration curves can be made for each calibrated probe. Each calibrated probe will have its own set of unique reference curves, and will then be mounted onto a viable UAS platform for flight testing. ABL measurements will be taken in an unknown flow field and the probe's data can be used to deduce the wind vectors from the preexisting calibration curves. A list of tasks to meet the goals and objectives of this work are as follows.

- Design various tip geometries and size MHPs
- 3D print high quality probes
- Design sensor board package for flight testing probes
- Design laboratory testing platform in wind tunnel
- Integrate systems to automate most of testing procedures
- Determine probe characteristics by wind tunnel calibration testing
- Compare probes with other commercially available probe data
- Flight test probe & board systems
- Evaluate probe flow characteristics with PIV

1.3 Outline of Thesis

The layout of this paper proceeds with Chapters II through VI followed by an Appendix. Chapter II: Review of Literature, covers all background and previous works studied and referenced in this body of work. Followed by, Chapter III: Theory, which covers a discussion on probe flow

theory that leads further into a discussion on MHP theory, specifically 5-hole probes. Probe application and governing equations used in this work are introduced in this chapter as well. Chapter IV: Methodology & Experimental Arrangement, discusses the tools and methods used to evaluate experimental procedures and the setup. Validation methods in calibration testing is discussed here. The last two chapters are Chapter V: Results and Chapter VI: Conclusions. Chapter V: Results, presents and discusses the experimental results derived from Chapter IV. Calibration results are presented in detail here. The last chapter, Chapter VI: Conclusions, follows giving a brief summary of the results and recommendations for this body of work. Future work is presented in this chapter for furthering this research area and ensuring that the research ahead is maintained with quality and a clear understanding of what still needs to be done going forward. An appendix is given at the end with results, figures, and data that could not be presented in previous chapters for reference.

Various MHP platforms and low-cost rapid prototyping methods have been used. This paper and work developed therein aim to evaluate and validate these low-cost rapid prototyping options. Examples of such are presented in Figure 1-2 and Figure 1-3 from the National Center for Atmospheric Research (NCAR) and the University of Kentucky (UK), respectively.

Figure 1-2 : 3D printed 5-hole probe mounted on NCAR's Albatross platform [5].

Figure 1-3 : Machined 5-hole probe mounted on University of Kentucky's X-8 platform.

NCAR have developed their own 3D printed 5-hole probes and tested them collecting weather data on their Albatross fixed-wing platform. Above the UK have mounted on their machined 5-hole probe on the nose of an X-8 fixed-wing.

CHAPTER II

2. REVIEW OF LITERATURE

2.1 Velocity Determination Through Pressure Measurements

The conventional Pitot-static tube is designed to measure the velocity of fluid flow. Facing an oncoming fluid stream, the flow hits the front hole and comes to a rest having an increase in pressure known as total pressure, while the downstream ports register the pressure of still flow as it does not see a pressure increase like the flow at the tip of the tube; it is this pressure difference relationship that reveals the fluid velocity.

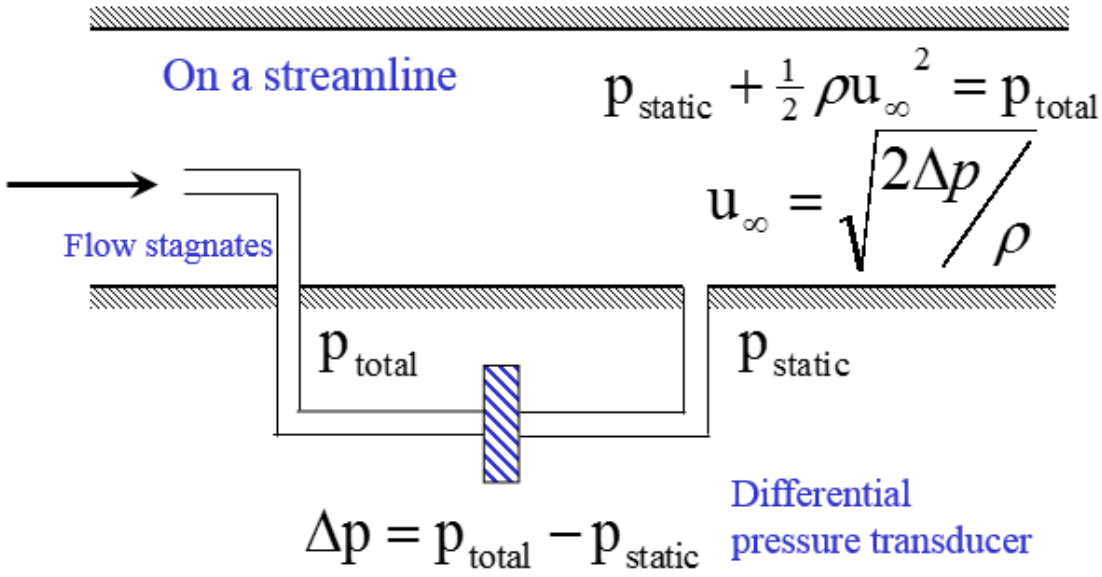

Figure 2-1 : Illustration of relationship between velocity and pressure measurements in flow. This is the basic theory in how a standard Pitot-static probe works.

This relationship was discovered in 1732 by Henri Pitot, a French hydraulic engineer and inventor of the aptly named Pitot tube [6]. The Pitot tube is simple by nature, and widely used then and today on ships and aircraft to measure water velocity and airspeed. It has been well documented that as a body is inserted into a stream of fluid (any fluid) that there will be a disturbance in the

flow as the pressure distribution over its surface will see a maximum pressure at the stagnation point [2], [3], [7], [8], [9], [10], [11], [12]. The maximum pressure is equal to total pressure, P_0, which is just the sum of static pressure, P_∞, and dynamic pressure, q. Described by Chue, dynamic pressure, for a point on a flow field is a difference between the total and static pressures at that same point which in isentropic compressible flows it is associated to the Mach number of the flow [7]. Thus, the velocity can be calculated for that point in the flow field by way of dynamic pressure measurement.

$$p_0 = p_\infty + \frac{\rho U_\infty^2}{2} + \rho g h \tag{1}$$

Where p_0 is the total (stagnation) pressure, p_∞ is the static pressure in the freestream, ρ is the fluid density, U_∞ is the freestream velocity, g is gravitational acceleration, and h is vertical distance (height). In this scenario, the potential energy term, $\rho g h$, is zero and is neglected.

For Pitot probes inserted into a flow, the inviscid incompressible form of Bernoulli's equation is used in determining flow properties along a streamline. These are for low speeds with Mach numbers below 0.2 where compressibility affects do not come into play [3]. Moreover, as said before of a body inserted into a stream, the pressure at specific points on the body's surface relates to the direction and magnitude of the stream's velocity [3], [7], [8], [12], [13]. The potential flow solution for spherical probes is well developed, however, it has several limitations, including angular range, that can only be applied to spherical probes making it necessary to calibrate. The analytical modeling of this relationship is in most cases cumbersome, and thus, it becomes more relevant and pragmatic to form this relationship by means of calibration and experimentation. This same principle of a simple Pitot-static probe measuring flow velocity is utilized on multi-hole probes. MHPs with one pair of pressure taps are utilized for two-dimensional flow direction measurements while probes with at least two pairs (5 ports and greater) are utilized for three-dimensional flow measurements. Since this paper focuses on three-dimensional flow measurements

the discussion will be focused on 5- and 7-hole probes at low subsonic velocities, hereafter referred to as 5HP and 7HP, respectively. The application of the 5HP has been around since Admiral Taylor developed it in 1915 for three-dimensional velocity vector measurements on a ship. Velocity vector probes are typically used in subsonic flow regimes only due to asymmetrical shocks that form upstream of the probe tip when placed in supersonic flows. The asymmetric shock will cause a significant change in the downstream flow from the probe inducing more error into the measurement. However, work on supersonic fast response MHPs are studied and tend to be much smaller with as small as possible spatial and temporal resolution as well as diameters as studied by Naughton et al. and others [3], [8], [14]. Better spatial resolution reduces the influence shocks may cause on probe measurements. These are calibrated and tested at Mach numbers between 2-4 and spatial resolution as small as 1 mm [14].

2.2 Probe Geometry & Design

Size, shape, and lengths of velocity probes and their components must be considered when designing the probe. Tip geometry of probes can provide varying operating characteristics on performance. By far hemispherical, conical, and pyramid geometries are the most common and have had extensive testing and research involved with them. It has been demonstrated that differences in conical and pyramid tips is primarily based on performance of how flow separation behaves around the probe. The main differences as summarized in the literature shows that with smooth surfaces (see hemispherical or conical) separation occurs gradually. This is typically a desirable feature to have for a MHP, but can be quite sensitive to Reynolds effects due to the possibility of abrupt changes in the free-stream flow velocity. If flow is tripped and a transition to turbulent flow is induced, the point of separation will be moved further downstream. Pyramid (or faceted/chamfered tips) employs sharp corners that force separation along the corners, and thus, the calibration curves are less sensitive to Reynolds effects. However, this makes the pyramid type probes more sensitive to unsteady stall effects [3], [10]. Chamfers of cone and pyramid tips are

usually taken at 30^0 to 45^0 angles. Sitaram determined that 30^0 for 5HPs tend to be optimum while up to 50^0 still showed good sensitivity [15].

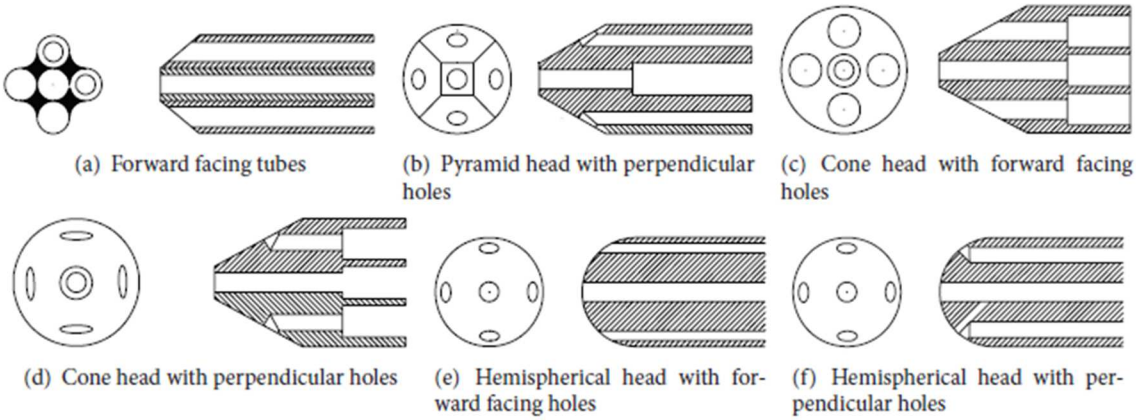

Figure 2-2 : 5HP tip geometry types [15]

There are no real, practical analytical solutions for the differing tip geometries except for hemi-/spherical probes; the potential flow solution can be applied and it presents a good approximation for pressure distribution. Although potential flow solution is valid for this tip type, manufacturing defects and unknown variations in field testing conditions make calibrating probes of any geometry type a necessity.

When designing a probe and keeping in mind tip variations it is desirable to design a head geometry that has variations in pressure measurements that can be related back to the local velocity vector's magnitude and direction. This is precisely what the pressure taps on the tip do to pick up measurable differences. As seen in the literature reviewed, most 5HP probes have an operating range between -25^0 to $+25^0$ (up to $\pm 55^0$), but with tip variation and some adjustments to calibration methods the angular ranges can be increased, some as high as $\pm 75^0$-80^0 [2]. These higher ranges were studied extensively in 7HPs and greater. These high angular ranges result from increasing the number of tip holes/pressure sensing ports. In general, the more holes, the more accurate the probe can be at determining the flow direction in larger angular ranges. Previous studies go into depth on

these aspects that will be discussed later with research from early 1960s up to more recent years [2], [3], [10], [11], [15] [16] [17], [18], [19], [20], [21], [22], [23], [24].

Pitot-static probes' response rates are dependent upon the diameter and length (spatial and temporal) of the pressure ports and channels within the probe. Small probes tend to have quicker response rates, but there is a point to where the small size can induce choked flow conditions as well as clogging with even some of the finest of particles [7]. To reduce measurement errors with larger velocity gradients in flow and maximize resolution, it is desirable for the pressure taps to be located close together. This minimizes the pressure differences due to the velocity gradient [12], [13], [18], [20]. This is the probe spatial resolution. Furthermore, it has been studied that as probe tip size decreases measurements in large velocity gradients improve [12] [13], [18]. The temporal resolution is improved the closer the sensors are to the pressure ports. As the distance is increased, the damping effects of pressure fluctuations will also increase [3]. As many factors can influence measurements taken from MHPs, the tip geometry largely impacts the probe response the most.

2.3 Calibration & Data Reduction Methods

Measuring 3-dimensional flow requires calibration of each probe due to the uniqueness of each set of calibration curves per probe. The purpose is to determine experimentally with pressure data sets that define the probe's behavior to a known flow field (total and static pressures, pitch and yaw angles, and velocity magnitude) which are typically expressed in non-dimensional pressure coefficient values. These relationships are used as functions of flow angle and compared to similar curves that are extracted from field testing in unknown flow fields. The relationships from the unknown flow field with measured probe pressures and the known calibration data sets will then give flow field velocity vectors that are useful in many applications. The result is that a fully empirical flow field is derived via calibration. These calibrations are taken within the expected testing parameters, such as, a known constant velocity, and range of Reynolds and Mach numbers, and traversed across a range of angles incremented by a known value over the span.

There are two main methods of calibration: nulling and non-nulling (also known as fixed-position) and are referenced extensively throughout the literature [2], [3], [8], [9], [10], [11], [12], [13], [21], [22], [23], [24], [25], [26], [27], [28], [29], [30], [31], [32]. In nulling mode, a probe is inserted into a flow and is mechanically rotated until the error signal across two opposing ports is nulled. The inclination angle at that position is the flow direction, and the velocity is obtained by measuring the pressure at that position. The nulling method is highly accurate, but requires larger space for traversing and takes long data acquisition time as the probe must be pitched and yawed until the opposing pressure ports are equaled. In the non-nulling method, the probe is in a fixed position and the pressure of each hole is measured as it is spanned across an angular range. A pitot-static probe upstream several specified probe diameters upstream of the MHP takes the tunnel flow velocity. This method requires less space than nulling method, but is still a tedious procedure. This method is well known and was introduced by Treaster and Yocum [10]. The probe must be placed in a wind or water tunnel in the middle of the test area and is typically calibrated at low speeds. Although most of the literature is extensively on 5HP, these methods can be used on any MHP as Zilliac and Shaw used non-nulling on 7HP and n-hole probes [24], [22], [23]. Data reduction methods presented in the literature for non-nulling method are variations of the same method described previously for getting the coefficients of pressure and only tend to extend calibration angle range and accuracy validation of measurements.

2.4 Probe Applications & Platforms

Much of the research for MHPs and current applications is in wind measurements. Being able to measure 3-dimensional wind vectors accurately, especially angle of sideslip, at a relatively low-cost is highly desirable amongst several research disciplines. In atmospheric and meteorological research this measurement is important for getting measurements in clouds and wind gusts/updrafts. Getting flight data with air data booms on manned aircraft has been done for years now, but with UAS becoming more reliable and instrumentation becoming smaller this

research is available to more researchers than ever before due to it becoming more cost effective. With so many UAS options researchers are able to fly more frequently and into areas manned aircraft would be deemed too dangerous to go.

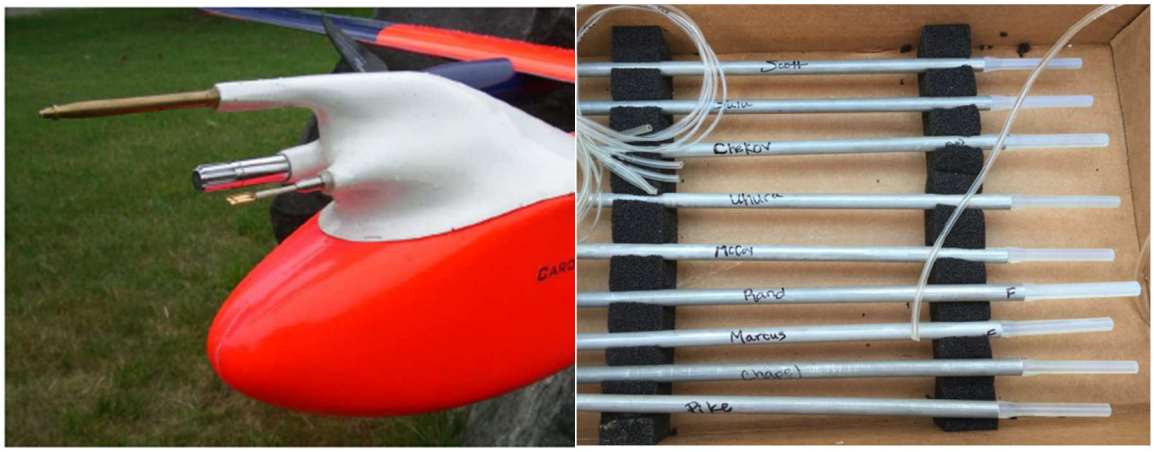

Figure 2-3 : M2AV ABL turbulence measuring platform with 5HP (left); 3D printed 5HPs used in turbulence studies by the University of Kentucky (right) [1], [33].

The M2AV UAS developed by van den Kroonenberg et al was used with a 5HP to take turbulent wind measurements in ABL [34]. The measurements when compared to an instrumented tower showed to be in good agreement and verified the endless possibilities of using instrumented UAS for in-situ measurements. Metzger et al was also able to verify this with "microlight" UAS measuring accurate 3D wind vectors. The research in this paper utilizes these UAS approaches in the literature [1], [34], [35], [36].

Applications of MHPs are varied with much research having been initially involved with naval ships to the application on wind turbines in the renewable energy sector by Fingersh [37]. Application to quantitative wake survey measurements done by Brune captured the use of utilizing 3D measurements for wake flow fields. An example is shown below with a schematic of a simple wing study setup.

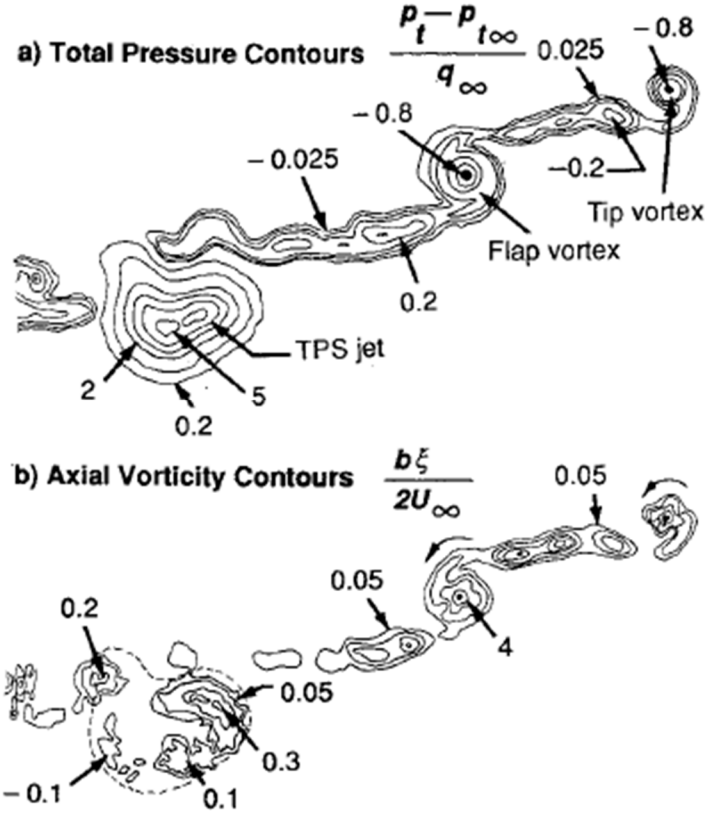

Figure 2-4 : Wake flow data of wing-body-nacelle combination in transport high-lift configuration [38].

In this study by Brune, measured crossflow velocities perpendicular to the tunnel axis were converted into axial vorticity and presented along with the measured total pressure contours [38]. This data, as described in Figure 2-4, gives understanding into the structure of wing wakes.

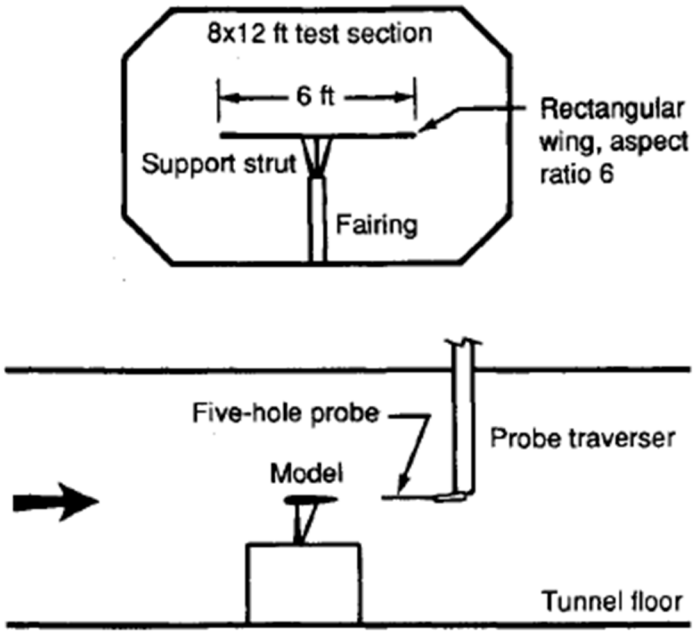

Figure 2-5 : Simple wing study model & 5HP setup in low speed wind tunnel for quantitative wake surveys [38].

CHAPTER III

3. THEORY

This chapter discusses the theory behind multi-hole probes, specifically 5-hole probes, as well as the applicability and science that drives it. The first section will describe the theory of MHPs followed by a discussion of the governing equations used for developing calibration curves which are fundamental to how MHPs are used in various applications. Section 3.2 will discuss theory in how it is applied and the science motivations.

3.1 Probe Theory

3.1.1 Multi-Hole Probes

MHPs use pressure data to find the 3-dimensional velocity vector in a flow. The probe acts as a 3-dimensional mean-velocity measurement instrument that can compare pressures to determine the pitch and yaw angles, and from there using Bernoulli's equation can derive the full velocity vector. The theory behind this is fundamentally driven by the examination of the non-dimensional pressure coefficients that compare the pressure differences across the probes' three axes: longitudinal, normal, and bi-normal. The main objective of MHPs, as stated previously, is to obtain the magnitude and direction of flow from the dynamic pressure that is measured through the pressure differences of the center and static holes. For a 5HP, the two holes corresponding to the pitching axis and two holes corresponding to the yawing axis are exploited to obtain the direction of the flow. Because the probe is inserted into a flow field, it will see a pressure distribution over its surface that varies from corresponding pressure ports that are dependent upon which way the axis or axes are oriented. This is the main principle of MHP measurements, that how the probe is oriented in the flow field means the pressure at specific points on the probe head's surface can be related back to the direction and magnitude of the flow velocity. A probe that is properly calibrated can be inserted into a subsonic unknown flow field and accurately determine the 3-dimensional

velocity vector by the way of recording the port pressures, and then comparing them with the calibration data. Where in the Figure 3-1, ports 2 and 4 relate to the pitch axis, 3 and 5 correspond to the yaw axis, and port 1 pairs with the static ports to give Pitot-static pressure. The relationships found between the pressures from calibration and in field studies are empirical in nature and represent the need for accurate and reliable calibration data.

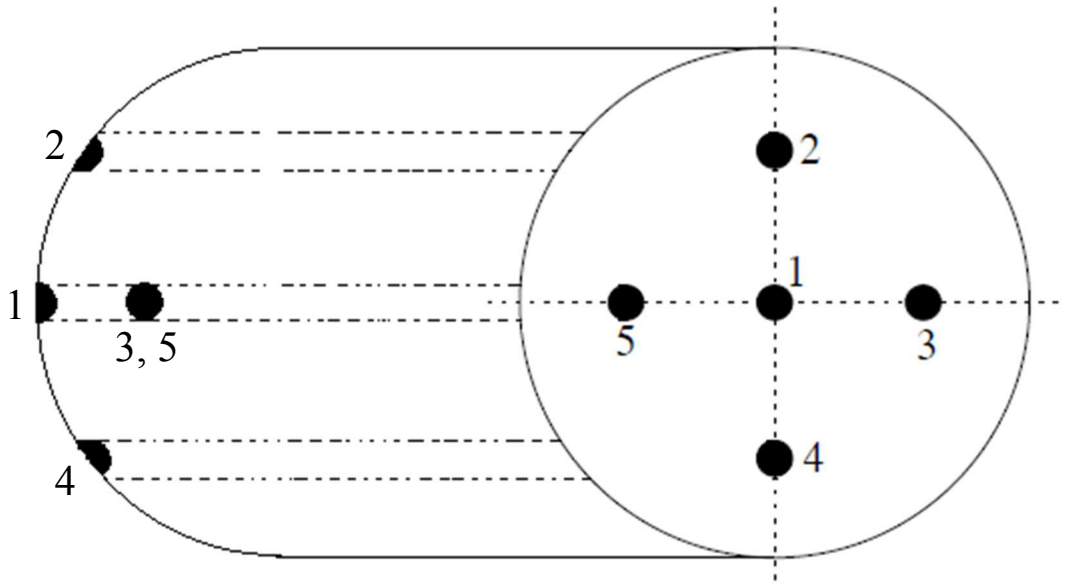

Figure 3-1 : Side (left) and front (right) views of 5HP [26]

For the front view of the 5HP, the hole #1 is on the axis of the probe. The other holes are symmetric about the center hole.

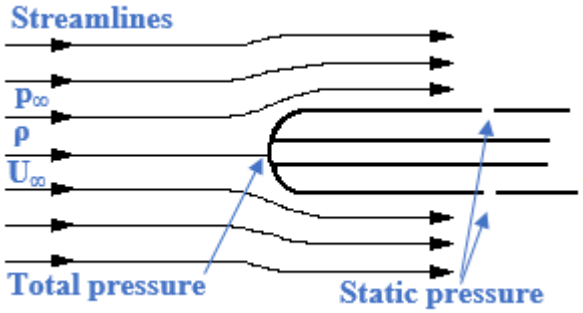

Figure 3-2 : Illustration of a probe inserted into a flow

Flow around a probe in low subsonic speed is treated as incompressible and the density remains constant. With these assumptions Bernoulli's equation is reduced to the relation between pressure, density, and velocity in a streamline. The velocity in this relationship is derived from the dynamic pressure which is also the difference between the static and total pressures. Velocity is tangent to the streamline at every point.

Some analytical models exist, but mostly for very specific geometries such as hemisphere (dome) probes. The hemispherical probe can be made with the assumption that the pressure over the front face of the probe would be nearly the same as that over a sphere. Therefore, the potential flow solution has proven to be a very accurate approximation. Research has been done to analytically model the probes, no good solution works in practice for probe geometries outside of a sphere. By default, that is largely why probe calibration methods must determine these relationships. It should also be emphasized that this is also required for no single probe is exactly identical to another probe as minute imperfections from manufacturing of the tip geometry or hole orientations cannot be 100% removed or replicated.

Also, as probe geometry discussed in the previous chapter affects the sensitivity of the probe's response it is important to calibrate to understand and optimize these features. Probes should ideally be able to produce a C_p curve with a linear region that correlates to the angle regime it will see in the field. Maximizing the angle regime can come down to tip geometry and resolution, spatially and temporally. The spatial resolution will affect the sensitivity of the probe's ability to pick up pressure responses while the temporal resolution will essentially affect whether the response is under or overdamped. To minimize the errors in flow direction when measuring at steep velocity gradients, the holes should be located close together to reduce pressure difference caused by a velocity gradient [12], [13]. Too short of lines from the probe tip to the pressure transducers can cause over oscillated responses that will affect the data read, while distances from tip to sensor being too long will overdamp the system's response producing responses with quite a bit of lag.

The relationships between the probes geometries, spatial and temporal resolutions greatly affect the quality of data these probes will be able to collect in calibration and field studies.

3.1.2 Governing Equations

Calibration of the probes and the curves associated with those are what make the simple idea of the MHP work. There are not many equations derived in MHP theory; however, it is of great importance to understand mathematically how the data is modeled. The pressure coefficient is a non-dimensional feature that is defined by the pressure difference over the dynamic pressure. Dynamic pressure is defined as,

$$\boldsymbol{q = p_o - p_\infty = \frac{1}{2}\rho_\infty U_\infty^2} \tag{2}$$

which is the seen to be the difference between the total pressure and the static freestream pressure. Since dynamic pressure is a difference between total and static pressures it can be found using the center probe port with the static port or ports along the circumference of the probe shaft. Since many MHPs are not easy to manufacture with the static ports the static pressure can be found as a normalization parameter by taking the peripheral ports around the center hole and averaging them together. The pressure coefficients are defined below along with the ports' pressure average, P_a, acting as the static pressure. The accompanying figure illustrates the theoretical curves the pressure coefficients for both axes should see typically in a traverse through an angular range. The angles for pitching are denoted by θ, whereas, the yaw angle is denoted by ϕ,

$$C_{p\theta} = \frac{p_2 - p_4}{p_1 - p_a} \tag{3}$$

$$C_{p\phi} = \frac{p_3 - p_5}{p_1 - p_a} \tag{4}$$

$$p_a = \frac{1}{4}(p_2 + p_3 + p_4 + p_5) \tag{5}$$

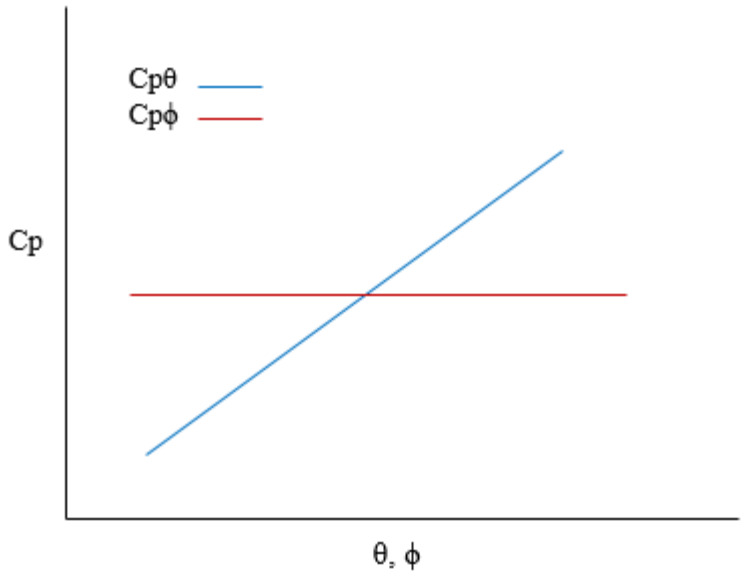

Figure 3-3 : Notional pressure coefficient curves for pitch and yaw depicting a 5HP traversing on the pitching axis while the yaw axis is nulled.

As shown above in Figure 3-3, the axis being tested ($Cp\theta$) has a slope of some gradient related to the probe's overall sensitivity, whereas, $Cp\phi$ is nulled and has zero or nearly zero sensitivity. This is further illustrated in Figure 3-4 by the varying curve slopes on the left. A steeper slope means a more sensitive probe in flow. Another significant parameter for probe response is angular range. As the figure on the right depicts, the further along the curve within the linear range gives the angular range. As stated before, different probe tip geometries affect the probe's sensitivities, which includes angular sensitivity. Out on the fringe in the nonlinear range of the curve, angular sensitivity is less, therefore, maintaining values of *Cp* that correspond to the associated angle is harder to correlate.

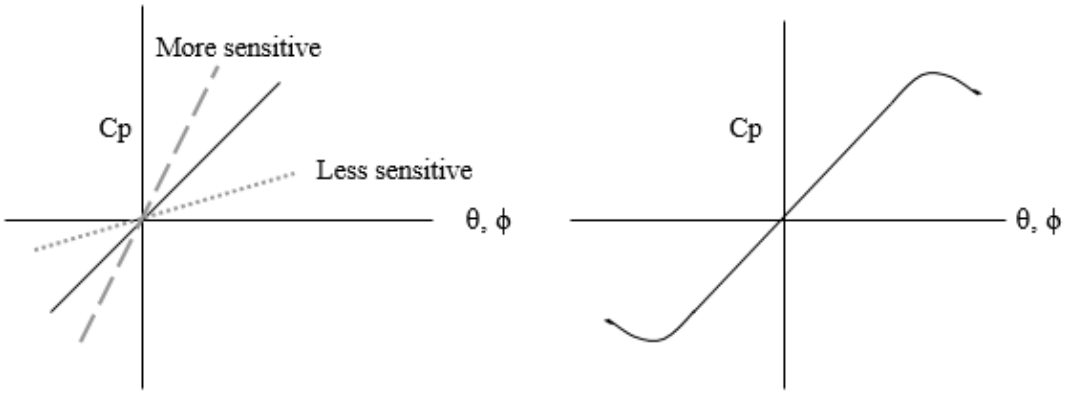

Figure 3-4 : Illustrations depicting pressure coefficient sensitivity (left) and range (right).

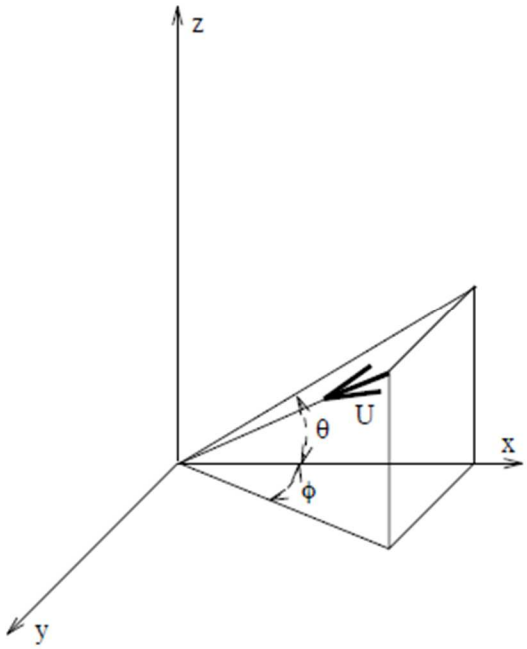

Figure 3-5 : Orientation of Vector pitch and yaw angle [26]

Figure 3-5 shows the decomposition of velocity, *U*, where the rotational axes for pitch and yaw are θ and ϕ, respectively. These are determined from the pressure differences on their respective axis and correspond to Equations 3 and 4.

As shown in Figure 3-5, the magnitude of the velocity vector can be resolved directly by using Bernoulli's equation.

$$U = \sqrt{\frac{2}{\rho_\infty} q} = \sqrt{\frac{2}{\rho_\infty}(p_o - p_\infty)} \tag{6}$$

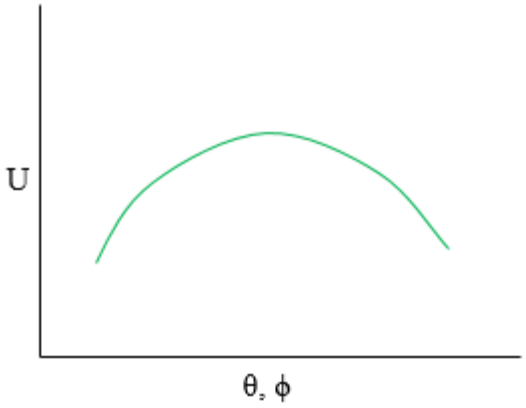

Figure 3-6 : Notional velocity magnitude curve.

Figure 3-6 illustrates a typical velocity magnitude curve with symmetry about the angular range of θ and ϕ. Ideally, the curve should be symmetric about θ and ϕ since the probe is symmetric. After calculating the magnitude and obtaining the direction of the velocity, the three velocity components can be calculated by,

$$\boldsymbol{u} = Ucos\theta cos\phi \tag{7}$$

$$\boldsymbol{v} = Usin\phi \tag{8}$$

$$\boldsymbol{w} = Usin\theta cos\phi \tag{9}$$

These velocity components are with respect to the *x*, *y*, and *z* axes of the probe. While the equations presented in this chapter are for a 5HP geometry, it can be extended to any probe geometry in general.

3.1.3 Reynolds Number Effects on Calibration

Since the main parameter sought after in MHP applications is velocity, it is natural that the effects of Reynolds number should be considered during calibration. Increasing the speed of the wind tunnel will increase the Reynolds regime as well due to its relationship with velocity.

$$Re = \frac{\rho U_\infty D}{\mu} \tag{10}$$

During calibrations a range of Reynolds should be determined; it typically makes sense to choose those Reynolds based on the Reynolds numbers expected to be seen in the field flights. Total pressure along with the pitch and yaw coefficients are typically unaffected by variations in Reynolds; however, the static pressure coefficient will see a measurable change [10]. The following table, Table 1, shows typical Reynolds numbers based on probe diameters tested within similar sizes, geometries, and flow velocity conditions.

Table 1 : Typical Reynolds numbers based on similar probe diameters: Treaster and Yocum (left); Lee and Wood (right) [10], [11].

Reynolds	Diameter	Reynolds	Diameter
$2.0x10^3$-$7.0x10^3$	9.52 mm (0.375 in)	$4.0x10^4$	3.175 mm (0.125 in)
	Hemisphere probe	$8.1x10^4$	Hemisphere probe

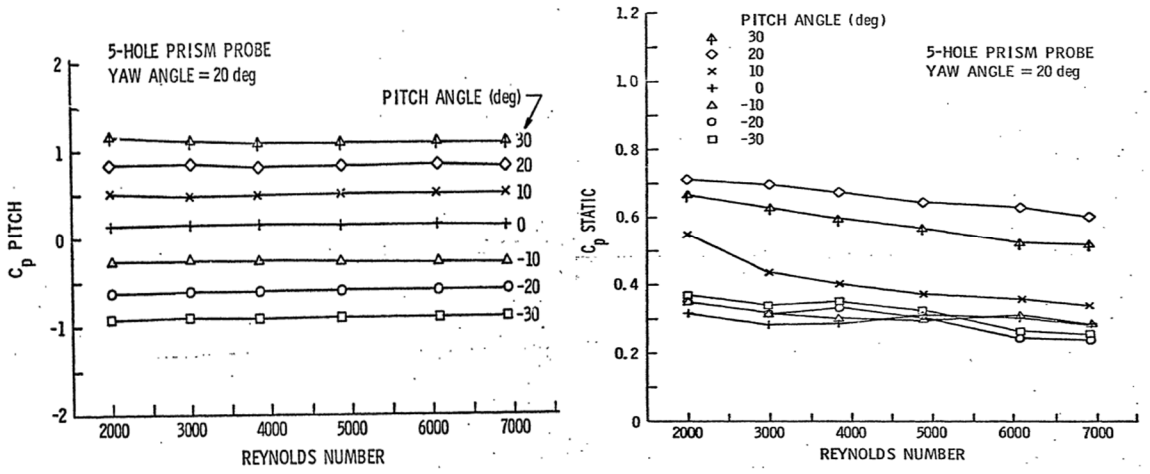

Figure 3-7 : Typical Reynolds number effects on calibration data for Cp_{pitch} (left) and Cp_{static} (right) [10].

It can be extrapolated from Figure 3-7 that Reynolds numbers have a weak effect on the measurements for pitch pressure coefficients. Similar results were observed for yaw and total

pressure coefficients. However, as shown in the figure above, the static pressure coefficients are affected to some degree by Reynolds numbers.

3.1.4 Wall Effects on Calibration

It is known that errors in boundary layer measurements are a function of the local velocity gradient as well as the size and spacing of the holes of the probe. According to Treaster and Yocum, they concluded that the problems that arise in boundary layer measurements are those of probe selection rather than that of calibration [10]. Since distance is the primary factor in wall effects, it is a good idea to observe this phenomenon especially having a probe span in a smaller wind tunnel. Figure 3-8, from Treaster and Yocum, show three calibration data sets as functions of distance for various yaw angles . It follows that the changes in the calibration data curves for these yaw angles appear to be similar suggesting that the wall proximity effects are almost exclusively a function of distance only [10]. In these tests, a plate was placed near the probe, and the probe was moved to different distances through the plate.

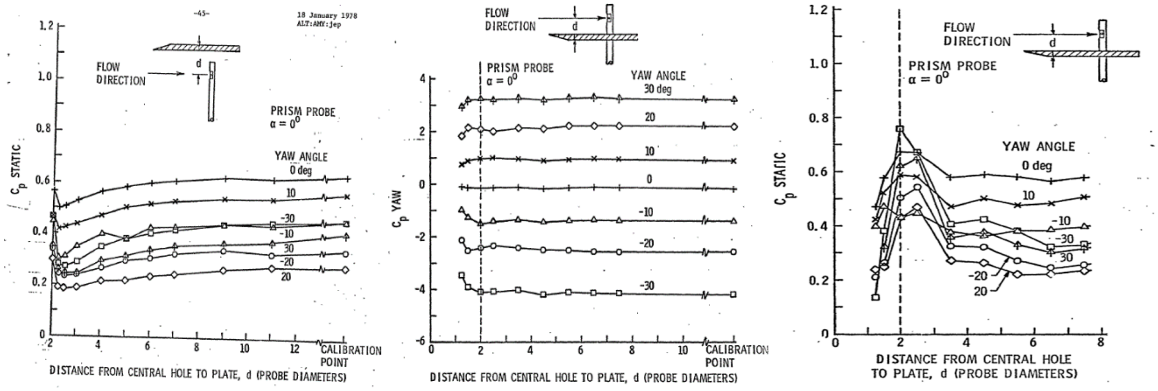

Figure 3-8 : Typical wall proximity effects on calibration data as a function of probe diameter distances: all three curve sets show wall effects taking place at approximately two probe diameters [10].

It was observed that calibration coefficients were effected within two probe diameters of the plate. Therefore, they concluded that measurement taking had a limitation of two probe diameters from the wall before the measurements were considered invalid for these specific probe geometries.

3.1.5 Transient Response

The mass of fluid in a sensor vibrates under the influence of fluid friction. This tends to have damping effects on the oscillatory motion. These fluctuations are common in many pressure systems. An example of how this works is illustrated in the figure below.

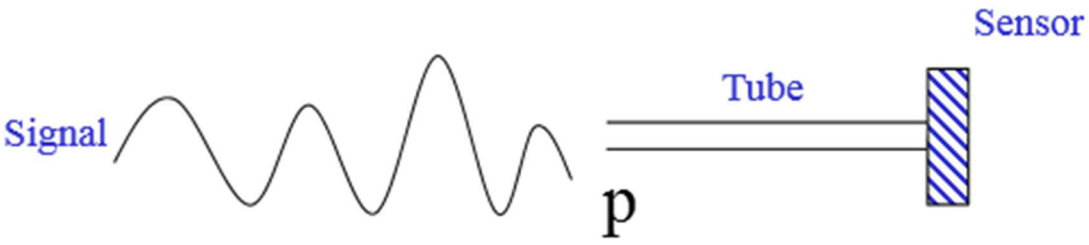

Figure 3-9 : An arbitrary input signal to a pressure sensor.

For a pressure sensor, the tube is small and the flow can be assumed to be laminar. An expression for this behavior is given as a pressure-amplitude ratio,

$$\left|\frac{p}{p_0}\right| = 1/\sqrt{[1-(f/f_n)^2]^2 + 4h^2(f/f_n)^2} \tag{11}$$

where f is the frequency of the pressure signal. The natural frequency f_n and the damping ration ξ is given as,

$$f_n = \sqrt{3\pi r^2 c^2 / 4LV} \tag{12}$$

$$\xi = \frac{2\mu}{\rho c r^3}\sqrt{3LV/\pi} \tag{13}$$

L is the length of the pressure tube (probe), r is the radius, V is the sensor volume, and c is the speed of sound. Density and dynamic viscosity of the fluid are ρ and μ, respectively. The behavior of the transient response for the pressure system attenuates as a function of the input signal frequency.

3.2 Application

3.2.1 Surveys

MHPs have been used in wake surveys due to the desire to accurately map out the complex 3-dimensional flow field that results from a vortical wake. Vorticity distribution in a vortex wake

is complex, and measurements of that distribution are essential in understanding and determining the stability characteristics of the wake. To further understand vortex wake roll-up, wind tunnel tests have been done using 5HPs in wind tunnels [26].

Qualitative applications on wake surveys utilizing wake imaging have been extensively used to verify most aerodynamic flows of interest. These types of surveys have significance in better understanding aerodynamic performance by visualizing the flow field around the obstacle being surveyed. To add to breadth and depth of wake surveys and aerodynamic understandings it is useful to characterize the quantitative aspects of wakes by surveying their 3-dimensional flow. With this information gathered, it allows for separate measurements in drag (induced and profile) and lift, including the spanwise distributions of drag and lift [38]. In these surveys MHPs are used to record pressure and velocities that are converted into aerodynamic forces. A wing model or object it mounted into a wind tunnel and a MHP is mounted at a specified location in the wake. By varying the angles of attack at multiple Mach and Reynolds number regimes, the probe can then map the wake created behind the object. In turn, the pressure and velocity data collected in these surveys can be used as validation information for CFD analyses. An example of the type of wake survey data that can be obtained is in the following figure.

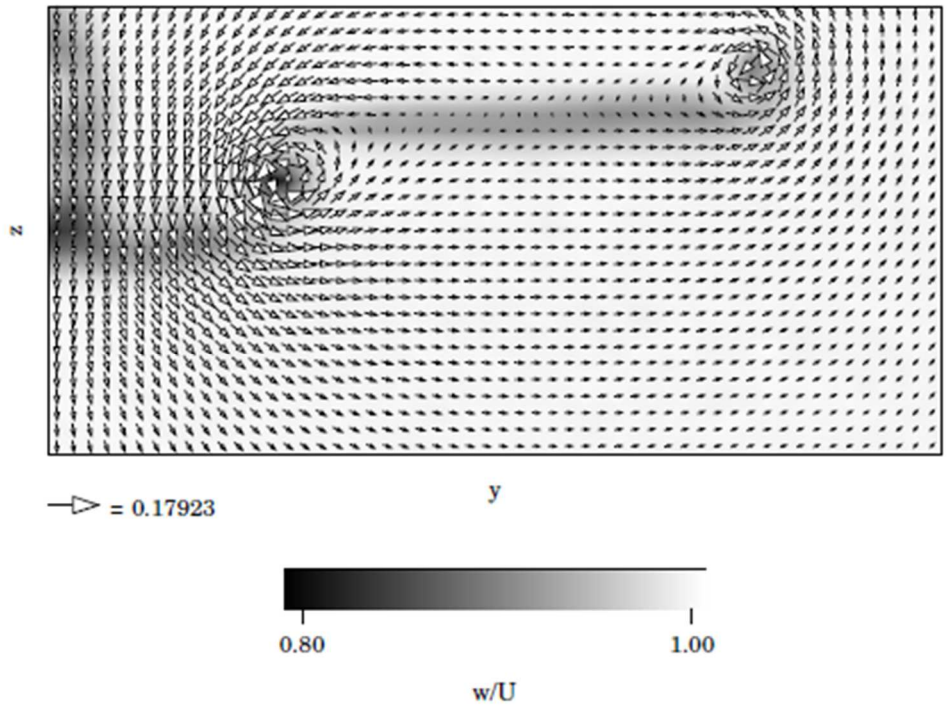

Figure 3-10 : Example 5HP data plot of the right half of a circular arc airfoil with flap-span at 30%. Velocities are scaled with the free-stream velocity U=15 m/s. The greyscale indicates the streamwise velocity deficit [26].

3.2.2 Air Velocity Aloft

Air velocity booms for MAP studies typically allow measurements of air pressure, temperature, and 3D airflow data. MHPs are mounted on a boom in a freestream flow away from the vehicle to measure the clean air. The probes are packaged with specified sensor packages to collect air data used in many meteorological and ABL research areas including but not limited to: severe weather and tornadic wind velocity modeling to help in predicting severe weather and tornadic formations, various turbulence studies, as well as many other meteorological interests. Vertical and horizontal movements in the atmosphere are of major interests at different scaling factors coming from small turbulent diffusions in the air all the way to large global wavelengths that typically occur in the upper troposphere [39]. In many of the meteorological sensor packages measuring limitations, such as, sampling rates are mostly dictated by the relative humidity sensor. This affects the overall sampling rates and measuring accuracies for the air data boom sensor

packages the probes are mounted to. These factors as discussed by Kroonenberg affect more sensitive measurements in determining the fine, small scaled structures within the stable portion of the ABL [1]. These include the varying layers, sheets, fossil turbulence, intermittent turbulence and waves, and a low level jet influence on these processes.

Figure 3-11 : M2AV taking turbulence data in Antarctica [1].

To better understand the necessity for reliable and high level wind velocity booms for understanding critical components of ABL physics it is necessary to understand things like turbulence and its complexities from its dynamics and internal interactions. Understanding these important transport processes is crucial. Turbulence within the ABL happens through a balance of shear stress presented by the surface buoyancy effects introduced by surface heat flux via temperature and humidity gradients. These surface gradients affecting the turbulence in the ABL layers are of great interest to understand as spatial characterizations of the turbulent structure is still relatively poor. Turbulence data is typically obtained as temporal information from anemometer readings that typically have a temporal response of 20 Hz with a spatial resolution close to 10s of centimeters [33]. Through UAS platforms utilizing air data booms with better equipped sensors and MHPs the possibilities of obtaining characterizations in the spatial reference of the turbulence

structure are greater as UAS can collect more data in ABL regimes that manned aircraft would not go due to risk of life. The use of MHPs enables the study of large-scale turbulent structures by determining all three velocity components in a more robust way than a typical hotwire probe can.

Measuring wind velocity with a 5HP mounted on a boom on a UAS vehicle will have six degrees-of-freedom in rotation and translation. The probe should be mounted along the aircraft's x-axis. To obtain the wind vector from the sensor measurements, the probe will sense the velocity of the aircraft relative to the velocity of the air it is traveling through. It is thus imperative to define the relative velocity recorded by taking the difference between the vehicle velocity and the wind velocity (atmosphere). Components of the relative velocity will be extracted from the sensors via the 5HP ports along the tangential, pitching and yawing axes [33]. Thus, the addition of MHPs on air data booms are of high interest as accurate measurements of sideslip angles are still difficult to come by and critical in ABL layer characterizations.

Measurements of vertical and horizontal air movements in ABL are important in understanding weather conditions and other meteorological interests. As discussed by Axford, being able to measure up- and downdrafts in cumulus clouds and horizontal and vertical components of turbulent air are just a few types of measurements that are of high importance to atmospheric scientists and meteorologists. Accuracy of these measurements are highly important for fast and potentially life-saving weather forecasts. Using an inertial platform like aircraft as a stable reference during flight instrumented with a MHP can evaluate the vertical and horizontal components of wind shear in real time. The measurements in up-/downdrafts can be distanced as far as 1-2 km in convective clouds [39].

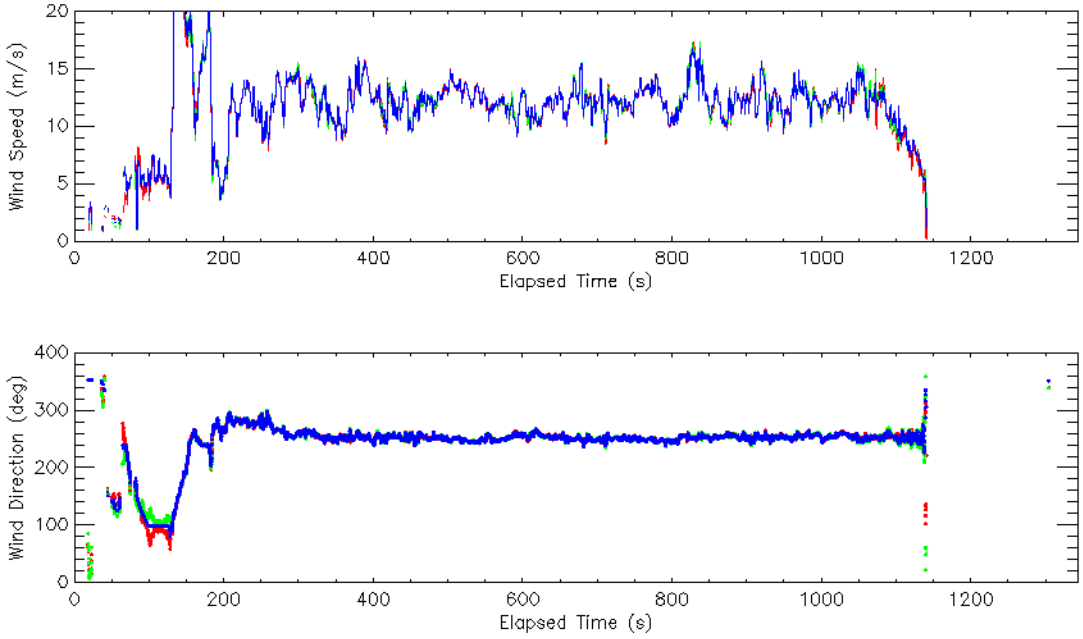

Figure 3-12 : Wind speed (top) and wind direction (bottom) NCAR 5HP data via Rain Dynamics [5]

Figure 3-12 shows data taken by a prototype 5HP system that measures 3D wind vectors, humidity, temperature, pressure. latitude, longitude, and altitude data. A high-performance INS system is integrated into the air data probe sensor suite. This data was taken on the Applied Aeronautics Albatross UAS (see Figure 1-2) with wind velocities up to 16 m/s and data acquisition at 5 Hz (approximately 10 m resolution) [5].

3.2.3 Data Booms for Aircraft Performance

Application of MHPs for aircraft performance on data booms are used to detect the flight velocity vector with respect to the airframe axis (probe axis). This can be used for both manned and unmanned vehicles for detecting the flight velocity vector to predict airframe motion caused by the wind changes in the air; adding flight stabilization control. This is referred to as an "air active control aircraft" [19]. This essentially acts as an enhanced Pitot-static probe, however, now aircraft performance can be observed and evaluated in more detail by simultaneously mapping the three-dimensional velocity vector components: pressure for angle of attack (pitch axis), pressure for angle of sideslip (yaw axis), as well as total and static pressures. Mach number can also be calculated

[40]. Maintaining control for proper attitude is done merely by the detection of the signal. Using this in parallel with an on-board flight controller the MHP can aid by extracting air data into a feedback loop for the flight controller to make aircraft performance adjustments in attitude and engine thrust control necessary for steady and level flight. An example schematic in Figure 3-13 shows an air data boom that integrates with a flight controller for feedback performance control.

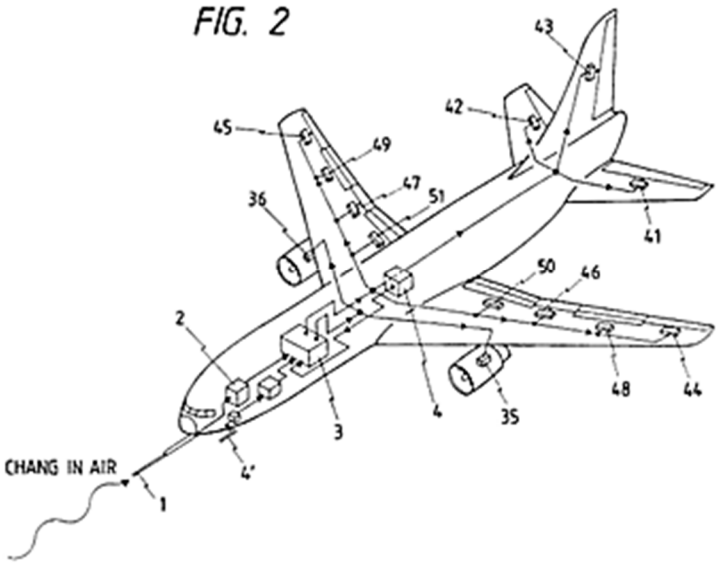

Figure 3-13 : A cartoon illustration from a patent of an air data boom system for aircraft performance enhancement [40].

CHAPTER IV

4. METHODOLOGY & EXPERIMENTAL ARRANGEMENT

This chapter discusses the tools, methods, and experimental setups that were used to develop the probes, sensors, and evaluate the calibration process. The first section will go into detail on probe design and selection processes as well as discuss the manufacturing approach for rapid prototyping each probe. The second and third sections discuss the calibration and data reduction methods, respectively. The benefits of those specific approaches over other methods are discussed while section 4.4 discusses the calibration testing setup in the wind tunnel. In subsequent subsections a discussion on the mounting procedures to verify alignment of the probes, probe types, testing specifications, sensors and other hardware/software specifications are discussed. A discussion on the approach for finding the time response is presented in section 4.5. Flight test setup is presented in the next section with detailed board and sensor layout followed by and uncertainty analysis evaluation on the experimental procedure in the last section of this chapter.

4.1 Probe Design

Each probe manufactured and tested was 3D printed in the Formlabs printer. It is crucial to observe and scrutinize the manufacturing approaches as accurately and precisely as possible to truly evaluate the probe performance by reducing outside error common in calibration processes. Each probe was checked before testing to verify the holes were not blocked and to the best that is most humanly possible. The first set of printed probes were made using fused deposition modeling (FDM) prototyping method. FDM uses a thermoplastic material and is deposited in layers which could be visible after printing the probes. An issue with FDM and the resin used was that the probes were brittle, and over time cracks began to accrue along the probe axis. Another method was used with stereo lithography (SLA) using a photopolymer tough resin. The SLA method also works with additive materials, but layers the tough resin as a liquid. The tough resin is designed to simulate

ABS plastic and gave the best results for prototyping probes. The latest iteration of probes used the tough resin SLA printing and it was easier to identify fluid passage blockages. Additionally, the probes were not as brittle and less prone to cracking and breaking than previous probe iterations using FDM. It was observed that orientation of the probes during the printing process greatly affected the outcome of their quality. For quality control purposes, each probe has a wire (pipe cleaner wires work best) passed through each hole to check for blockages or constrictions. After each probe was newly printed it was useful to immediately check and clean the holes before the resin hardened. Isopropyl alcohol proved to be a good cleaning agent on the probes' internal passages. Over several iterations and variations of probe geometries and sizes, a more optimized procedure for printing the probes developed. As far as designs of the probes, for the span of this research project typical probe geometries were chosen to test first with the printing process over more complex geometries.

4.1.1 Probe Design Considerations

The probe designs in the scope of this project were kept relatively simple even though experimenting with 3D printing for rapid prototyping was the manufacturing goal. The benefit of 3D printing is that complexity of design becomes less of an issue with the build; whereas, manmade probes have to remain relatively simple internally due to human manufacturing capabilities. Once the printing process proves optimized and can consistently reproduce high quality probes, then printing smaller probes with more complex internal and external geometries will be done to test design optimization. It is noted that as 3D printing technology and materials become more advanced, the limitations currently seen in this project with maintaining consistent print quality will soon likely be overcome and 3D probes commonplace.

Figure 4-1 : Progression of 3D printed probes. Old-to-new from left to right. 3D printing of left 6 probes in the FDM method, and the 7 probes to the right are manufactured by SLA tough resin.

Many studies have shown that the smaller the probe tip diameter the greater the accuracy when traversing shear layers. Tip size, including hole diameter size, is directly related to spatial resolution quality. Minimizing tip size of the probe increases the spatial resolution. However, as the probe tip diameter decreases, so does the response time. Smaller probes require more time to allow the pressure sensors' readings to settle between each traverse position. One study demonstrated that it took 3.4 times longer to traverse a complete test regime with their smallest probe diameter as compared to their largest (0.99 mm & 2.67 mm) [41], while another found it took approximately 8 hours with a tip diameter of 1.22 mm [18]. To reduce settling times, it is found that minimizing the length of the probe's internal holes/tubes accomplish this followed also with the length of the tubes externally of the probe, i.e., the tubing that connects the probe to the sensors. This overall distance from the probe tip to the pressure transducer is known as temporal resolution. Minimizing the distance between will increase the temporal resolution and give quicker response times for readings. The same study found that applying these techniques to design on the probe reduced the traverse time in their experiments by 71% while keeping a very high accuracy [41].

Hence, size of the probe (outer and internal) are directly related to the resolution and accuracies of the probe's characteristic performance.

The problem with designing very small probes comes down to two main factors: 1) manufacturing quality and 2) response times. These are significantly important details when experimental (laboratory and field) data is the goal. The science will ultimately drive the direction of the design, but the manufacturing of the probe will influence due to limitations. As the probe's performance required does depend on the data taken for the science. For example, in turbulence studies, it is desirable to have the quickest response times, and therefore, having small probes with minimized distance from the sensors is more ideal. But there is a tradeoff as discussed above; having a smaller probe may not make sense if the science needed does not require faster responses. Additionally, too short of distances between tip and transducer can result in extra noise since the tubes act as a high-pass filter. The tubing length on the probe can be thought of as a filter, adding length will dampen out some of the response. Finding the balance between is key to having accurate measurements. So to reiterate one of the main dilemmas in designing a probe: 1) in order to have higher accuracy the tip diameter should be minimized and 2) to have faster response times the tip diameter must be increased.

Probe tip geometries (tip and hole) is another consideration to take when designing the probe as geometries affect the sensitivity of the probe. It was found that 45 degree angled tip holes and chamfers have a good balance between static pressure and flow angle sensitivity [20].

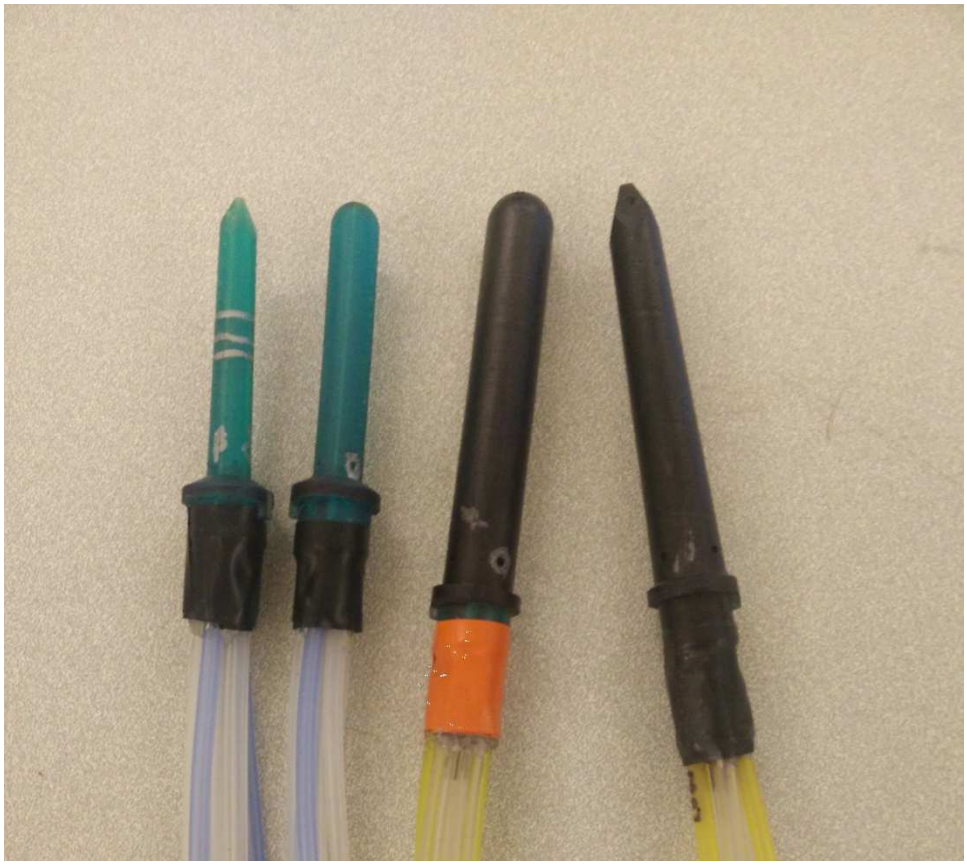

Figure 4-2 : Scaled down pyramid and hemisphere probes (left) compared to the large hemisphere and pyramid probes (right).

4.1.2 Probe Design

Probe designs for this project started with two main geometries, and then varied in sizes to compare performance characteristics of each design. The tip geometries evaluated included a hemispherical and a pyramid probe each of two different sizes. Variations of sizes in between these 4 were made, but due to print qualities only the 4 probes made in the last iteration produced the best quality to thoroughly evaluate. Major issues with 3D printing MHPs came from quality of printing. Externally the quality of the probe tip must be considered as tip geometry affects sensitivity to the flow and response. Internally, ensuring that the hole and tube diameters remain consistent is generally the most important to quality of measurements. Some probes printed with hole constriction inside the tube due to printing quality. It was found orientation of how the probe was printed affected the quality as much as the type of resin used in the print.

Table 2 : Probe dimensions for the two probes sizes.

	Hemisphere/Pyramid	Small Hemisphere/Pyramid
Tip diameter	12.7 mm (0.50 inches)	6.60 mm (0.26 inches)
Hole diameter	1.78 mm (0.07 inches)	1.27 mm (0.05 inches)
Probe length	98.3 mm (3.87 inches)	58.93 mm (2.32 inches)
304 SS tubes ID	2.03 mm (0.084 inches)	1.30 mm (0.051 inches)
Tygon PVC tube ID	2.38 mm (0.094 inches)	1.59 mm (0.0625 inches)

Each probe (both geometries) was constructed with 45 degree angled holes. The pyramid had 45 degree angled chamfers at the tip. The following figures are of the probe designs.

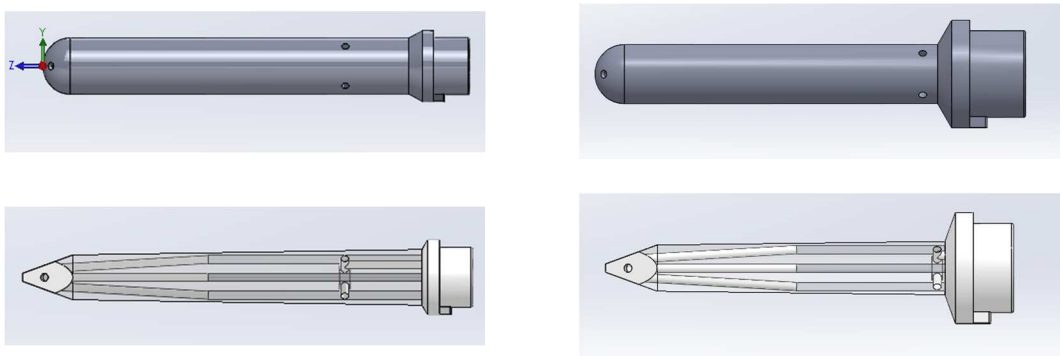

Figure 4-3 : Probe designs: large hemisphere and pyramid probes (left); small hemisphere and pyramid probes (right).

Each probe, for mounting purposes, has a protruding notch at its base that fits into a female notch on the mount to lock the probe in place to ensure axis alignment. The base of every probe is the same size and geometry to make all mounting procedures as simple and easy to follow allowing for the same boom mount to be used in the wind tunnel and in the field no matter probe size. A discussion on probe mounting and alingment procedures is presented later in this chapter.

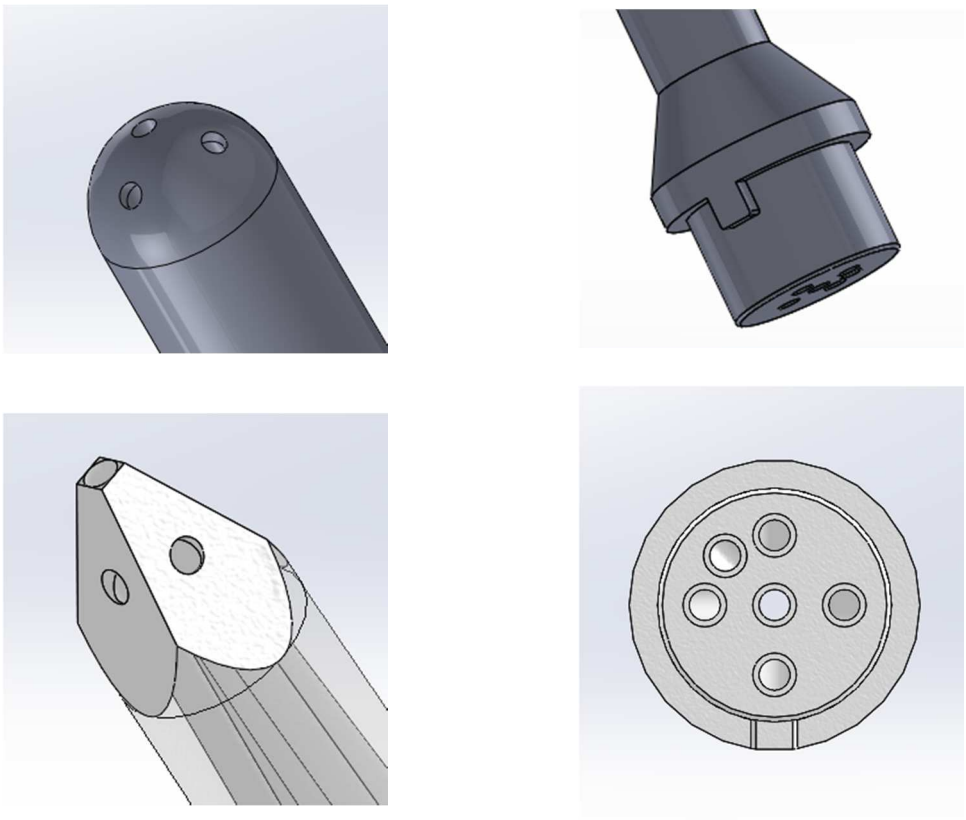

Figure 4-4 : tip geometry (left column); base of small probe showing notch (top right); hole layout of all probes (bottom right).

All probes had stainless steel hypodermic tubing inserted into the base of the probe that connected the base to the tygon plastic tubing that connected to the transducers.

4.2 Fixed-position or Non-nulling Method

This section addresses the fixed-position also known as the non-nulling method. The other widely used method is the nulling method. The nulling approach became less popular as the fixed-position approach was found because the sophistication required of the traversing system and long data acquisition time makes it overly cumbersome in the data collecting and data processing schemes. Nulling method has the probe mounted on a five degree-of-freedom traversing system that lines up parallel to the flow. In this method, the probe must be pitched and yawed at each measuring point until the four peripheral pressures around the center hole are equalized, or nulled

[27]. This method requires more space for a wind tunnel and is a much longer process than using the non-nulling technique, which also makes it more expensive to implement.

In the non-nulling method, the probe is mounted at a constant angle on one of its axes while the other axis is traversed and incremented over a flow field at an angle range determined by the user. It measures all port pressures at each angle increment within its span. With all of the pressures measured, the data can then be related back to the pressure coefficients and velocity vectors as discussed in previous chapters. Through the calibration process the probe will reach its maximum angle it can accurately read before flow separates from the probe. The wind tunnel has a pitot probe upstream of the 5HP for recording environment data that will be used and compared with. More details with the probes will be discussed in the next chapter for experimental setup. Developed by Treaster and Yocum, this technique is simple and elegant by comparison to the nulling method [10]. However, at calibrations for large angles in pitch or yaw singularity is encountered. In this method at large angles, the total and static pressure (averaged pressures) they begin to deviate from the actual total and static pressures and then begin to not behave as dynamic pressure [25]. Singularity, in short, occurs when the denominator goes to zero producing a singularity. This issue should not be too much of an issue for this project as expanding the angle range is only secondary to evaluating the actual probe performances.

4.3 Data Reduction Methods

A goal of this research is to reduce the number of pressure transducers from five to three by utilizing the pressure coefficient relationships that are explained in further below,

$$C_p = \frac{\Delta P}{q} \tag{14}$$

Instead of having a pressure transducer connected to each individual probe pressure port, it was decided to test the viability of using only three transducers being one for each pair of holes associated with a specific test axis. Transducers 1-3 go to the pitot-static ports, the pitching axis ports, and the yawing axis ports. In the wind tunnel a fourth pressure transducer is used for the wind

tunnel pitot-static probe. With reducing the number of transducers it leaves room for other sensor integration eventually and reduces costs of manufacturing sensor packages with custom made boards. By reducing the number of transducers it also minimizes the time it takes to process data by having two fewer sensors. This arrangement also reduces the impact of bias error.

Validation of this approach is to be done by also calibrating with a scanivalve that is connected to a barocel manometer to record the pressure differences in each of the 5HPs' pressure ports along with the upstream pitot probe. Then the averaged pressures in the denominator for the dynamic pressure can be evaluated and compared to the other methods. Just as before, the procedure will calibrate the probe in the pitch and yaw axes by varying the angles in incremental steps small enough to map out a good calibration curve.

4.3.1 Replacing the denominator, P_1-P_a, *with the constant* P_0-P_s

Replacing the P_1-P_a denominator, which is the dynamic pressure measured by the 5HP's averaged peripheral pressure holes, is also evaluated. The dynamic pressure measured in the freestream by the wind tunnel pitot probe was used in the hopes of helping overcome what is known as singularity as was developed and tested originally by Pisasale et al [25]. This was used as a means of data normalization to help reduce data scatter and implement and easy way to process calibration data. This method is noted by Pisasale to have possibly drawbacks, by examining the pressure coefficient in one of the axes it is possible for the angle associated with that axis, i.e., yaw and the sideslip angle, to become multivalued at a very large angle. For example, they noted that at some angle point the pressure coefficient for the yaw axis loses its one-to-one relationship with the sideslip angle, ϕ. This is something to take into consideration when going through the different data reduction techniques.

4.3.2 Replacing the denominator, P_1-P_a, *with* P_1-P_s

One technique evaluated is replacing the typical P_1-P_a denominator with the pitot-static pressure difference on the 5HP. When using this approach for the denominator there is no problem

encountered with multivalued calibration coefficients. Although that issue is resolved it is still prone to singularity encounters. Evaluating this method against the other two should give good comparison results for validation.

4.3.3 Test Matrix

A test matrix was developed for refining the approach in wind tunnel testing. Three Reynolds and Mach number regimes were determined over the varying angle for each test axis. This was implemented for each probe type. There are two probe geometries evaluated in this scope with the goal to evaluate their performances against a professionally manufactured 7HP by Aeroprobe company. Table 3 illustrates the testing matrix used in calibrating the 5HPs. Reynolds numbers were calculated based on the two probe diameter sizes in meters. *Re_D/m* and *Re_d/m* represents the Reynolds numbers for the hemisphere/pyramid and small hemisphere/pyramid probe diameters, respectively. Wind tunnel velocities were largely determined based on the physical output the wind tunnel could perform. At higher velocities it was observed that the wind tunnel motor speed would vary and cause velocity fluctuations at the high end of the tunnel motor's RPM capabilities.

Table 3: Test Matrix of calibration testing parameters for subsonic test regimes

Geometry	Diameters	Angle Span	Velocity	Re_D/m	Re_d/m	Axes
Hemisphere	12.7 mm	-45^0	10 m/s	$8.4x10^3$	$4.4x10^3$	pitch, θ
Pyramid	12.7 mm	$+45^0$	15 m/s	$12.6x10^3$	$6.6x10^3$	yaw, ϕ
Small Hemi	6.6 mm	5^0 increment	20 m/s	$16.8x10^3$	$8.7x10^3$	
Small Pyr	6.6 mm					

4.4 Wind Tunnel Setup

4.4.1 Sensors and System Layout

The wind tunnel is on the Oklahoma State University campus and is a subsonic low-turbulence Flotek 1440 wind tunnel. Designed to deliver up to 33.5 m/s (132 fps) it has a test section of 12" x 12" x 36" and is a closed tunnel. It is designed for turbulence of 0.2% or less, straight-line (laminar) airflow with variable speed 2 hp direct current industrial Baldor motor. Tunnel schematic is shown in the next figure.

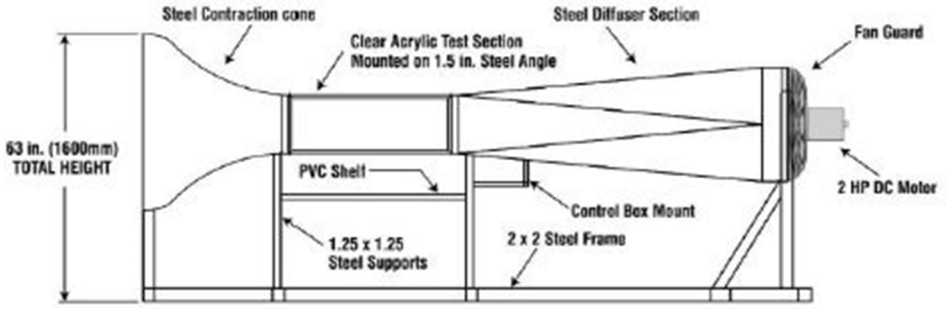

Figure 4-5 : Flotek 1440 Subsonic Wind Tunnel: The Oklahoma State University Low-Turbulence Wind Tunnel. Test section is 12inx12in.

Underneath the test section a 12 to 48 Vdc voltage input, 100mA to 3.0A current Arcus Technology NEMA 23 USB stepper motor (DMX-UMD-23 model) is integrated with 1000-line incremental encoder. It has USB 2.0 and RS-485 (9600-11k bps) communication capability, but is being used solely on USB communication protocols. The stepper runs integrated with National Instruments' data acquisition system, NI USB-6295, that runs LabVIEW. Four 0-25 Pa to 0-12.5 kPa, OMEGA PX653 pressure transducers with a 1-5 Vdc output are connected to the National Instruments data acquisition system. Data is sampled at a sample rate of 1 kHz. The pressure transducers are connected to the 5HP by tygon tubing to stainless steel tubing of the same internal diameters (2 different sizes for 2 probe diameter sizes). These components are shown in the next figure.

Figure 4-6 : DMX-UMD-23; NI-6259; OMEGA PX653

These components integrated together with the wind tunnel are presented in the following figure. Airflow comes into the test chamber from the right to the left as the probe traverses a predetermined, incremented span and the pressure transducers take analog voltage readings converted into differential pressure.

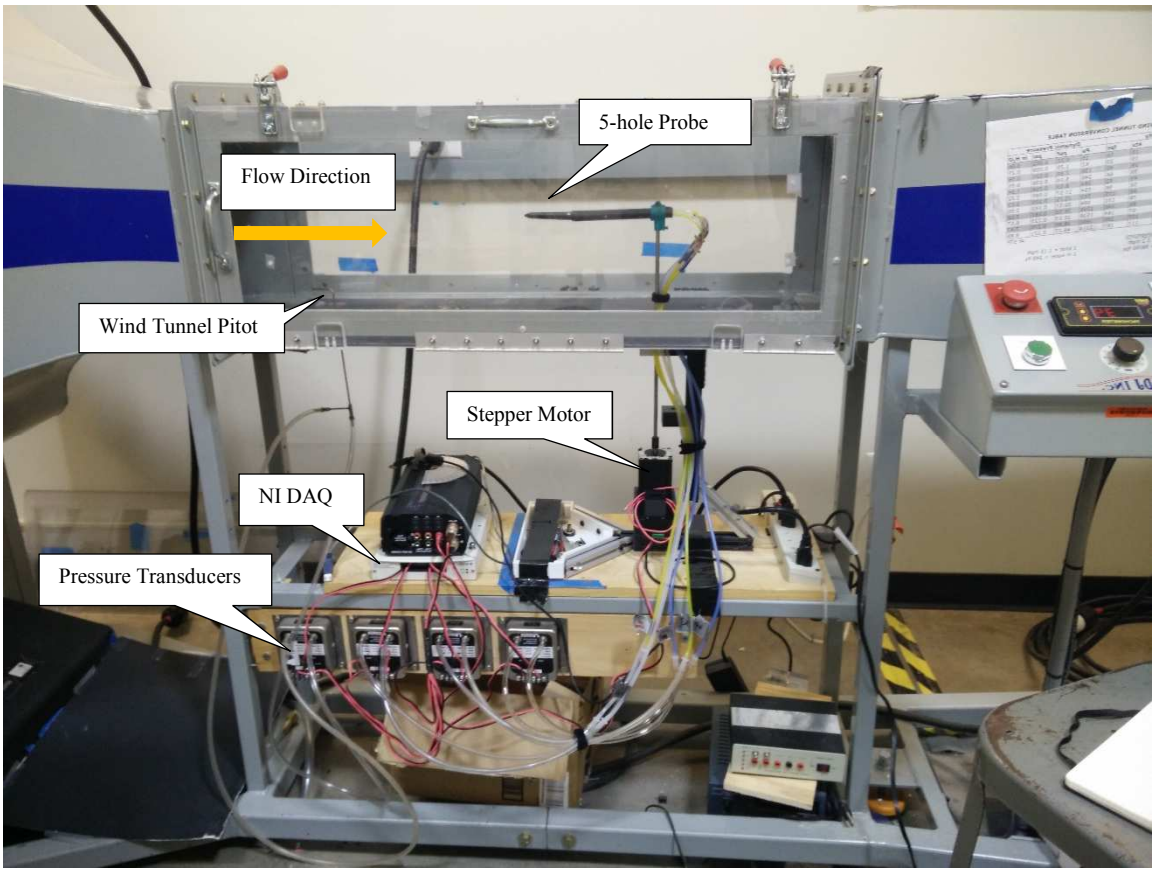

Figure 4-7 : Wind Tunnel setup with Pyramid probe mounted.

Figure 4-8 : Pyramid 5-hole probe side and top views

4.4.2 Mounting and Alignment Procedures

A significant determining factor in quality of data is properly mounting and verifying the probes are oriented correctly. This reduces the overall human error associated with experimental testing. Careful precaution was taken to mechanically ensure the probe was always mounting correctly, but this assumes the mount itself is positioned correctly. This portion of the calibration and testing processes tend to be the most tedious and cumbersome as any variation from alignment in any of the axes can cause distortion in the data readings.

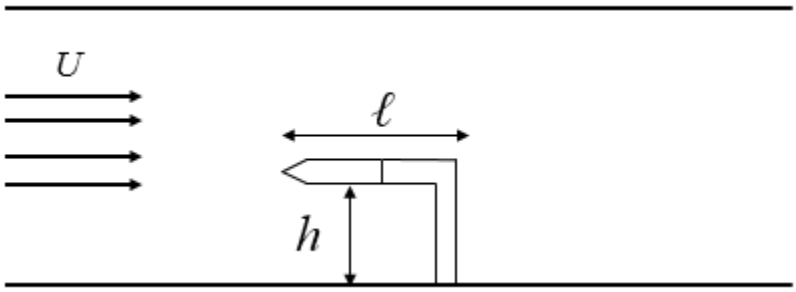

Figure 4-9 : Schematic of probe setup in the wind tunnel.

Aligning the probe with the accuracy of the stepper motor greatly reduces aligning the probe axis (x-axis) with the flow and angle increments. However, setting the boom the probe is mounted into must be carefully placed so that the roll axis is aligned correctly while remaining level in the pitching rotational axis of the mount. If improperly mounted the pitching and yawing axes will be

offset from their vertical and horizontal axes. A lot of time and consideration was taken to reduce the setup time for testing as this stage. The following is a procedural description of how each alignment step was taken and validated:

1. *Boom & Probe Alignment*: The boom the probe is mounted to is a standard carbon fiber tube (ID: 0.503 in and OD: 0.505 in) that has had notches cut into both ends. At the backside of the boom it is notched on the bottom side and slides into the mount that has a protruding notch the fits into the boom's notch. On the front end of the boom are two more notches cut at 90 degrees apart from each other with one of the notches cut exactly 180 degrees (opposite) from the notch on the back end of the boom. It is notched on the top side front end with the secondary notch 90 degrees from it on the same plane. The notches on the front end are from mounting the probes into the boom without having to take time to align the pitch and yaw axes before testing. The following figure illustrates the mating process between the probe and boom.

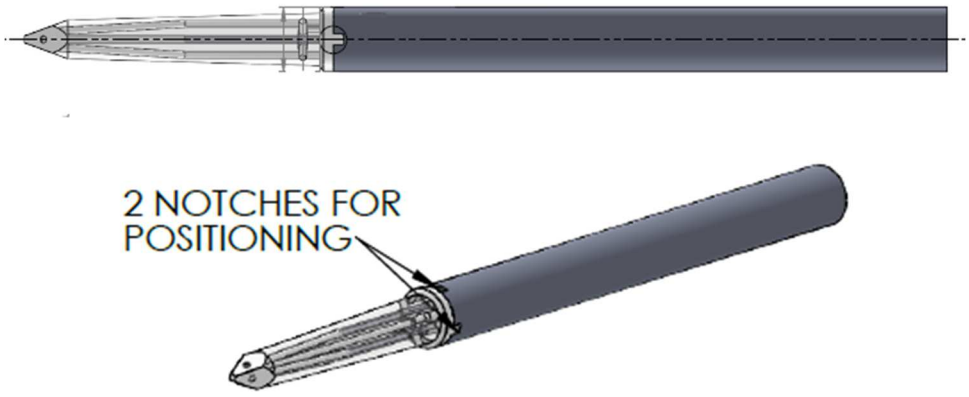

Figure 4-10 : Boom and Probe notch mating.

As long as the notches are cut correctly on the boom the probe can easily slide in without having to measure it. The mount and probes are 3D printed so they are premeasured in the CAD file and printed to specifications. After printing they were checked for any inconsistencies.

2. Spanning Axis Alignment: Within the wind tunnel, tape was put down and lines for -45, -30, 0, +30, and +45 degrees were measured with a protractor and drawn out to aid as a visual for probe/stepper angle steps. With this it can easily be seen if the stepper motor is positioned wrong before the tests begin as this was a concern in previous testing before the stepper was integrated. A check to see if the probe x-axis is lined up with the flow axis is also done by observing that the highest pressure is read from the pitot-static ports on the probe. At 0 degrees, the probe should get the highest differential pressure reading from its center (total pressure) and static ports. Another check is observing that the calibration curves have symmetry.

Once the mounting and stepper motor is setup within the program the alignment process is done. Prior to adding mechanical guides and the new mounting system, it was up to the user to hand measure everything out for each test setup. By doing this approach it cut down setup time considerably.

4.4.3 Calibration Testing

In calibrating, the purpose is to determine the relationships of the measured pressures from the probe holes and local static and total pressures. The relationships are found and expressed in the form of dimensionless pressure coefficients that are functions of flow angularity. The objective of calibration is to experimentally determine the pressure data in a controlled, known flow field. The probe's response can then be determined with the set of calibration curves. Whereas, in-field experiments, the opposite is true; the flow field (total and static pressures, pitch/yaw pressures and angles, and the magnitude of velocity) is not known. Thus, the relationships between the probe pressures from calibration are then used to compare and extract these parameters in the field.

Calibration of probes followed the procedures and methods of Treaster and Yocum as described in chapter 4 [10]. Each probe was calibrated 3 times. Ambient conditions in the laboratory were taken at the start of each testing session day, and were checked as the day progressed. Typically, the conditions within the same test day period did not change, but were checked as

testing multiple probes could take several hours. Mounting and alignment procedures were done as described previously. Each calibration test was implemented by traversing a probe in the specified axis (pitch or yaw) from -45 to + 45 degrees at 5 degree steps. Each 5-degree step was sampled for 2 seconds at 1 kHz sampling rate. Each probe axis (θ and ϕ) was tested 3 times at 3 different Reynolds numbers (velocities).

Flow velocity was set in the wind tunnel and the pressure transducers read the voltages as the probe traversed the test section. A LabVIEW code with the National Instruments data acquisition device was used to read and process data into corresponding pressures. Voltages were read through the 3 OMEGA sensors, and pressure and velocities calculated through LabVIEW. The wind tunnel pitot-static probe was located 16 and 17.5 inches (32 large 5HP diameters and 67 small 5HP diameters) from the large and small probe tips, respectively. Wind tunnel conditions were also read by an OMEGA sensor. Before any calibration testing began, the OMEGA sensors were calibrated and their voltage versus pressure relationships were found, the data for which can be found in the appendix. The following two figures are examples of the interface of the Arcus stepper motor and the example block diagram code for LabVIEW.

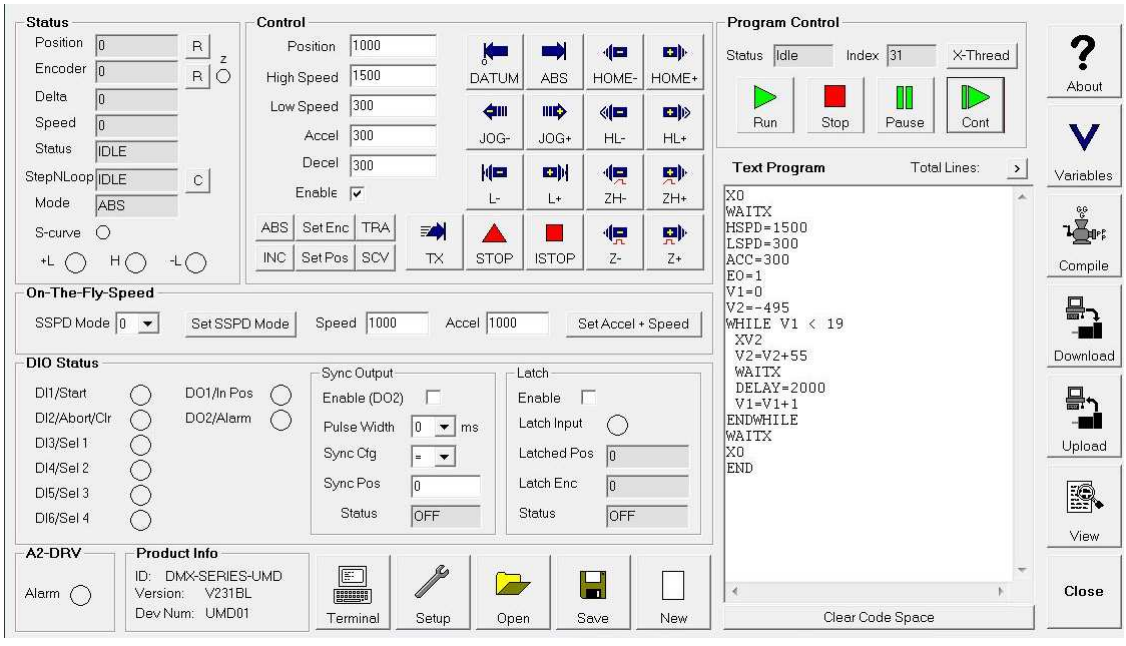

Figure 4-11 : Arcus stepper motor and encoder interface with a simple traversing code.

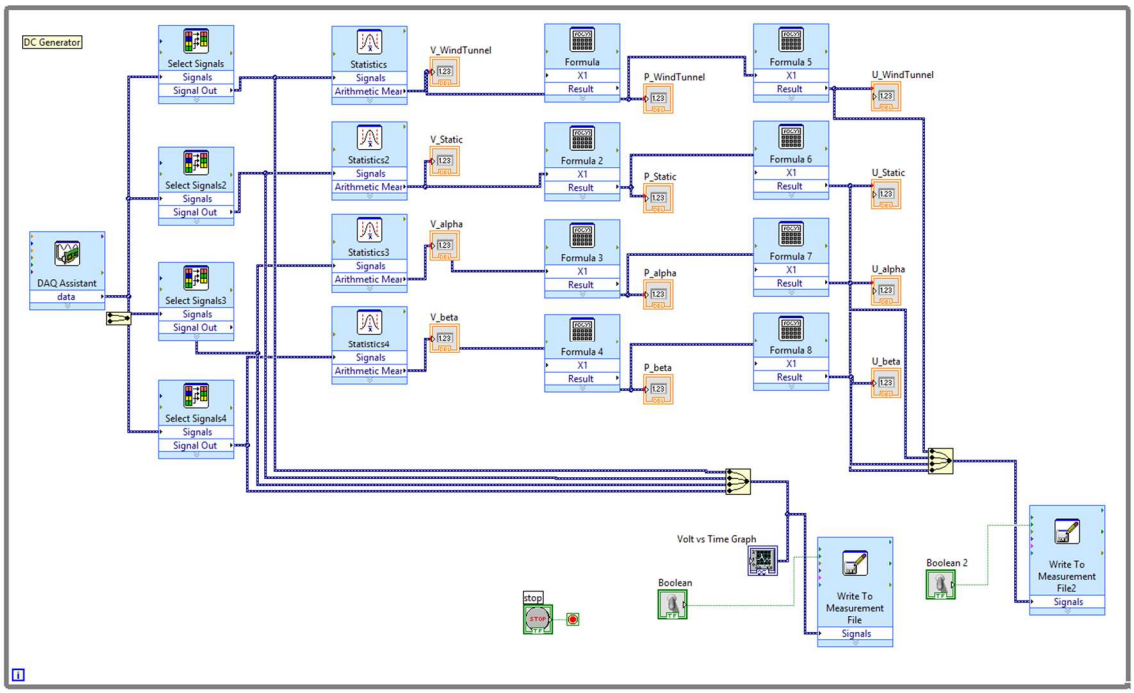

Figure 4-12 : LabVIEW block diagram that processes the voltage and pressure data.

4.5 Time Response

Settling time defined as the time taken for the output response to match the step response within a given error [41]. Step response is measured by the transducer. Settling time is sensitive to internal diameter of the tubing due to a d^2 term in the damping factor. Uncertainty in the internal geometry of the probe and tubes is a factor in accurately predicting settling times.

To determine the time response, the probe is subjected to a step input where the probe is first inserted to a flow at a 0-degree inclination at a determined flow velocity, then it is suddenly stepped to an angle offset. At this angle input the probe's response is observed until it reaches steady state. This will determine the time it takes to respond to input in a flow and will validate or invalidate the time increments used in calibration and flight testing maneuvers. The time response determined that satisfied both probe sizes was 2 seconds per increment was sufficient.

4.6 Flight Testing

The probe was installed on an Albatross fixed-wing unmanned aircraft by Applied Aeronautics. A boom to mount the probes was attached to the bottom-starboard side of the Albatross and positioned approximately 1 foot ahead of the nose for clean freestream flow. The distance from the tip of the probe to the pressure transducers on the board is 28 inches (71.12 cm). Figure 4-13 shows a planform of the Albatross and mounting location of the probe.

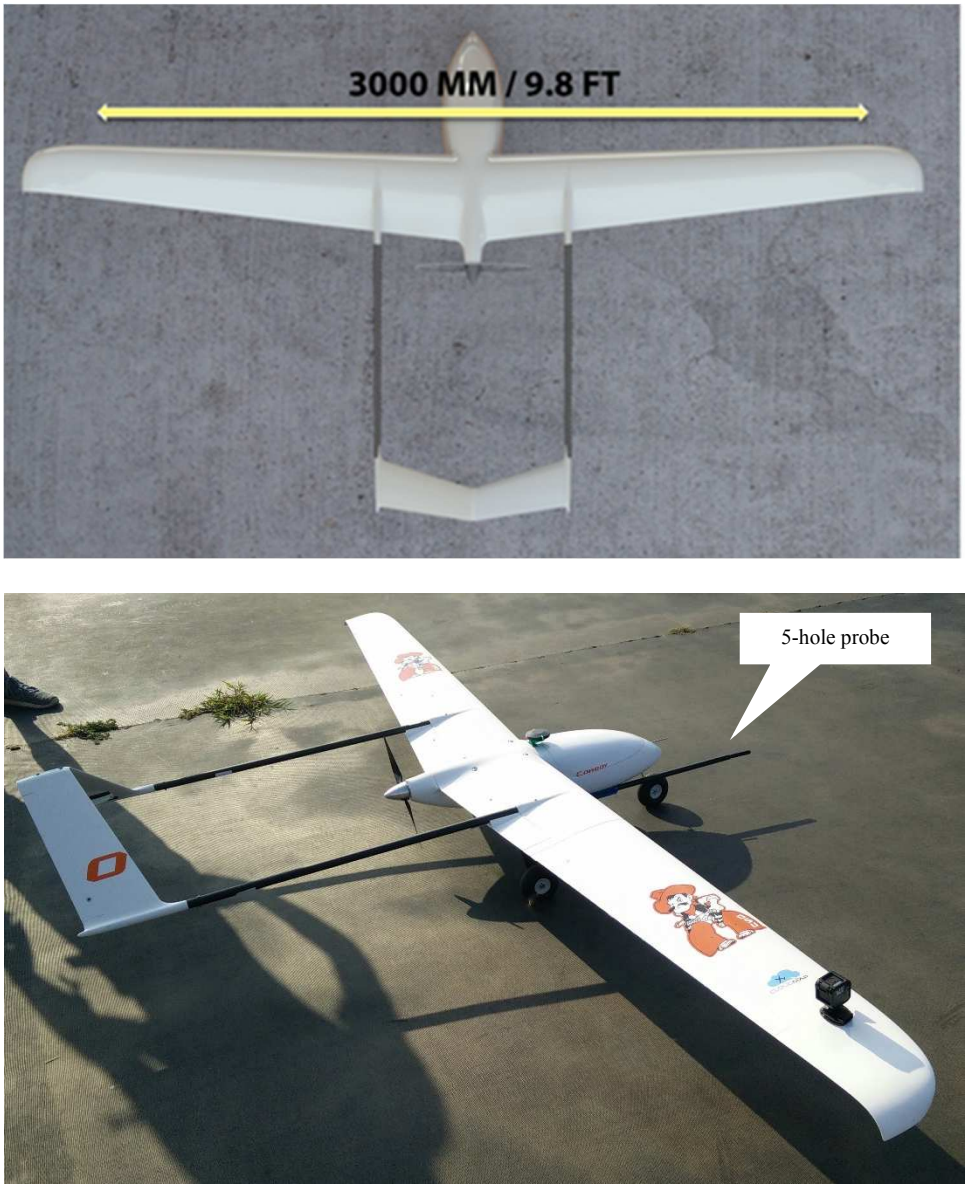

Figure 4-13 : Albatross planform view with dimensions (top); probe mounted preflight on Albatross bottom-starboard side (bottom)

As can be seen from the above figure, the 5HP is mounted on a boom mounted to the Albatross. A hole was drilled into the side for connecting the probe to the payload bay with a custom 3D printed mounting hardware made for the probe and other sensors. 24 inches (60.96 cm) of Tygon tubing is used on the probe to connect to the board. This amount of length has loosely been determined to be of good length for response time, but is not yet confirmed from flight testing.

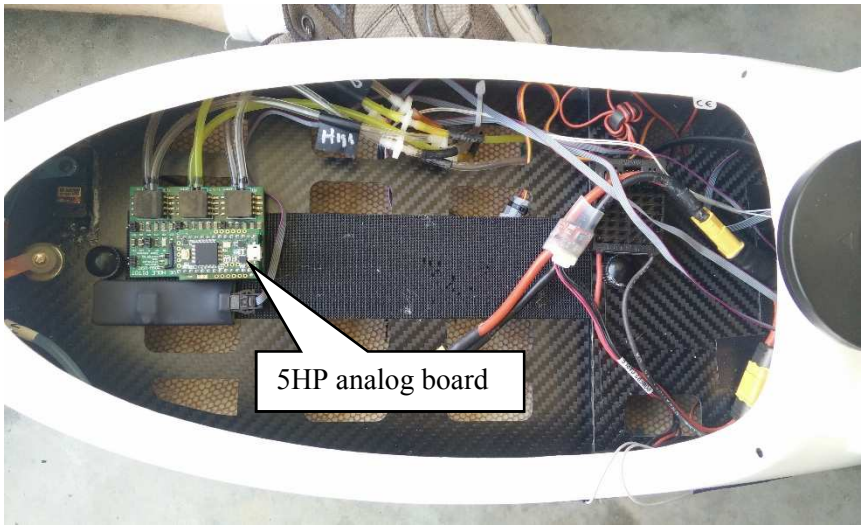

Figure 4-14 : 5HP implemented into the Albatross preflight

4.6.1 Sensors and System Layout

The custom analog board designed and built for flight testing uses a Teensy 3.2 by PJRC for data acquisition and processing. Teensy 3.2 is a 32-bit ARM processor, 72 MHz speeds with 3.3V signal. It takes 5V to power and is low-cost. It is stacked with an SD card adapter that takes micro SD cards to write and store data. Teensy uses an Arduino-based code which makes it easy to start working with an Arduino background. However, since the Teensy 3.2 only has 2 I2C ports using more than 2 sensors requiring I2C communication would require a work around needing multiple sensor addresses and limits the amount of sensors. The goal is to eventually use A/D sensors and adding other sensors with an IMU /dual-GPS (VN-300) for attitude awareness needed for finding the pitch and yaw angles. A barometer is to be added with temperature and humidity sensors. This will require a step up from a Teensy 3.2 eventually. As a proof of concept, several board iterations

have been made using NPX Freescale MPXV7002 surface mount differential pressure transducers. These were tested in flight at CLOUD-MAP during the summer 2017 campaign. The Freescale pressure sensors have a ±2 kPa pressure range, supply voltage of 5 Vdc, and an operating range of 10 to 60°C. Figure 4-15 shows the board schematic and circuit diagram.

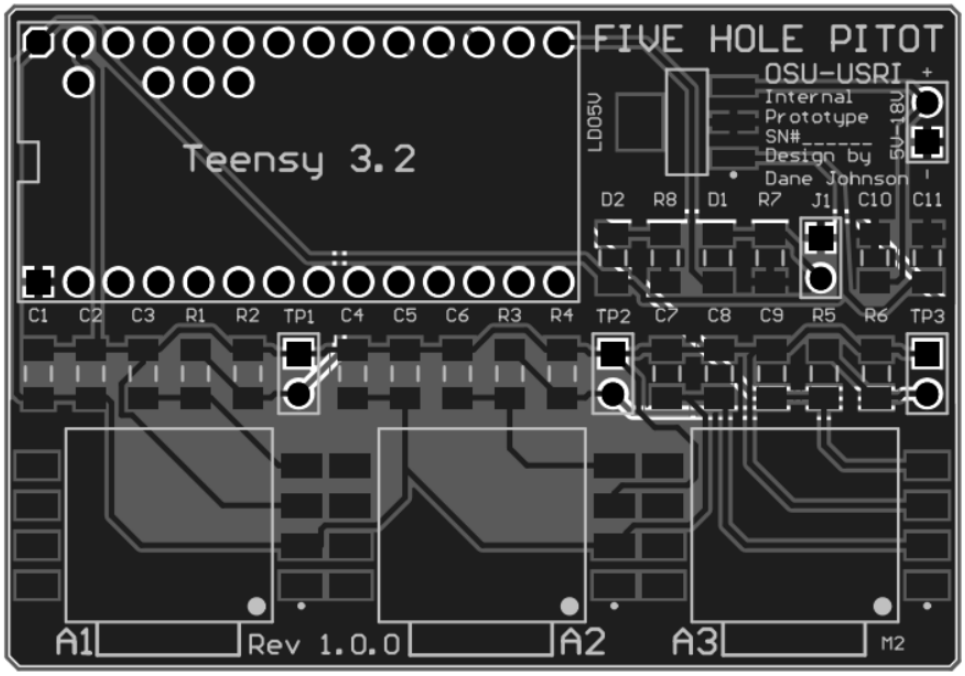

Figure 4-15 : Analog board layout showing component placements.

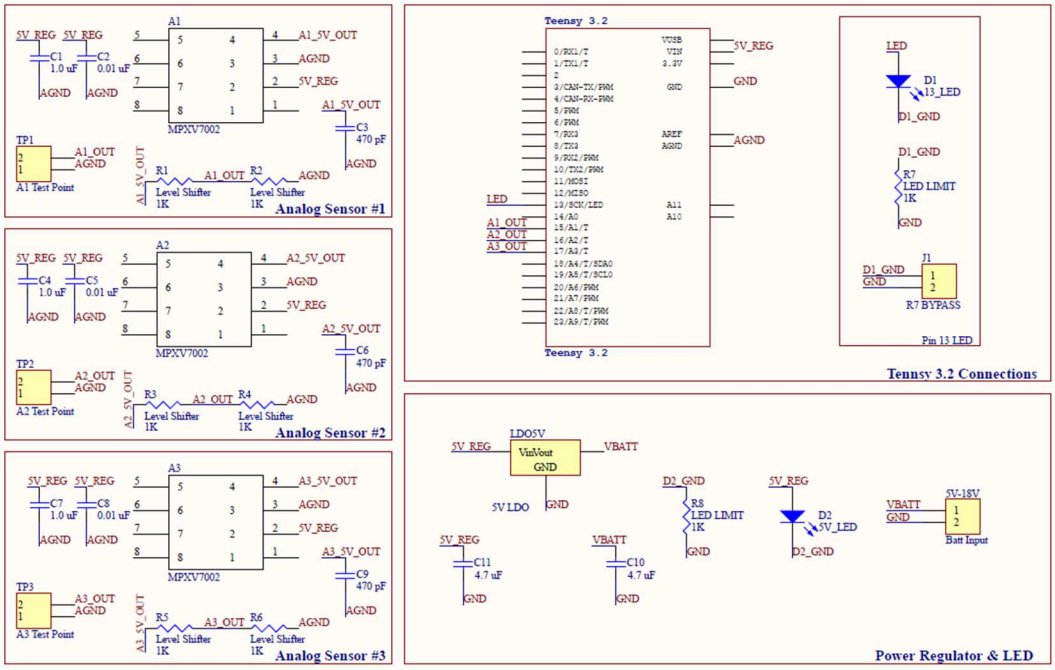

Figure 4-16 : Circuit schematic of the analog board.

Figure 4-17 shows board iterations for the analog concept 5HP boards. The far-right is the most current and will be the last analog board made before going to the digital custom board.

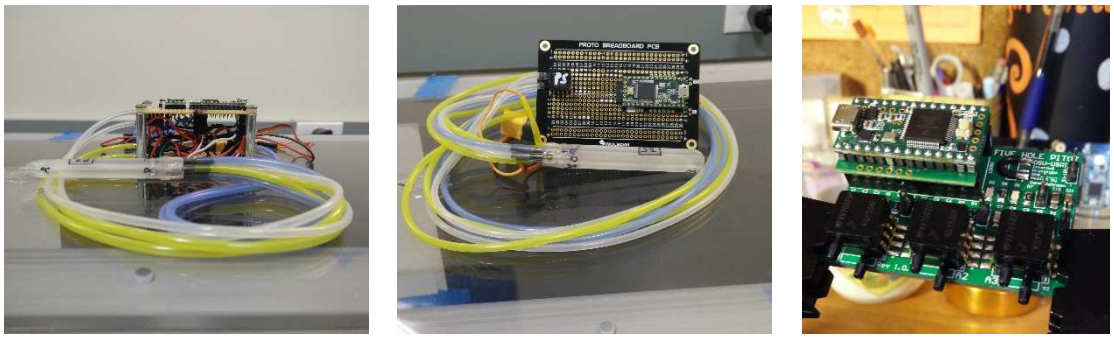

Figure 4-17 : Board iterations for the analog proof-of-concept. Last analog board iteration (far right).

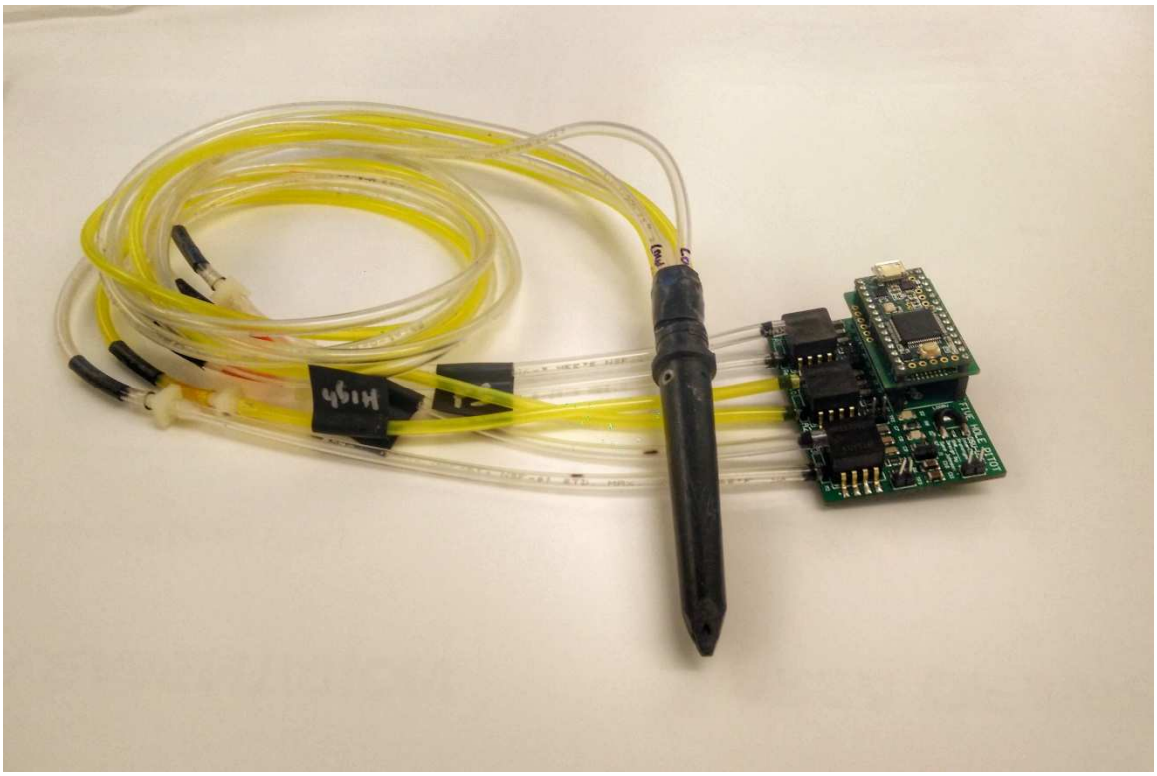

Figure 4-18 : Full flight test system (analog board and pyramid probe).

4.7 Uncertainty Analysis

An error analysis was performed to determine the uncertainty of the 5HP. Error is the difference between the true and observed value of a quantity. Since the true value is unknown, estimates of the error must be made. Uncertainty is determined as a possible value of that error, known as the experimental error. In this experimental setup the uncertainty of the pressure coefficient and velocity magnitude for the 5HP calibration scheme were examined. Uncertainty is made up of two components, bias error and precision error. Kline and McClintock methods for uncertainty analysis provide a reasonable estimate of uncertainty and is a standard for experimental analysis [42]. It has been shown that uncertainty in a calculated result can be determined with reasonable accuracy using the root-sum square method (RSS).

The standard deviation was determined to represent a calculated precision (random) error over four main steps:

1. the sample mean over the 3 runs
2. sample variance
3. variance of sample mean
4. standard deviation

The final equation for determining the standard deviation with the steps above combined is as follows,

$$S_x = \sqrt{\frac{1}{N}\sum_{i=1}^{N}(x_i - \bar{x})^2} \tag{15}$$

Precision error represents a statistical Gaussian distribution making the calculated standard deviation a reasonable fit over the experimental values. In determining the bias in the overall experiment, the RSS of the sources of error are found with the equation below.

$$Bx_i = [(B_{cal})^2 + (B_{acq})^2 + (B_{red})^2]^{1/2} \tag{16}$$

Where B_{cal} is bias error in calibration, B_{acq} is bias errors in data acquisition, and B_{red} is bias in data reduction. The main sources of bias error in this setup comes from the pressure transducers (OMEGA) accuracy. Other instruments, such as, the Venier barometer used to take ambient lab conditions are examined; however, the bias error percentage was found to be so small its affects were deemed negligible. Another source was the error due to probe angle alignment. Since a high precision Arcus stepper motor with an integrated encoder correcting for position was used, the accuracy level and precision made this value insignificant in the overall calculation of bias error as well. This was confirmed visually as well as checked within the encoder readings. The only other source of alignment error comes from the mounting procedure from the initial probe mounting, but this is difficult to determine and since each run for a single axis on a probe was done without removing the probe (for three tests each), it was ignored. With the transducer error being large enough to overcompensate the other bias terms, the overall bias error was found using the RSS for

its full-scale accuracy. The final determination for the overall uncertainty, U_x, is then the RSS of the precision and bias errors.

$$U_x = [B_x^2 + S_x^2]^{1/2} \tag{17}$$

The main sources of error considered in calibration were from flow velocity magnitude and pressure coefficients as resultant errors. The random transducer error, bias transducer error, probe angle, and residual error in curve fitting. All of these, with the exception of the bias error, were accounted for in the quality of the curve fit calculation. These are shown in the chapter for results with error bars and for both velocity magnitude and pressure coefficient curves. Uncertainty tables are shown in the Appendix.

CHAPTER V

5. RESULTS

The results presented in this section are derived from the methodology and experimental setup previously discussed. The results are presented in correlation to their relevance to the objectives and goals of this research. Since the main focus was on calibration procedures to low-cost probes and their performance the following chapter will firstly discuss those results. Then followed by the results from supplemental tests and a discussion on flight testing.

5.1 5HP Calibration Results

Calibration results for the large hemisphere probe are presented below with error bars for both pressure coefficient and velocity magnitude curves. These errors are derived from the standard deviation as part of the uncertainty analysis of the data sets for multiple runs. The standard deviation and sample mean variability parameter give reasonable descriptions and illustrates the experimental repeatability for each test.

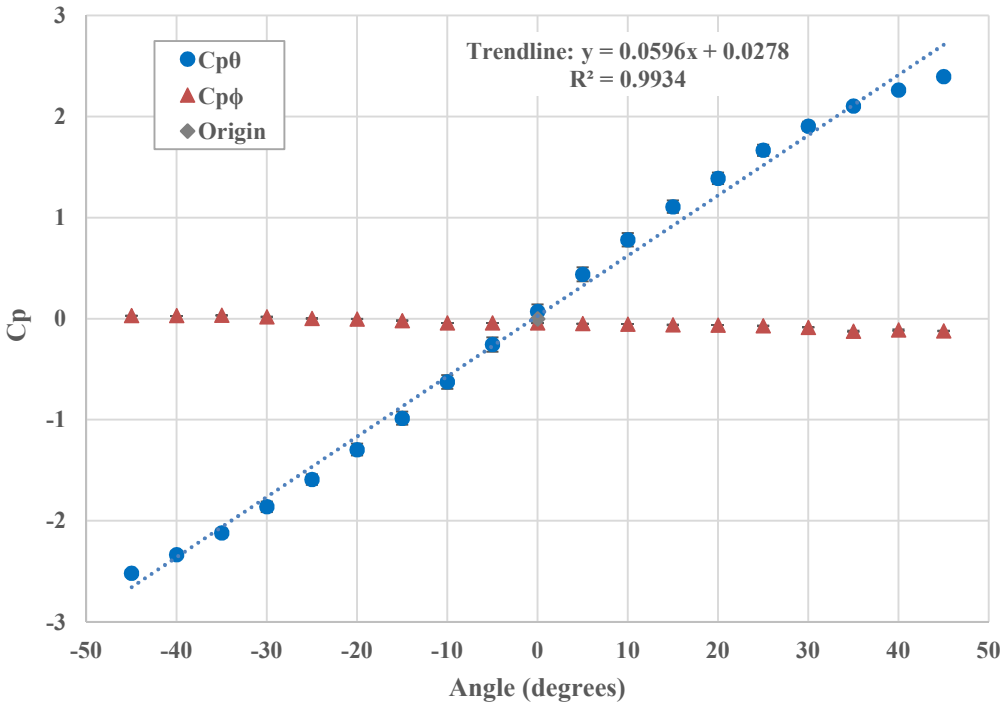

Figure 5-1 : Cp_θ versus angle calibration curve for large hemisphere probe shows a linear range in ±20° at $8.4x10^3$ Reynolds number (10 m/s).

Figure 5-1 has a clear linear range at approximately -20 to + 20 degrees as typical for most probes of this geometry and size. The highest angular sensitivity falls within this linear range. Measurements were taken for this figure at 10 m/s with a Reynolds number at $8.4x10^3$ along the pitching axis designated for the probe. The curve for the yaw axis falls nearly completely on the horizontal axis along the origin. Since the yaw axis is spanned for pressure it should be nulled having a zero/near zero sensitivity to angular displacement. The linear relationship is given as the trendline shown in the above figure, and the R^2 value at 0.99 (almost 1) indicates there is a good overall data fit. Since the probe is symmetric the *Cp* curve should run through the origin, which in this case it does. Some graphs off origin axis indicate the likeliness that the probe could have been mounted improperly misaligning one or more axes. The standard deviation of the sample mean shows small variance in the data. This can further be extrapolated by Figure 5-2 below with all three runs plotted for the same test axis.

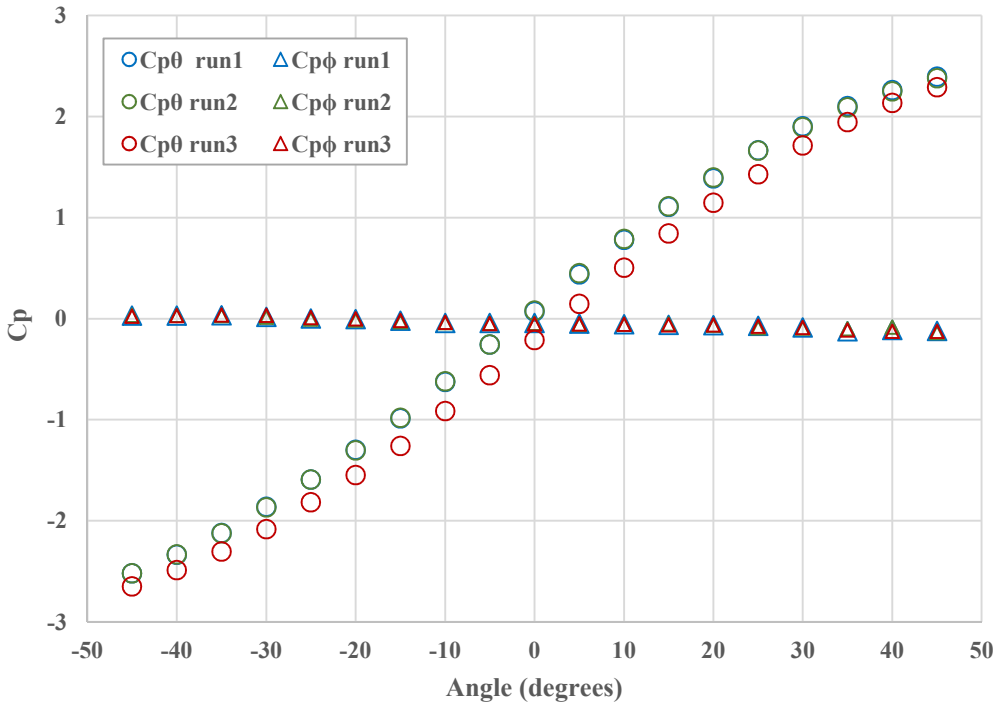

Figure 5-2 : Cp_0 calibration curve for large hemisphere probe at $8.4x10^3$ Reynolds number (10 m/s) for all three runs.

Figure 5-2 shows the variance for the three runs spanning the pitch axis. Due to these factors, the curves indicate good repeatability in the measurements.

The following magnitude velocity curve for the large hemisphere probe shows symmetry throughout the traverse from -45 to + 45 degrees. Error bars are provided on Figure 5-3 while Figure 5-4 depicts little variance from three runs at 10 m/s velocity regime. The wind tunnel Pitot-static probe shows a consistent flow velocity during each test.

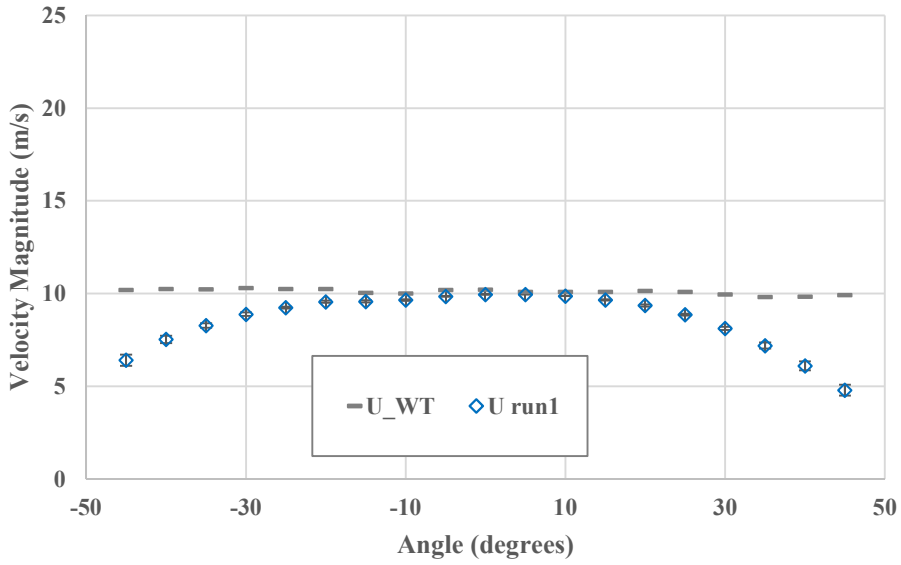

Figure 5-3 : Large hemisphere probe: magnitude velocity versus angle for pitch from ±45° at 8.4x10^3 Reynolds number (10 m/s). This shows a mostly symmetrical curve.

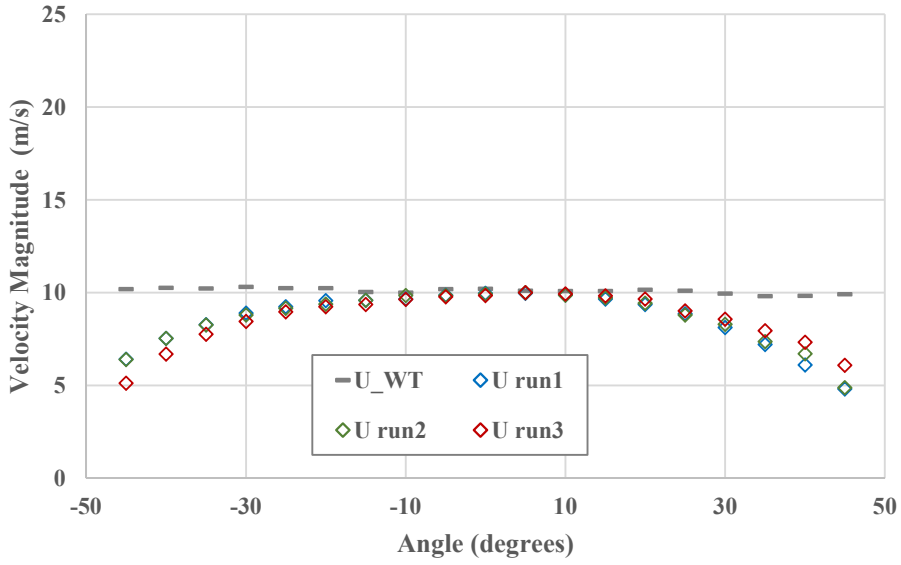

Figure 5-4 : Large hemisphere probe: magnitude velocity pitch curve with three runs at 10 m/s. This is a complimentary curve for Figure 5-3.

The next set of calibration curves for *Cp* versus angle and magnitude velocity versus angle are for the same Reynolds number regime and probe as the curves above, however, these represent

the data collected for the yaw axis of the probe. As seen below, Figure 5-5and Figure 5-6, show similar linearity as the calibration curves for the pitching axis. Small standard deviation (error bars are small) on both Cp axes sets are shown. Again, R^2 indicates a good data fit at 0.99 being very near to 1, and each run in Figure 5-6 falls nearly on top of each other with little sample variance.

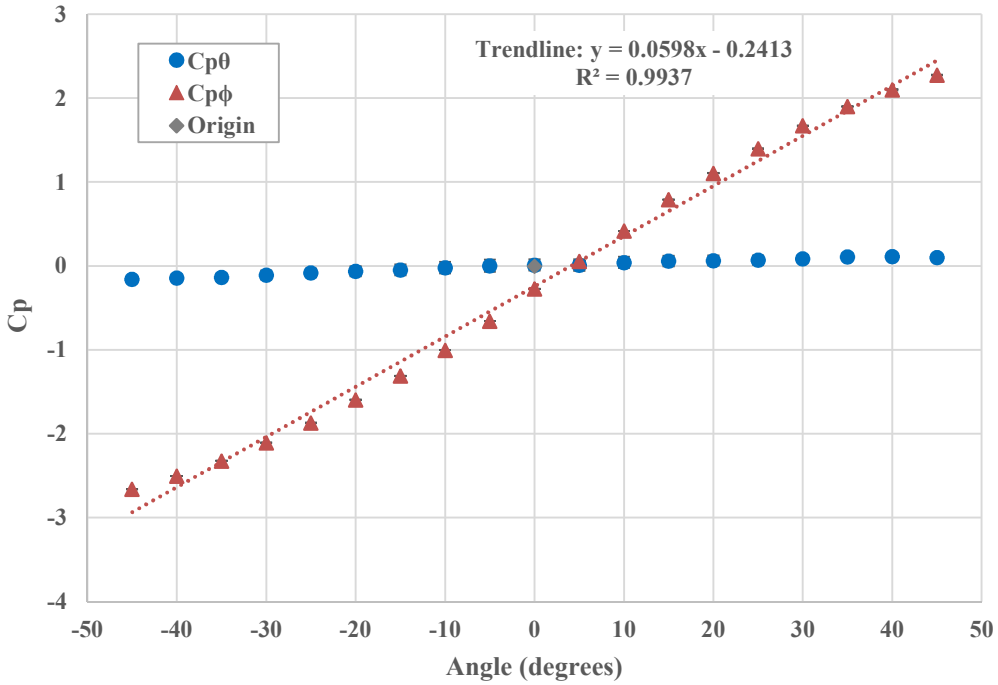

Figure 5-5 : Cpϕ versus angle calibration curve for large hemisphere probe with a linear range in ±20° at 8.4x10^3 Reynolds number (10 m/s).

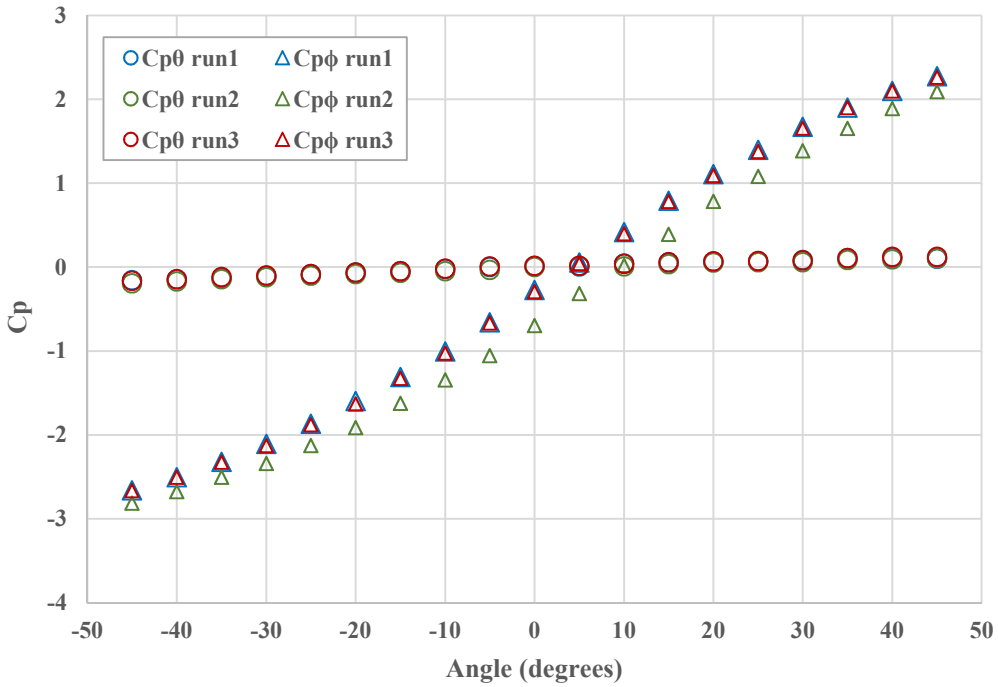

Figure 5-6 : Cpϕ calibration for large hemisphere probe at 8.4x10^3 Reynolds number (10 m/s) for all three runs.

The yaw axis at this velocity regime shows symmetry along the angle traverse, and each test run for this set is nearly identical to the others. Results a similar to the pitch axis tests.

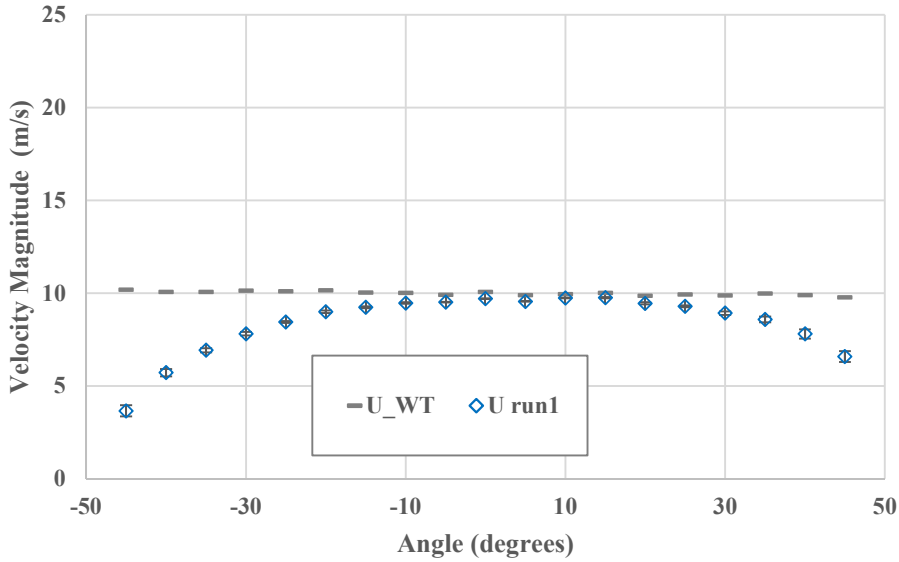

Figure 5-7 : Large hemisphere probe: magnitude velocity versus angle for yaw from ±45° at 8.4x10^3 Reynolds number (10 m/s). This shows a mostly symmetrical curve

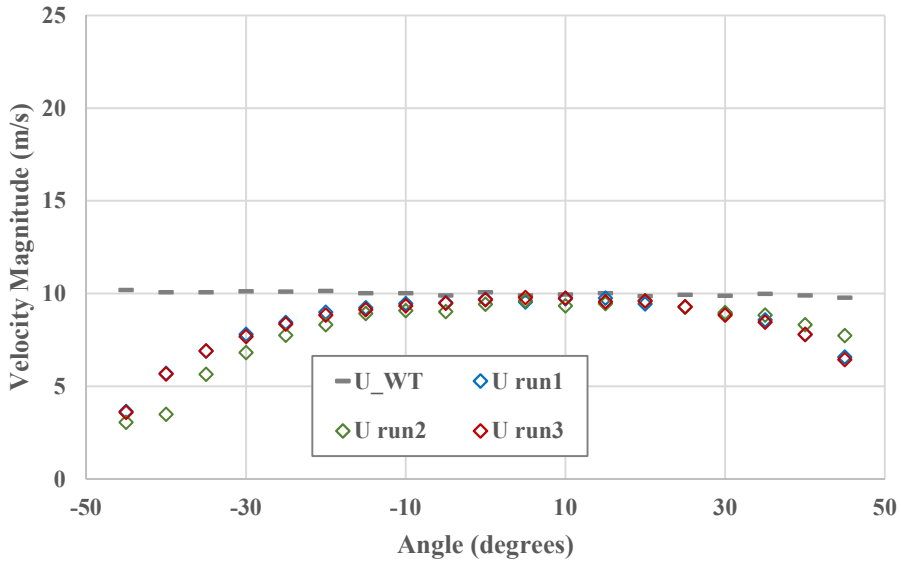

Figure 5-8 : Large hemisphere probe: magnitude velocity yaw curve with three runs at 10 m/s.

The next set of figures show the large hemisphere probe at a Reynolds number of 12.6×10^3 (15 m/s).

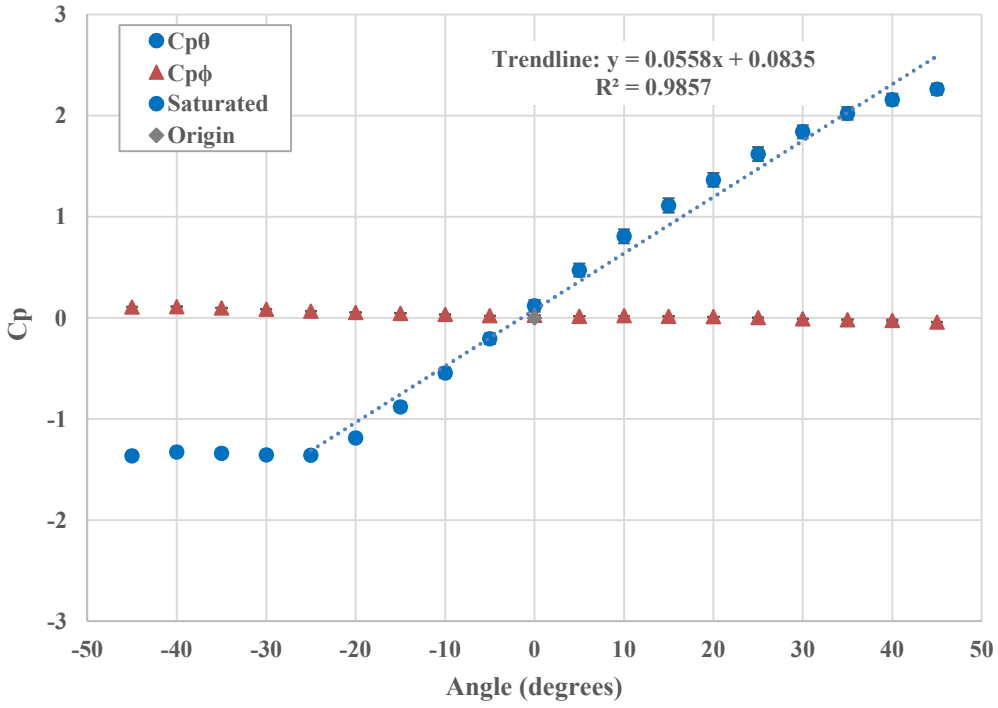

Figure 5-9 : Cpθ versus angle calibration curve for large hemisphere probe shows a linear range in ±20° at 12.6×10^3 Reynolds number (15 m/s). The flat line indicating pressure transducer saturation.

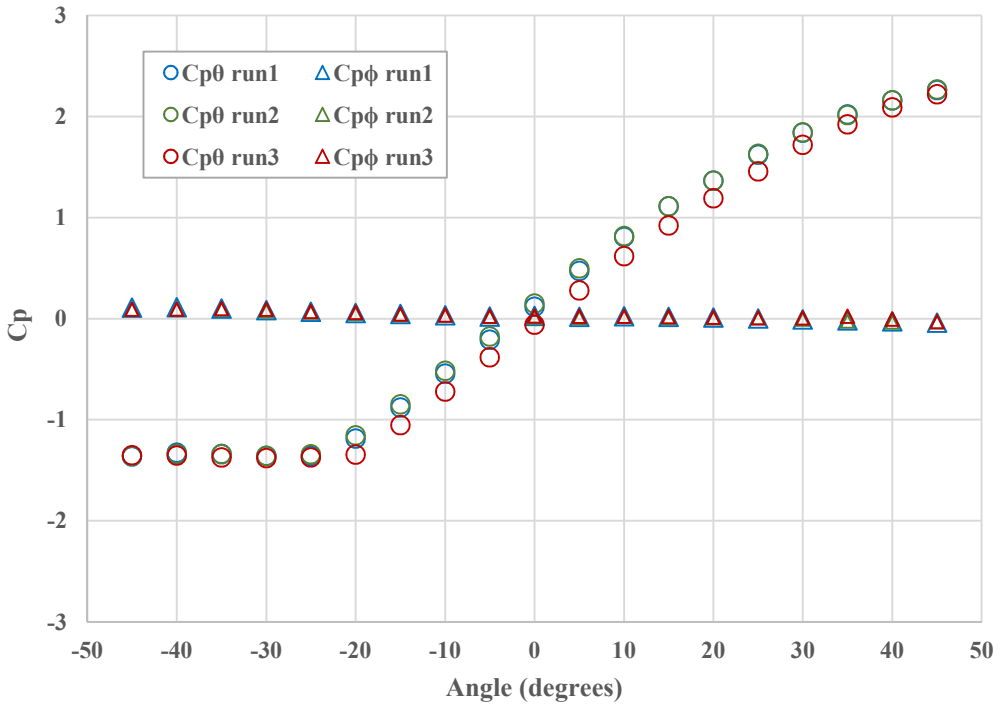

Figure 5-10 : Cpθ versus angle: Large hemisphere on pitch axis with saturation at larger negative angle values.

Each probe at higher velocities saw a pressure transducer saturation on the higher "negative" or low pressure side. The OMEGA PX653 transducers are differential and measure based on high and low pressures it is a clear indicator of saturation on the high negative which is the low pressure side of the diaphragm. This occurred on every run for velocities at 15 and 20 m/s on both test axes. Figure 5-9 shows saturation occurring from -45 to -30 degrees range, taking this into account the trendline and R^2 values were taken from the readable transducer range of -25 to +45 degrees. The linear range for the probe still shows ±20 degrees range and R^2 is still reasonably close to 1 as shown in Figure 5-9. Figure 5-10 illustrates good data repeatability and also reinforces the saturation of the pressure transducers showing each run converging to the flat line at the previously specified range.

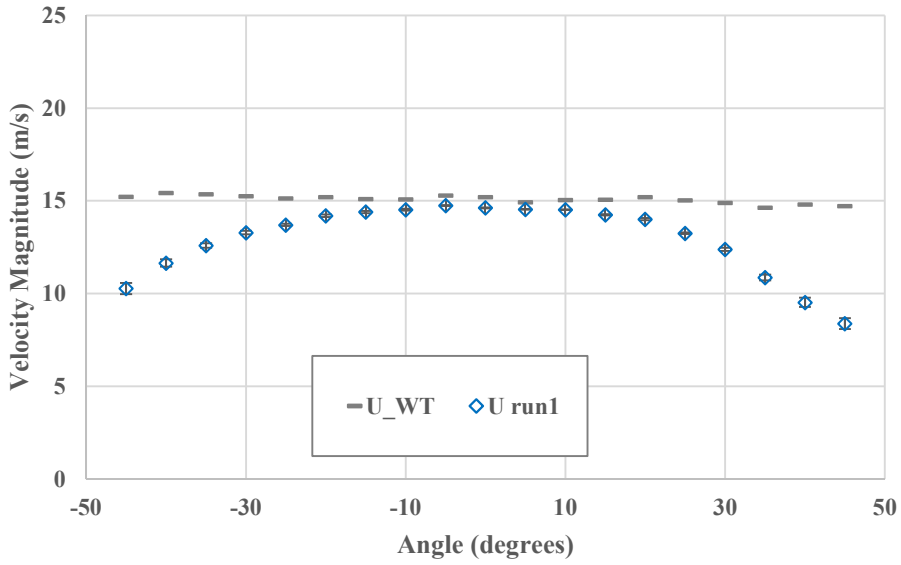

Figure 5-11 : Magnitude velocity calibration curve for large hemisphere pitch axis at 15 m/s.

The magnitude velocity calibration curve in Figure 5-11 shows continued symmetry for the large hemisphere probe as seen in the lower velocity and Reynolds number range.

The large hemisphere probe results indicate probe symmetry and good linear ranges typical of a 5HP at ±20 degrees. Error from the standard deviation of the data sets show small spread in the measured values which also indicates low precision error in experimental uncertainties. This is a good indicator of repeatability as stated before, and the nature of this type of testing requires high precision and accuracy overall for calibration and validation of MHPs. The figures discussed for the large hemisphere probe are representative of the other curves not shown for this probe. For the linear range, relationship, data spread, and overall data fit, these figures represent a consistency throughout each probe geometry as will be discussed in further detail in this section. Saturation issues for the OMEGA transducers occurred for every probe at 15 and 20 m/s indicated by a flat line in the higher negative angle range for pressures.

Below, Figure 5-12, shows the calibration curve of the large pyramid probe with similar linear angle range and data fit trends as the large hemisphere probe. There appears to be some sensor saturation on this curve between -25 and -40 degree angular range. Symmetry is offset from

the origin approximately -0.5 for the pressure coefficient that is spanned. Most notably, the probe curves are off the origin and the *Cpθ* for pitch shows differential pressure fluctuations throughout the traverse for the yaw axis. This same anomaly is prevalent in every *Cp* calibration curve (each Reynolds' number regime) for this probe specifically for *Cpθ*.

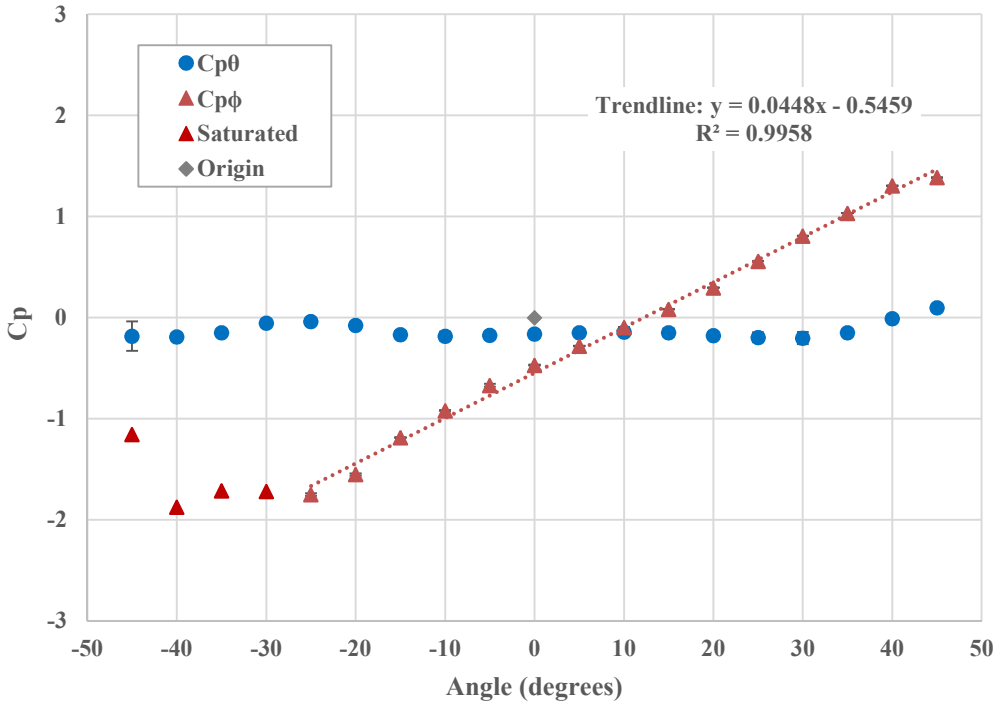

Figure 5-12 : Cpϕ versus angle calibration curve for large pyramid probe shows a linear range in ±20° at 8.4x10^3 Reynolds number (10 m/s). Off origin placement can be seen with sensor saturation occurring from -25° to -45°.

As shown in Figure 5-13, *Cpθ* as spanned through the angle range still has the same trend as in Figure 5-12. This likely indicates a geometry (internal or external) inconsistency on the probe. Inspection of the tip geometry for the large pyramid probe was conducted and two noticeable raised ridges were observed on the chamfered side for port 4 which is located on the pitch port axis. Figure 5-14 shows the probe tip with the raised ridge inconsistencies. The ridges appear to be a 3D printing irregularity and do not occur on other pyramid probe tips.

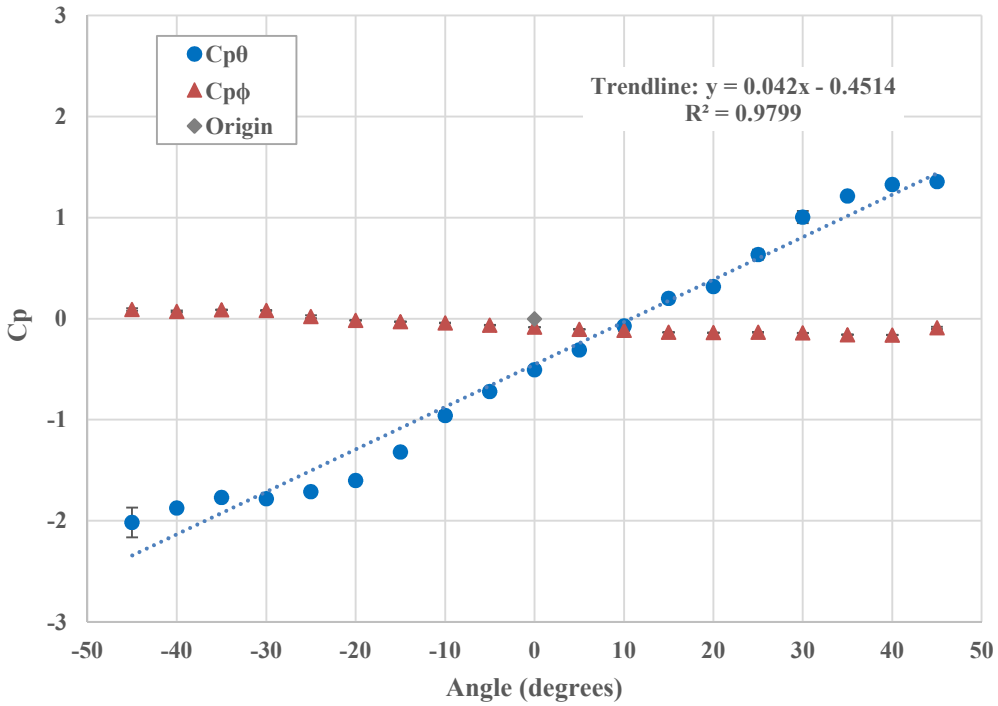

Figure 5-13 : Cpθ versus angle calibration curve for large pyramid probe axis pitch-yaw performance comparison to Figure 5-12 . Cpθ (pitch coefficient) fluctuates and has more data scatter than Cpϕ.

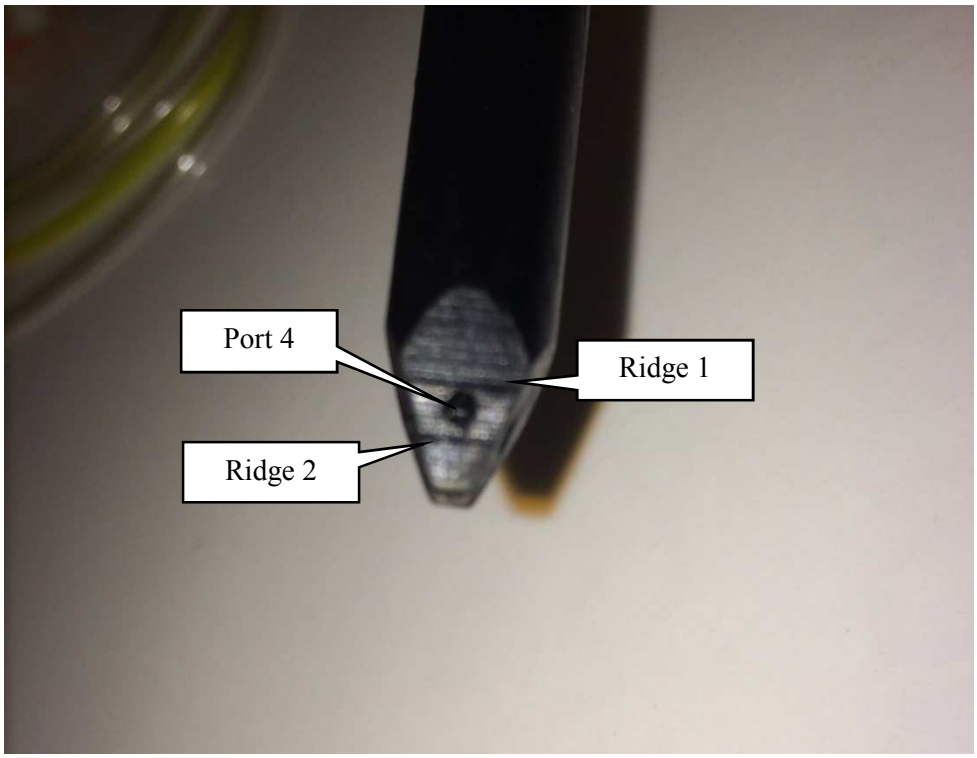

Figure 5-14 : Large pyramid with 3D print anomaly (2 raised ridges) on chamfered port 4.

The velocity magnitude in Figure 5-15 shows lack of symmetry with similar trends in the both pitch and yaw at every Reynolds number and velocity. The lack of symmetry is likely linked to the tip geometry anomaly from a misprint on the Formlabs printer.

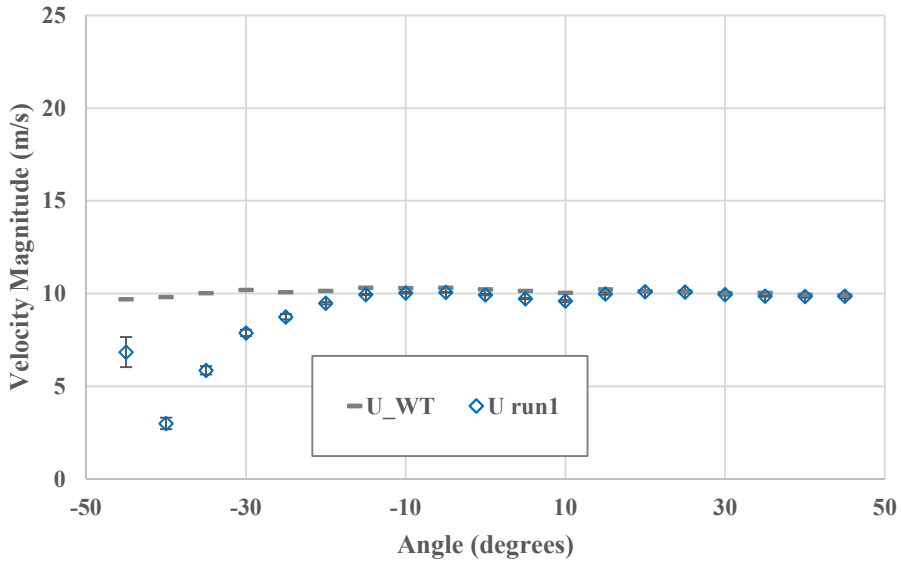

Figure 5-15 : Large pyramid probe magnitude velocity versus angle for yaw axis from ±45° at 8.4x10^3 Reynolds number (10 m/s). Clear asymmetry in the calibration curve.

The following figures, Figure 5-16 and Figure 5-17, are representations of a *Cp* curve that has been misaligned on both the rotational and the non-traverse axes. The lack of origin symmetry and the non-traversing *Cp* axis are shifted as well as picking up differential pressures adding slope to the respective curve. This is seen as a propagation error in the mounting procedure. The probe will always be mounted correctly assuming the boom and notched mount are correctly positioned.

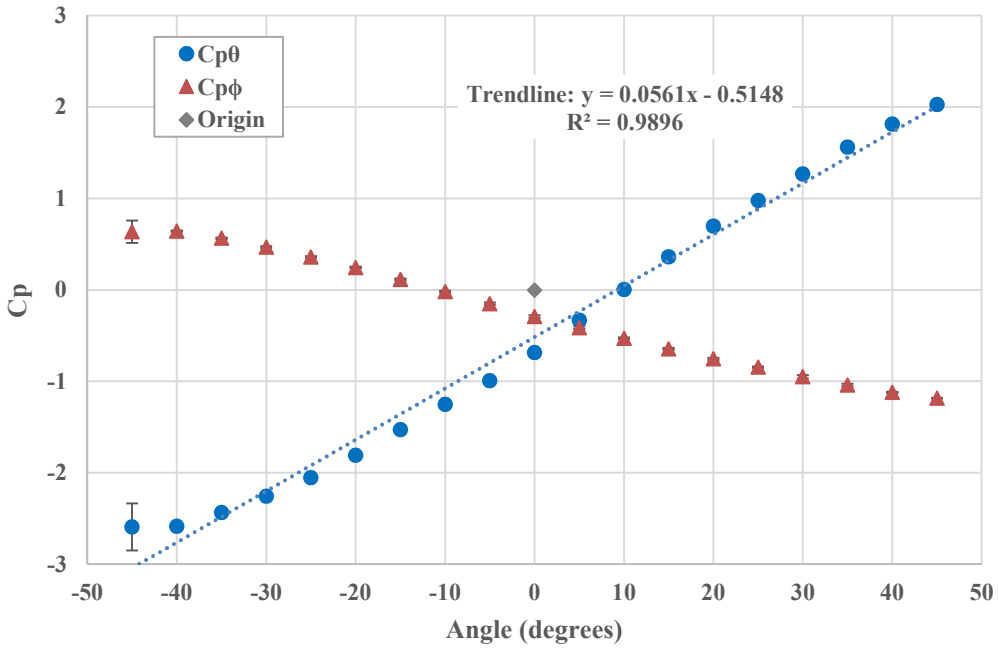

Figure 5-16 :Cpθ versus angle calibration curve for small hemisphere probe traversing pitch with a linear range in ±20° at $4.4x10^3$ Reynolds number (10 m/s). There is an offset from the origin and the non-traversing curve has a negative slope.

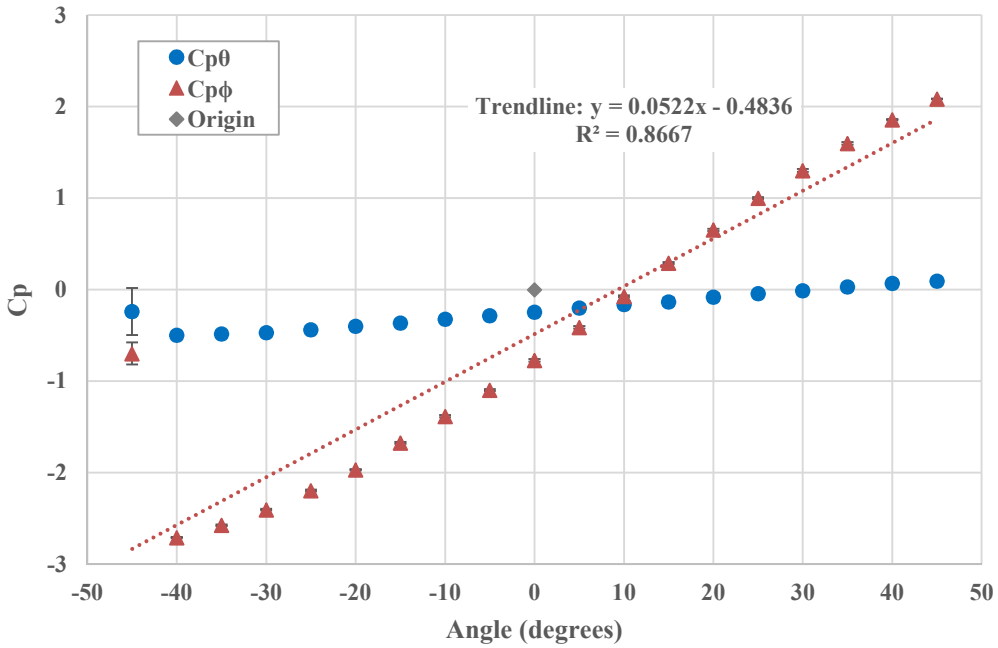

Figure 5-17 : Cpϕ versus angle calibration curve for small hemisphere probe traversing yaw with a linear range in ±20° at $4.4x10^3$ Reynolds number (10 m/s). There is an offset from the origin and the non-traversing curve (Cpθ) has a positive slope.

Velocity curve for both probe axis traverses have the same trend as Figure 5-18 does below. Similar shifted symmetries are shown for each probe with between 5 to 10 degree shifts to the right of the horizontal axis. This is another indicator of probe misalignment.

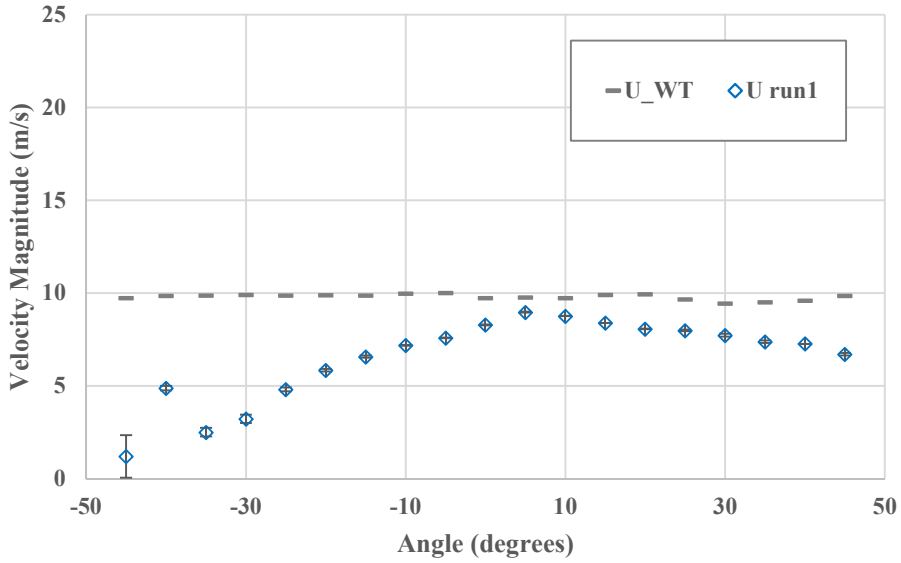

Figure 5-18 : Small hemisphere probe magnitude velocity versus angle for pitch axis from ±45° at 4.4x10^3 Reynolds number (10 m/s). Approximately a 5° shift to the right for the velocity curve.

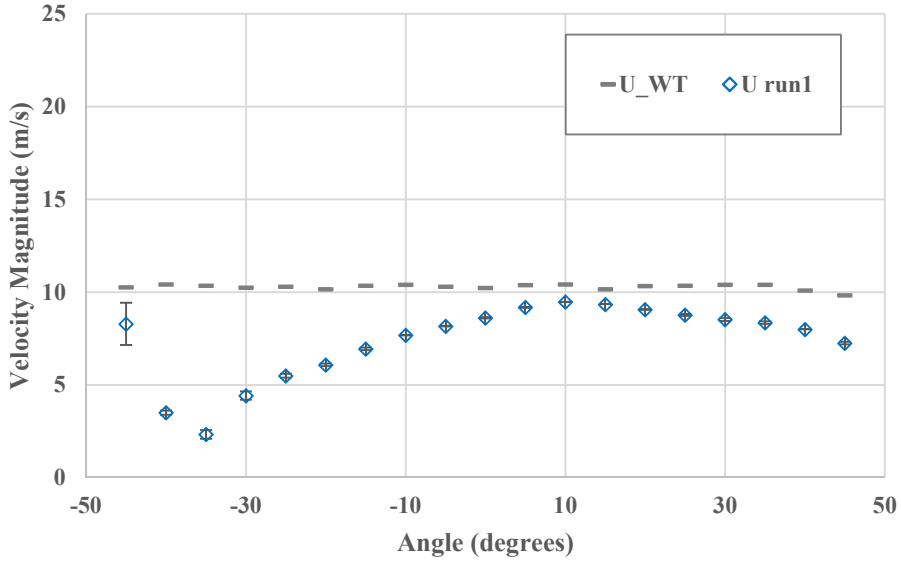

Figure 5-19 : Small hemisphere probe magnitude velocity versus angle for yaw axis from ±45° at 4.4x10^3 Reynolds number (10 m/s). Approximately a 10° shift to the right for the velocity curve.

Similar results as discussed above are prevalent throughout the rest of the data on this probe as misalignment affected both traverse axes on each test set. Further discussion and representation of other calibration figures will go into the Conclusion and Appendix, respectively.

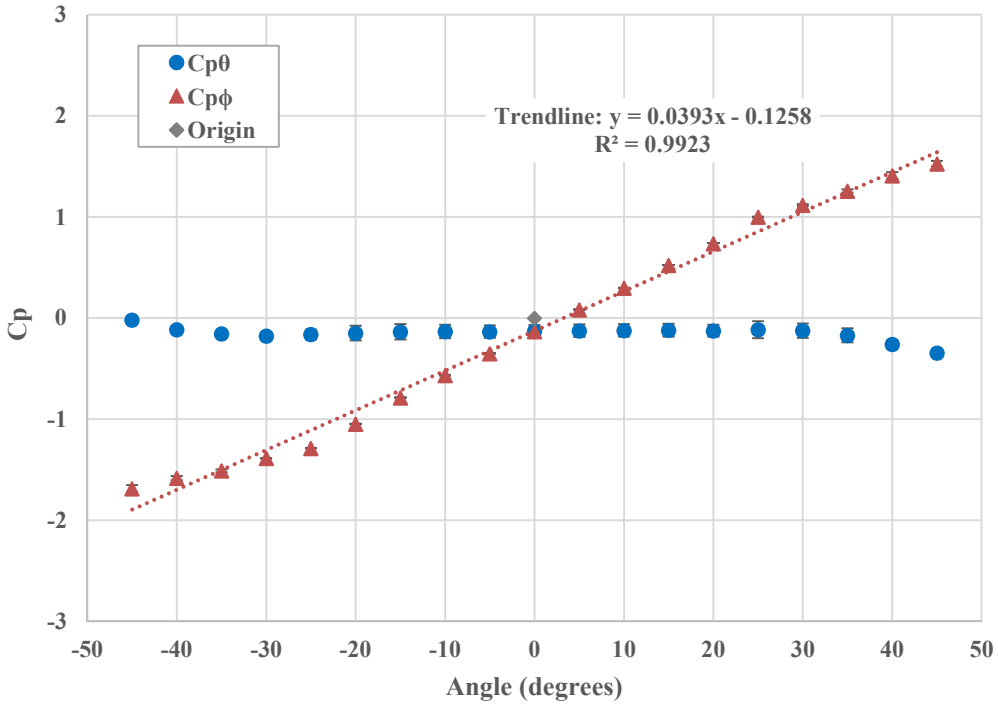

Figure 5-20 : Small pyramid probe Cp for yaw at Reynolds number $4.4x10^3$ (10 m/s).

The small pyramid probe shows symmetry at each Reynolds number regime with origin symmetry as well as curve symmetry. Saturation creeps in at the two larger Reynolds number regimes. The slope of each line decreases as the velocities increase. R^2 values for each of the three figures show good data fit. The curves for the pitch axis shows similar trends and can be found in the Appendix.

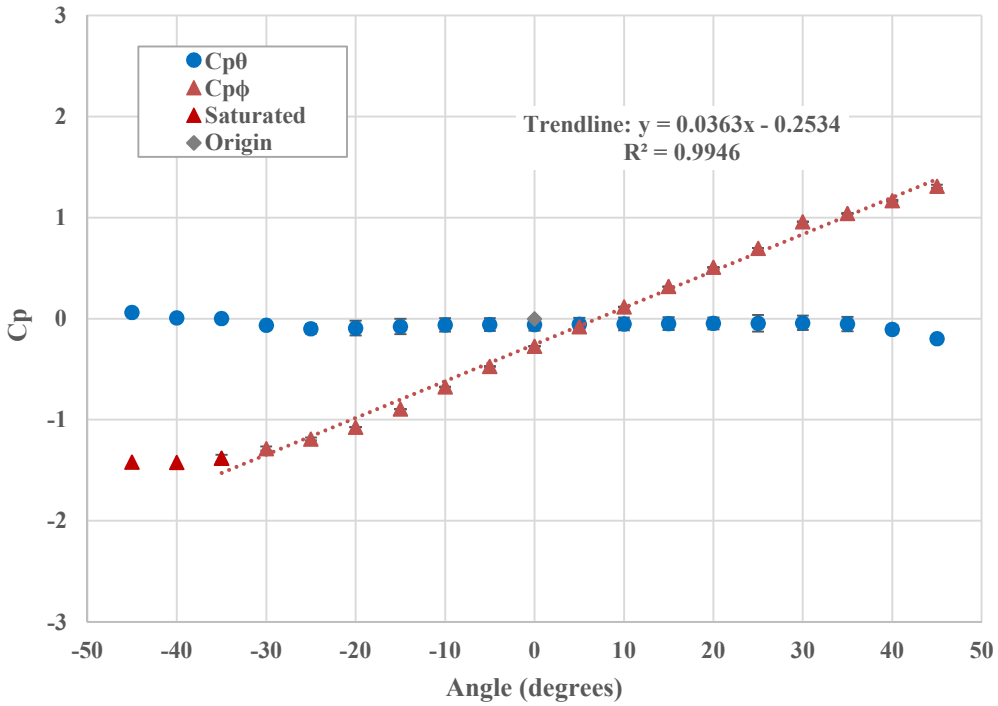

Figure 5-21 : Small pyramid probe Cp for yaw at Reynolds number $6.6x10^3$ (15 m/s).

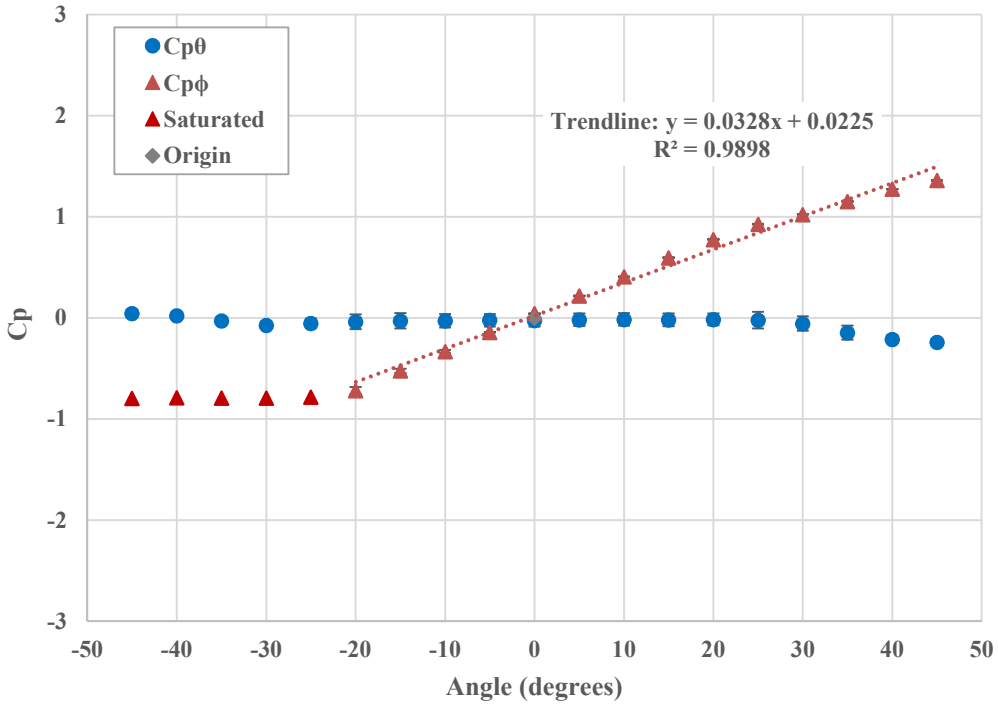

Figure 5-22 : Small pyramid probe Cp for yaw at Reynolds number $8.7x10^3$ (20 m/s).

All velocity magnitude curves show reasonable symmetry and little offset in angle. As shown in the figures below, as velocity increases in the wind tunnel environment, the 5HP velocity measurements became further from the wind tunnel measurement. Comparisons between the 10 m/s wind tunnel velocity to the 20 m/s velocity shows: the 10 m/s test determined the 5HP could pick up approximately 8 to 9 m/s; while the 5HP's maximum magnitude velocity was found to be approximately 17 m/s rather than 20 m/s.

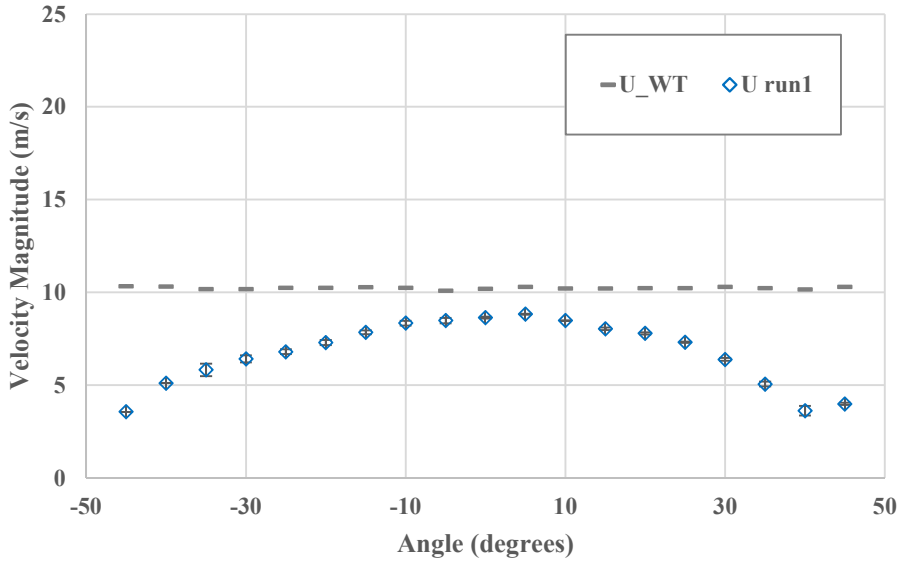

Figure 5-23 : Small pyramid probe Cp for yaw at Reynolds number $4.4x10^3$ (10 m/s).

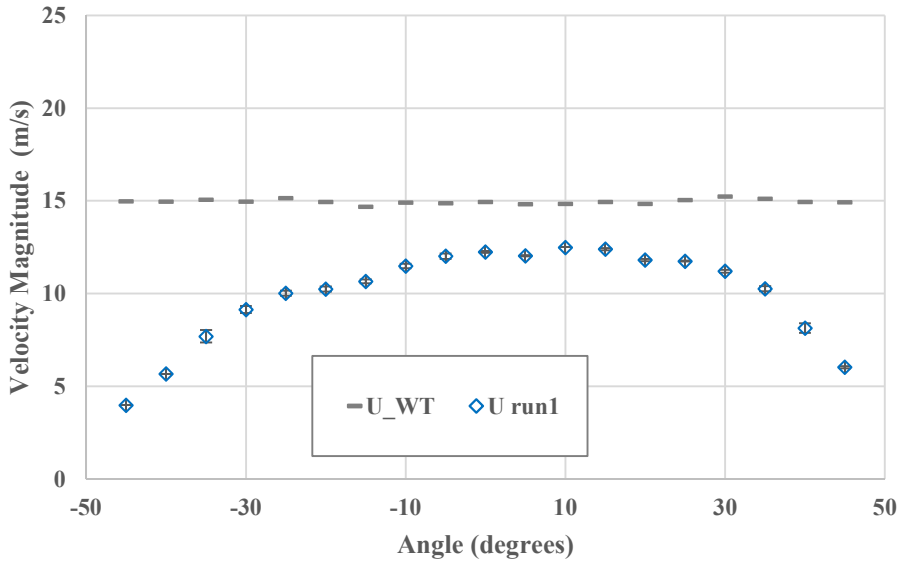

Figure 5-24 : Small pyramid probe Cp for yaw at Reynolds number $6.6x10^3$ (15 m/s).

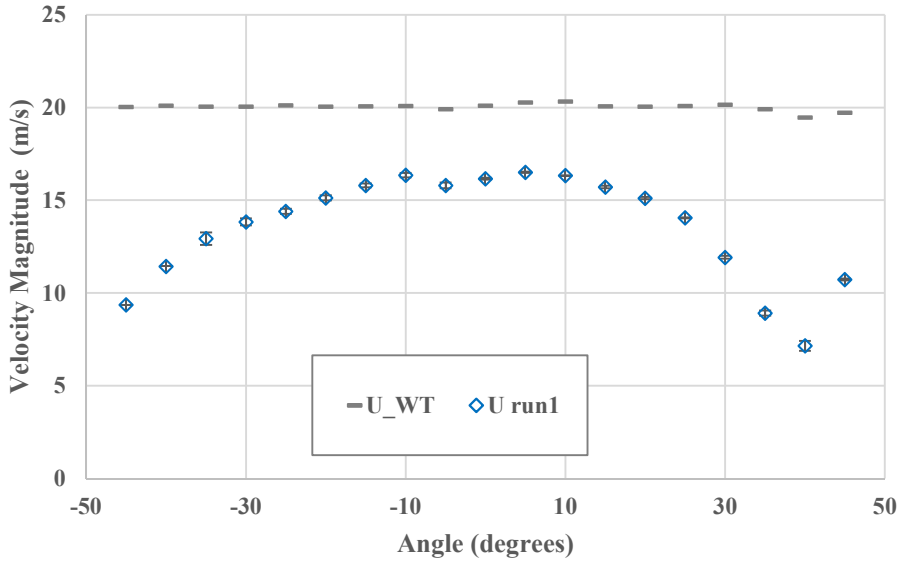

Figure 5-25 : Small pyramid probe Cp for yaw at Reynolds number $8.7x10^3$ (20 m/s).

CHAPTER VI

6. CONCLUSIONS

6.1 Summary

Four 5HPs were manufactured by 3D printing and calibrating in the Oklahoma State University Low-Turbulence Wind Tunnel. The probes were carefully mounted and swept through a ±45-degree range. The calibration data is in good agreement with repeatability as there is little variance between data sets and precision error was relatively low. Each probe was calibrated three times for each axis in the wind tunnel to verify repeatability of the data sets. Averaging of data sets help reduce scatter, as was shown by Treaster and Yocum in the development of the non-nulling method and data reduction scheme [10]. Three Reynolds regimes were tested for a low, medium, and high flight velocity regime various UAS would likely see in flight. It was observed that each test at the higher Reynolds and velocities saw a flat line in the "negative" region of the test traverse. This is an indication of sensor saturation and illustrates a need to reconsider pressure transducers for wind tunnel testing.

The large hemisphere probe showed the most consistency with symmetry about the origin and general curves. The large hemisphere had the highest sensitivity in all tests and displayed the best performance characteristics followed closely by the small hemisphere probe. The sensitivity is easily presented with the slope gradients of each calibration curve. The steepest slope, and therefore, most sensitive to flow is the large hemisphere as presented in the following figure.

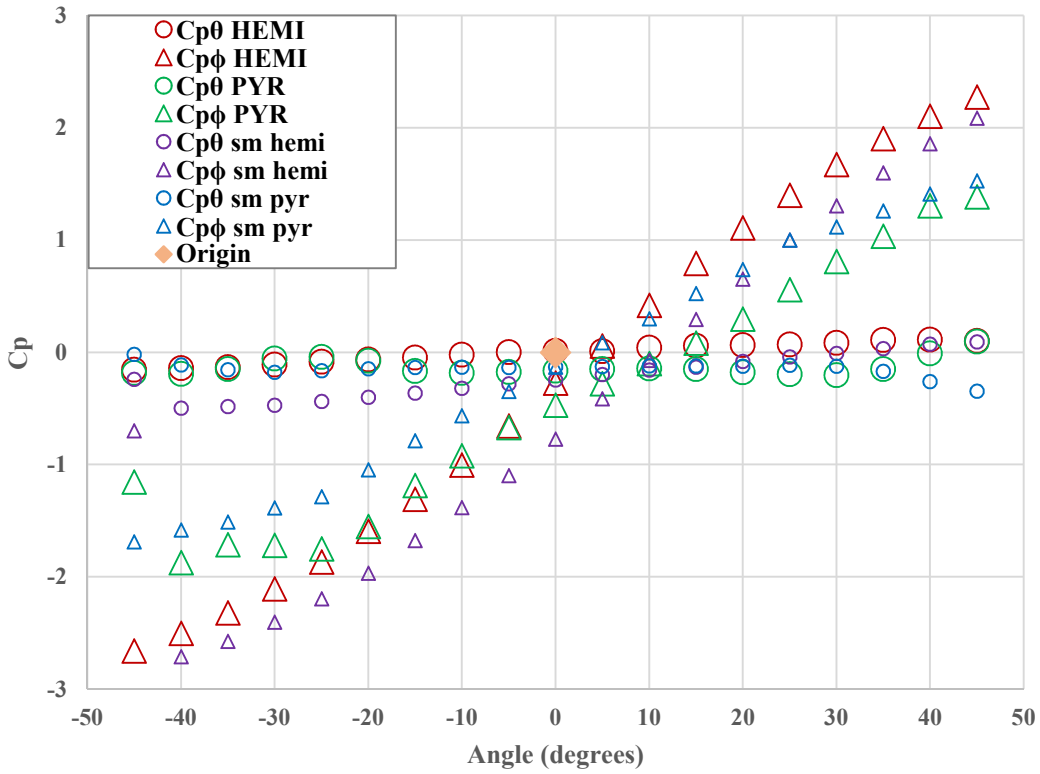

Figure 6-1 : Sensitivities indicated by slope steepness. The large hemisphere probe (red) and the small hemisphere (purple) are close to the same sensitivities. The large pyramid probe (green) has the worst sensitivity.

The objectives of this work were laid out into these main categories: calibration, data reduction, and flight testing; with a focus on designing and manufacturing MHPs and a data sensor package. These were accomplished through analyzing and experimenting with different methods in manufacturing, calibration, and data reduction.

6.2 Recommendations

For the Reynolds numbers tested, no measurable or conclusive effect on pitch and yaw were identifiable. Since Reynolds typically effects static pressure coefficient, more testing preferably with the scanivalve for each individual pressure will need to be done. Of the four probe types the large hemisphere performed the best having better linearity and symmetry in the *Cp* calibration curves throughout each test. Magnitude velocity curves were fairly symmetrical for each run at each Reynolds regime. The small hemisphere performed next best, but maintains issues likely

leading back to some misalignment in the probe in testing or internal inconsistencies that cannot be detected due to its size. An issue with the small probes of both geometries became apparent that the static ports were designed too close to the probe base. Since the last iteration of probes were given the same universal notched base for easy mounting, the small probes' bases were widened to fit the notched mounting boom. As such, the static ports are too close to the protruding base wall. A newer probe iteration has been designed by moving the static ports up the probe shaft to minimize any possible flow interferences. The pyramid probes of both size showed similar curve characteristics. Some mounting errors have been accounted for but were retested and the issues remained. Since the internals of the pyramid probes are much more difficult to examine to the hemisphere probes, it is assumed there is likely an internal anomaly from print quality or design deficiencies.

The goals presented in this work all highlight the need for low-cost MHPs for various research science areas. The evaluation of low-cost MHPs will hopefully contribute to a much larger UAS movement that can bridge these areas of interest with highly accurate packages for meaningful data collection and research. The results from the probes tested are promising, and indicate that although there is room for improvement in quality control and manufacturing optimization, there is still a reasonable foundation and path for further investigation and validation. Calibration testing was done using the two different normalization parameters for dynamic pressure to evaluate *Cp*, and can be further expanded into higher level data reduction methods. Normalization with the constant wind tunnel parameter gave more reasonable results for comparisons; however, refining this method along with uncertainty analysis is a good start in further validation of the probes' performances.

The analog sensor package system went through multiple iterations and proof-of-concepts that show refinement in approach and measurement taking. The base level results of these flight tests show a system that works, but still needs refinement. The details of the next board and other test refinements will be discussed further in future work. Flights tests were conducted during the

CLOUD-MAP campaign on June 27-29, 2017. A total of 6 flight tests were conducted with only 3 of them being usable due to human error. The large pyramid, large hemisphere, and small pyramid were tested (small hemisphere did not have time for testing). Each flight started with getting to altitude at approximately 250-300 ft. A series of 10 box pattern loops were conducted followed by 5-10 orbit flight patterns. One test could only do 5 orbits due to low battery and having to end the flight early. The Albatross has a 10 ft wingspan with a cruise speed of 17-20 m/s. Flight times were dependent on how soon the aircraft could get into the air and at altitude, but most flights were around 25-30 minutes per flight. Batteries had to be charged after the first flight which only left room for 1 more flight at the end of the flight day.

As stated previously, each flight ran a series of box patterns followed directly with orbit patterns. These patterns were conducted using a Pixhawk 2 autopilot set with waypoint to guide the aircraft. Altitudes were reached by a pilot and stayed within 250-350 ft regime, and the Albatross cruised between 17-25 m/s depending on the headwind. The test days all had fairly strong winds so flight patterns where some of the boxes and orbits were overshot by the aircraft trying to correct for wind. The gains likely need to be tuned to better account for that issue.

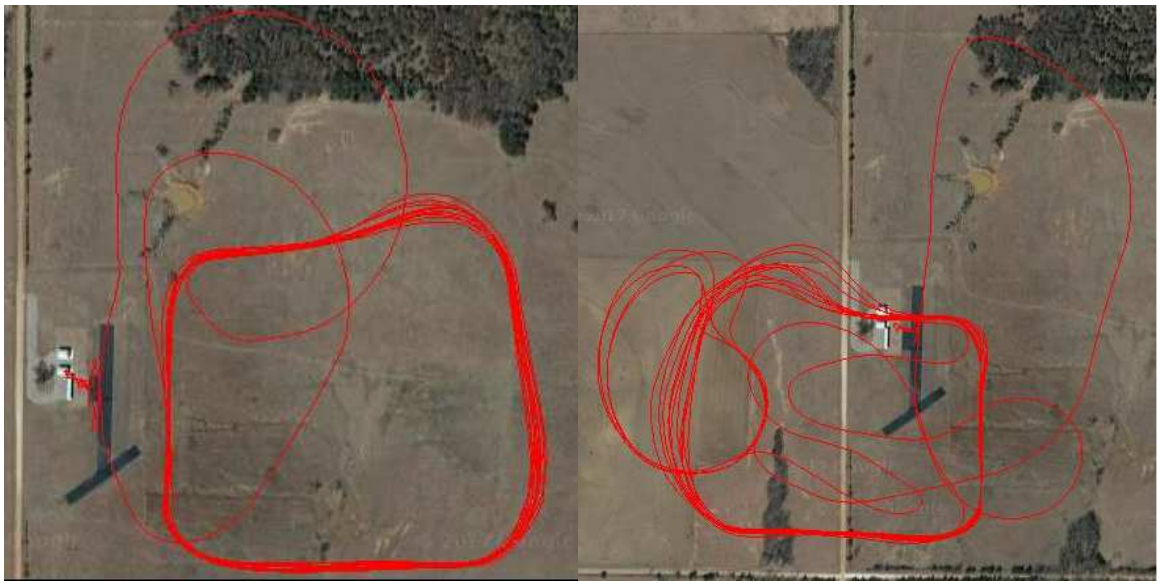

Figure 6-2 : Flight Paths for 2 flight days with varying wind conditions. Left image shows minimal overshoot. Overshoots in waypoints (right) resulting from greater wind conditions and autopilot gain tuning.

Ideally, it is the intention to compare flight test data with the local tower data and the anemometer data acquired by another in field aircraft taking measurements of the same kind. More flight tests in better conditions will be considered.

6.3 Future Work

For furthering this project and ensuring the quality of the research and investigation still ahead, this section of the chapter will layout the steps needed for future work in: probe design and optimization; calibration and data reduction refinements; board and sensor package design; flight testing; and PIV testing.

6.3.1 Probe design & optimization

Since the two geometries have been tested with varying results primarily from the pyramid design, it would be beneficial to do a redesign of that probe reducing the bends and possible constriction areas in the internal geometry of the pyramid probe. Printing and testing of the new probes (especially small probes) with the static ports moved away from the base is needed. Expand probe geometries to include cone and other angle variations. Doing these first few probe design

options while working to optimize the printing quality will expedite this process. With the wind tunnel calibration setup more in-tune a focus on probe design can be shifted in a meaningful direction. More in-depth testing to reduce probe size is a good start. Start developing a 7HP to directly compare with the 7HP Aeroprobe.

6.3.2 Calibration & data reduction refinements

Find a better way to automate by integrating the traversing system with LabVIEW or any program for better real time calibration results. Once this is refined, a shift to focus on the science taken for ABL research can be done easier. Test in the large wind tunnel to compare lab conditions. Less likely have wall effect issues in traverse. Swapping out the OMEGA PX653 differential sensors with better suited pressure sensors will likely improve calibration readings.

6.3.3 Board & sensor package design

Work on developing the new sensor board package for flight testing. Many of the hardware upgrades have been researched and design process has been done. Integrating the VectorNav VN-300 INS with dual GPS will greatly increase robustness and quality of measurements. Better data acquisition computer should be upgraded since the direction to Intel's Joule line has been pulled. Upgrade to digital sensors or upgrade analog sensors and add an A/D converter. This gives more control over level of precision wanted or needed for measurements rather than rely on the digital transducer's manufacturer specs. The idea to add a small LCD screen and LED lights for better user-interface interaction has been discussed. These are not high priority, but would greatly improve the packaging and usage of the sensor package itself.

6.3.4 Flight testing

More flight testing for validation and data collection needs to be done. Thus, telemetry data from the autopilot is extracted to attempt to correlate the necessary data for pitch, yaw, and roll orientations with the pressure sensor data since the current board iteration does not have a separate IMU integrated into it. This will be added to the new board iteration.

6.3.5 PIV testing

Particle image velocimetry should be conducted for understanding the flow at high angles around probes of different geometries. Flow visualization will aid in understanding tip geometries angle ranges.

7. APPENDIX

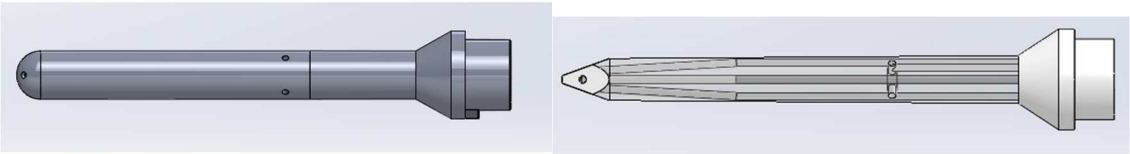

Figure 7-1 : CAD images of most recent probe designs. The static ports have been moved further up the shaft.

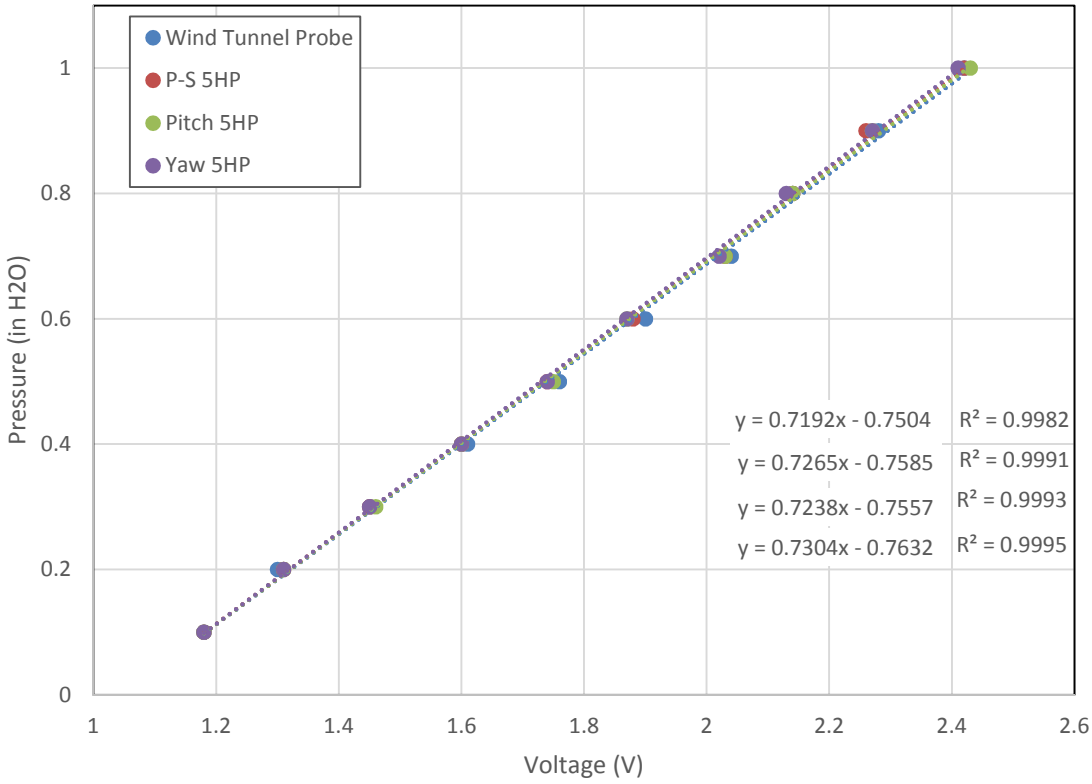

Figure 7-2 : Calibration results of the OMEGA PX653 sensors: Differential Pressure versus Output Voltage.

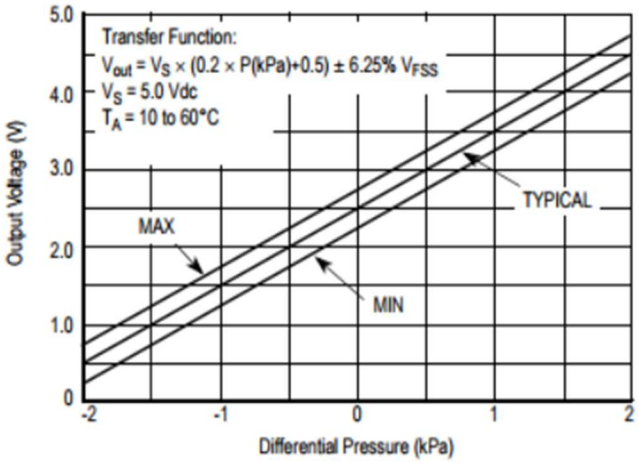

Figure 7-3 : Output versus Pressure Differential [43].

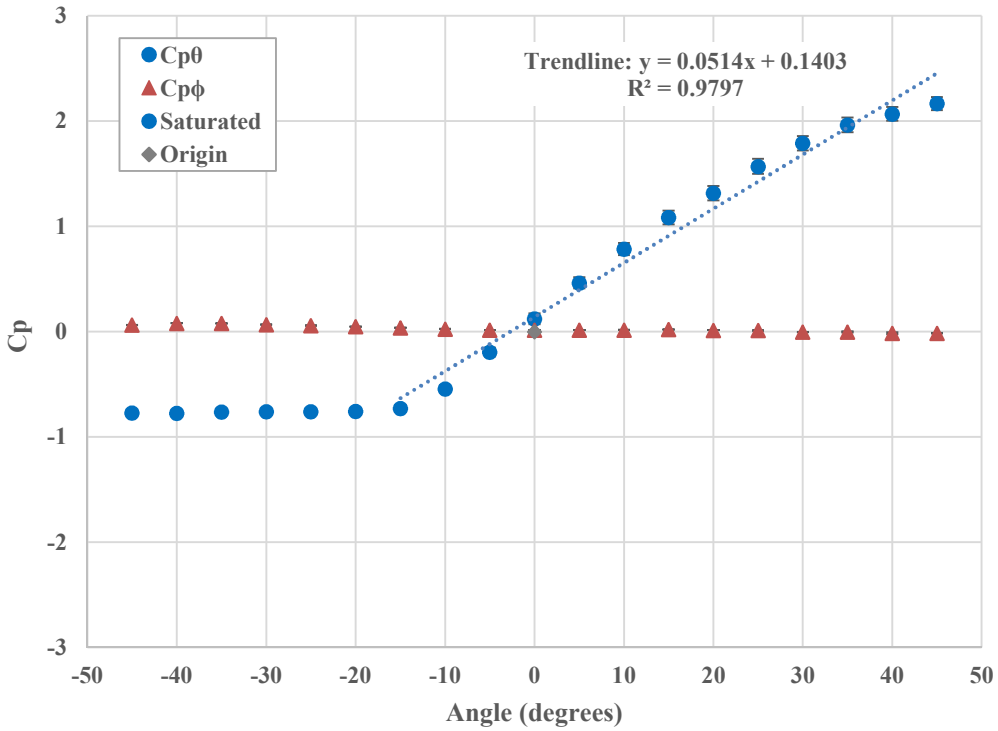

Figure 7-4 : Large hemisphere probe: Cpθ vs angle, 12.6×10^3 Reynolds (20 m/s).

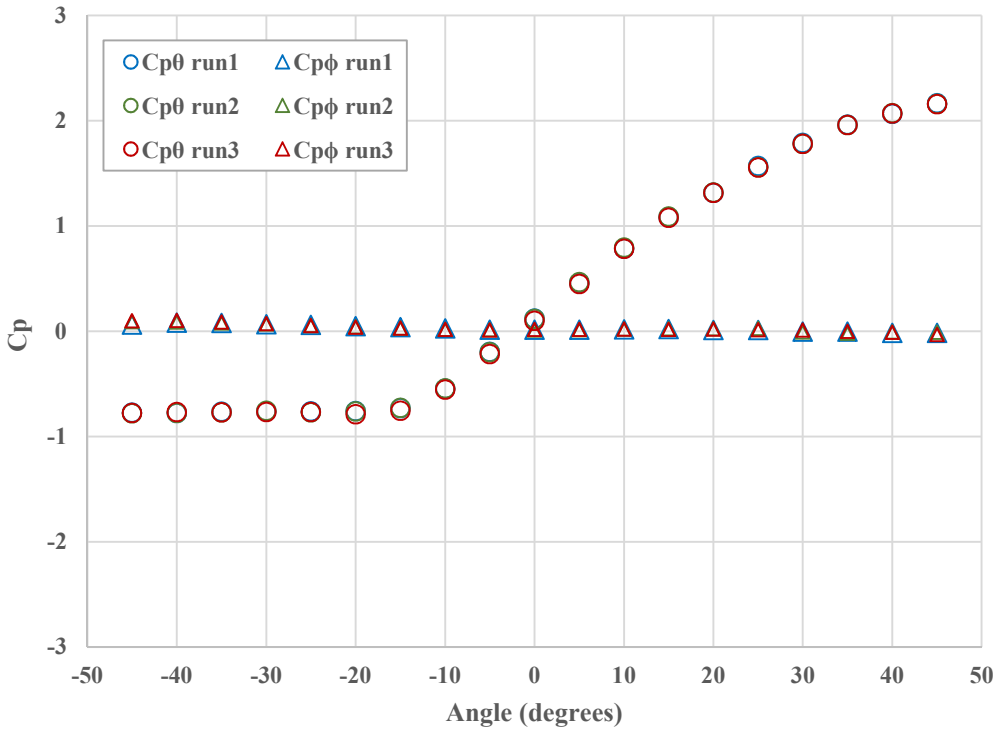

Figure 7-5 : Large hemisphere probe: Cpθ vs angle, 12.6x103 Reynolds. All runs.

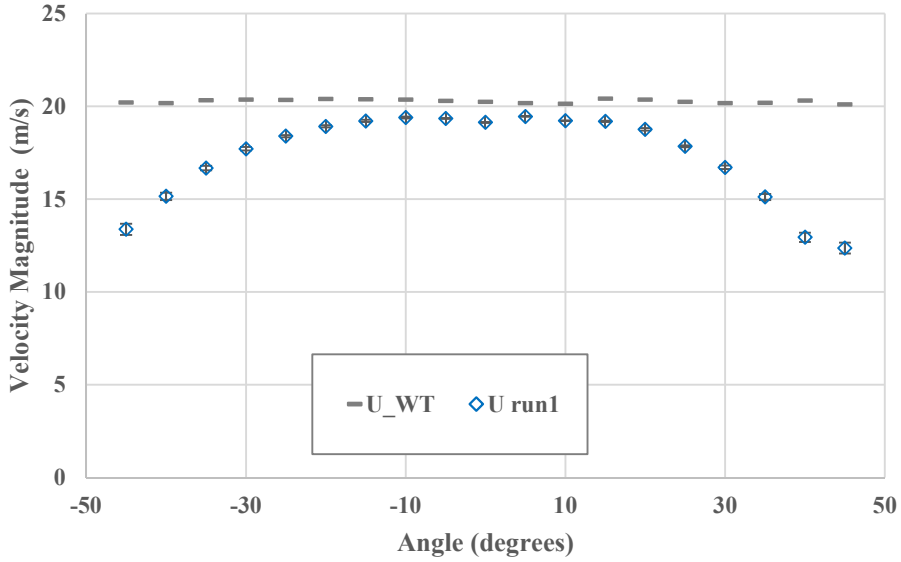

Figure 7-6 : Large hemisphere probe: Magnitude Velocity, 12.6x103 Reynolds. All runs.

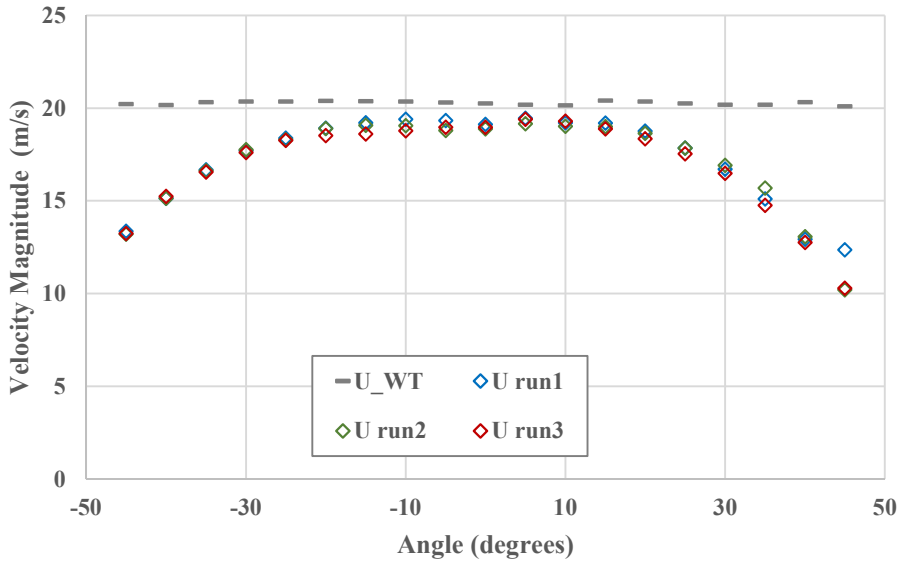

Figure 7-7 : Large hemisphere probe: Magnitude Velocity, 12.6x103 Reynolds. All runs.

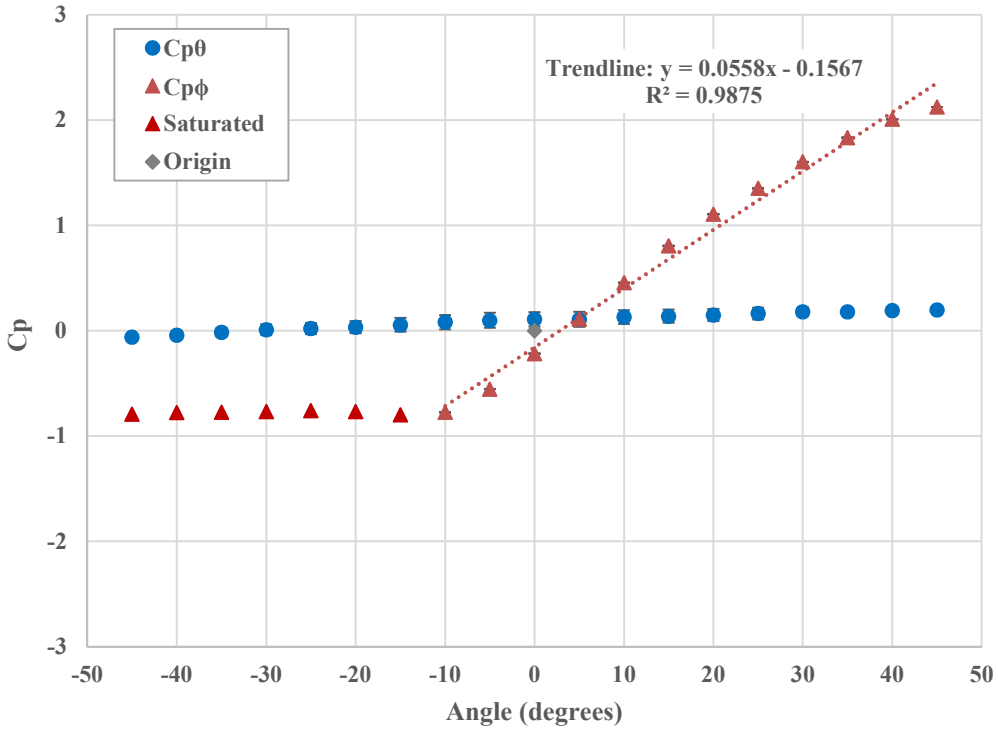

Figure 7-8 : Large hemisphere probe: Cpϕ vs angle, 12.6x103 Reynolds (20 m/s).

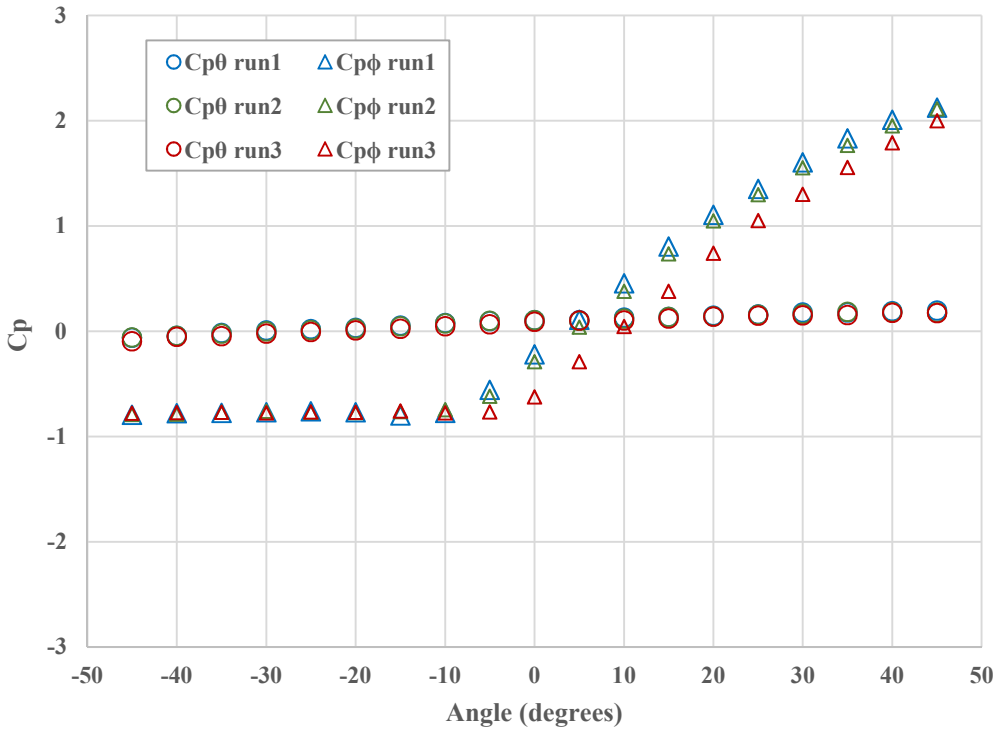

Figure 7-9 : Large hemisphere probe: Cpϕ vs angle, 12.6x103 Reynolds (20 m/s). All runs.

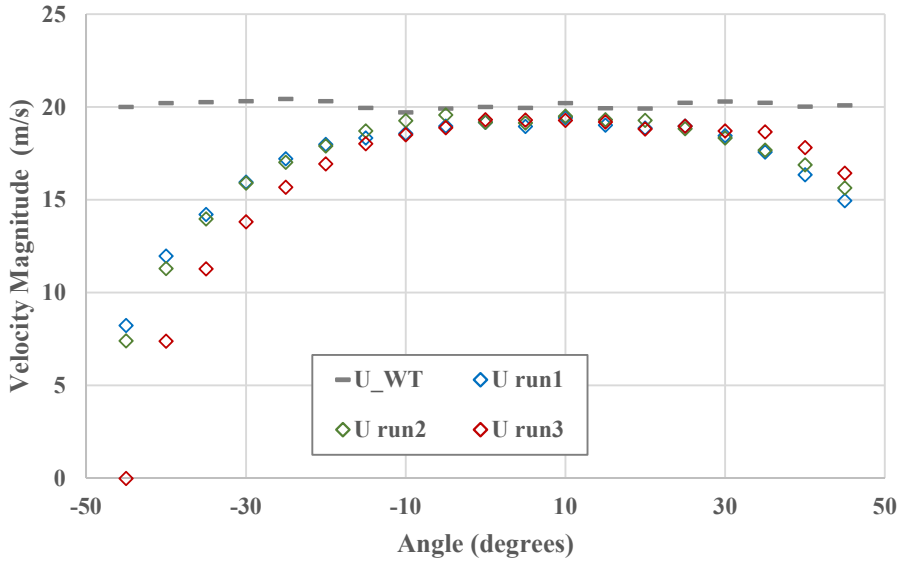

Figure 7-10 : Large hemisphere probe: Magnitude Velocity for yaw, 12.6x103 Reynolds. All runs.

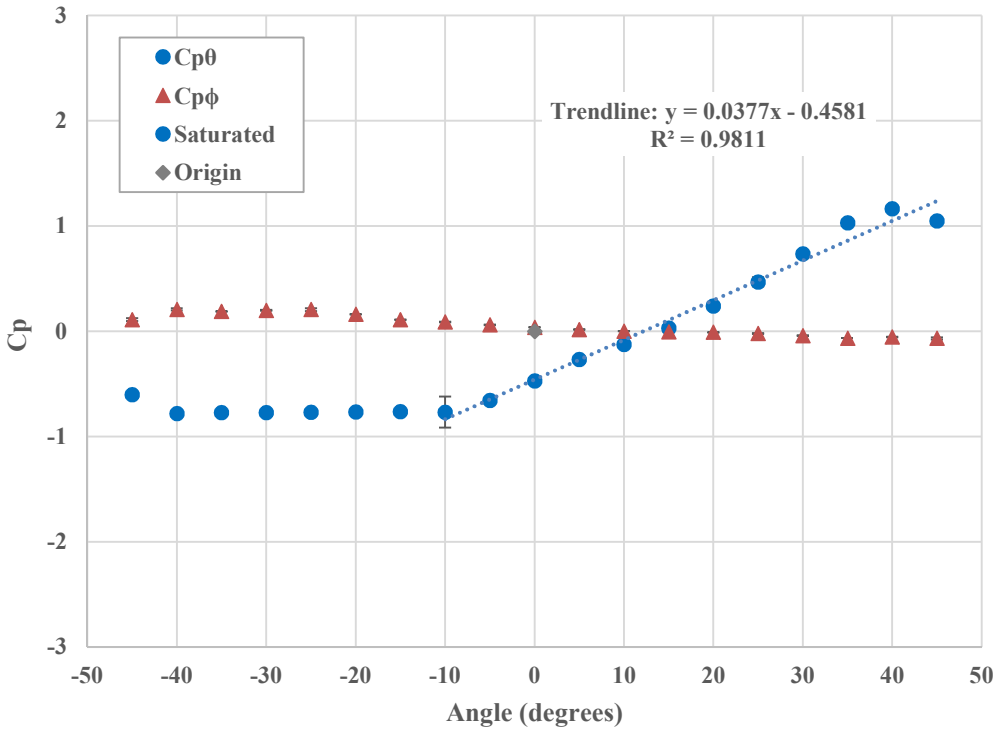

Figure 7-11 : Large pyramid probe: Cpθ vs angle, 12.6x103 Reynolds (20 m/s).

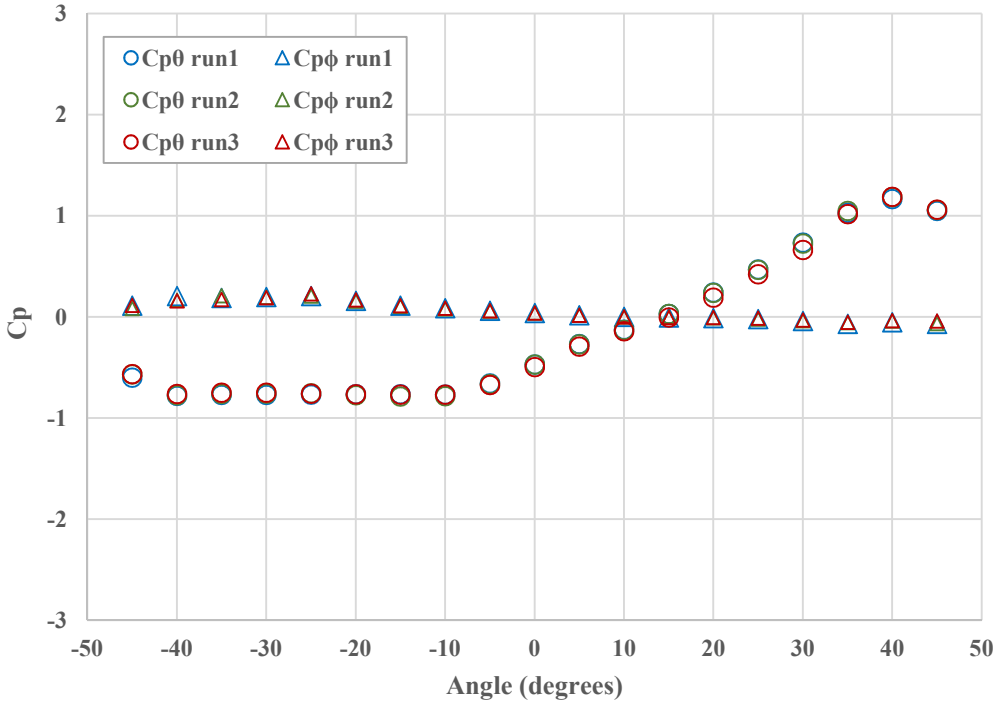

Figure 7-12 Large pyramid probe: Cpθ vs angle, 12.6x103 Reynolds (20 m/s). All runs.

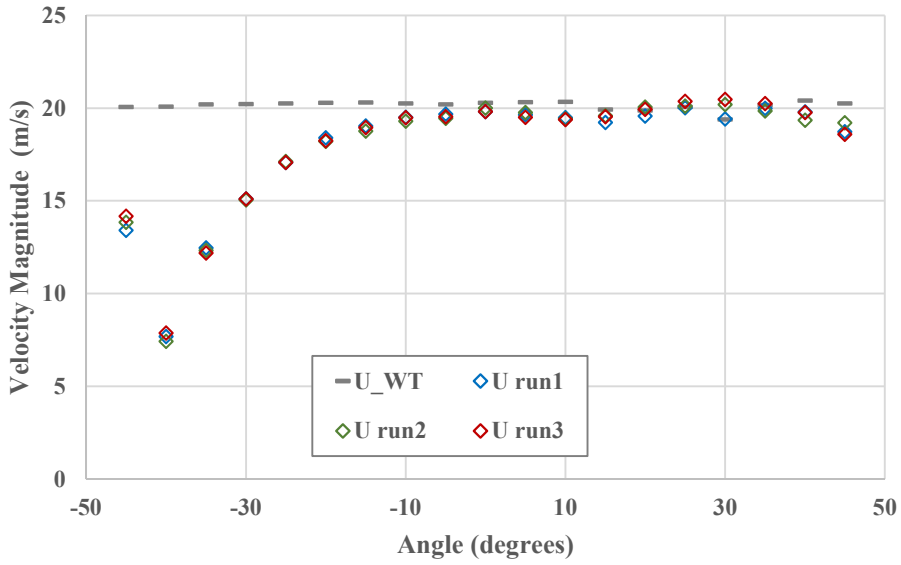

Figure 7-13 Large pyramid probe: Magnitude Velocity for pitch, 12.6x103 Reynolds. All runs.

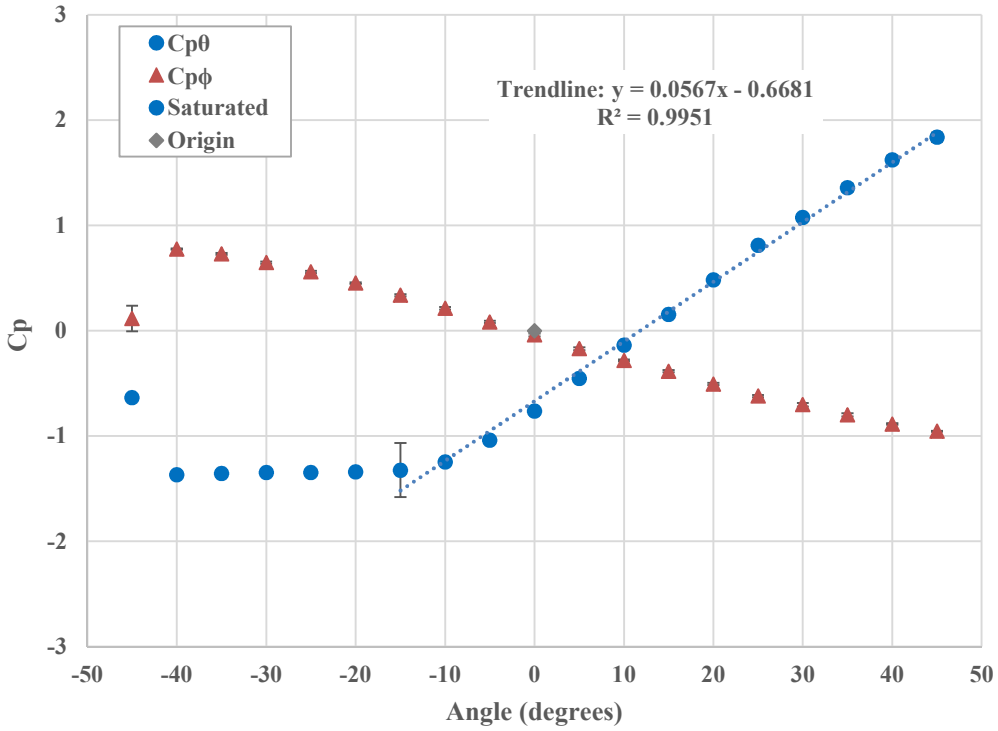

Figure 7-14 : Small hemisphere probe: Cpθ versus angle, $6.6x10^3$ Reynolds number (15 m/s). There is an offset from the origin.

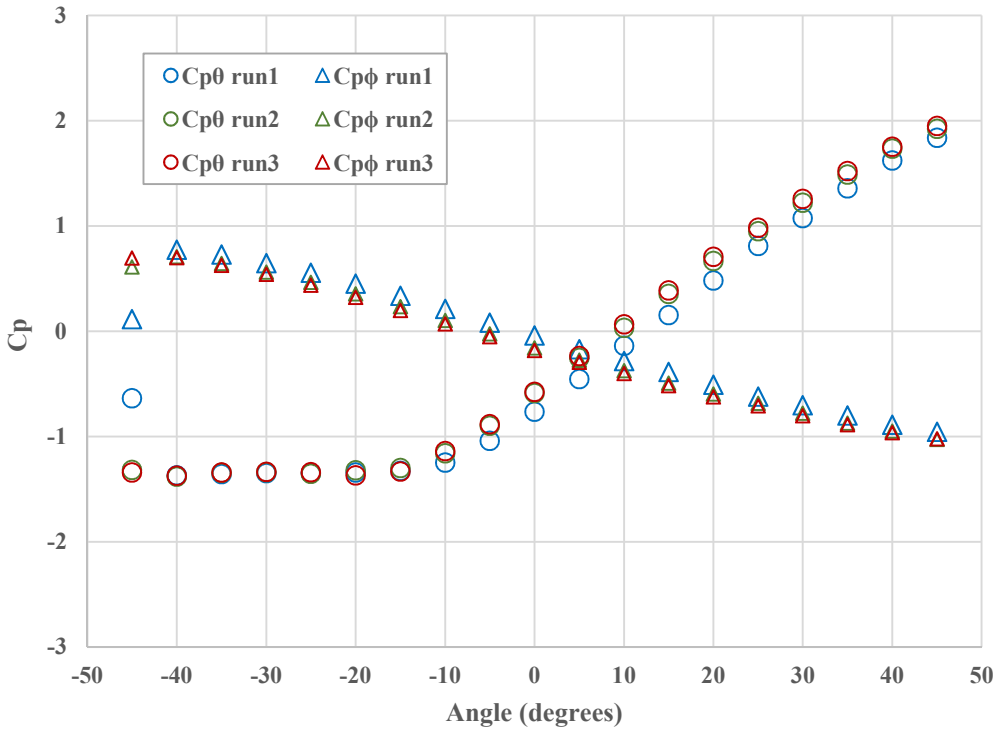

Figure 7-15 : Small hemisphere probe: Cpθ versus angle, 6.6x103 Reynolds number (15 m/s). There is an offset from the origin. All Runs.

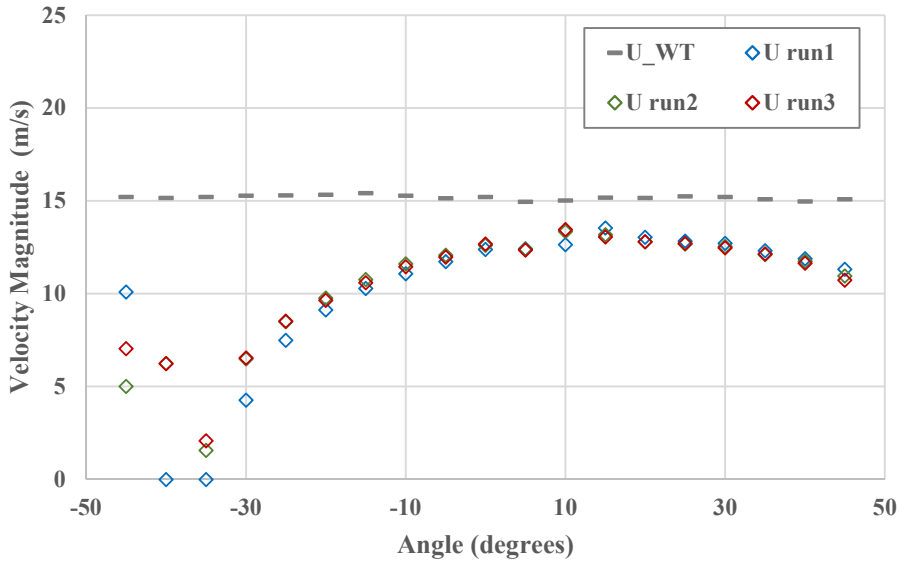

Figure 7-16 : Small hemisphere probe: Magnitude velocity versus angle for pitch , at 6.6x10^3 Reynolds number (15 m/s). Approximately a 10° shift to the right for the velocity curve.

Table 4 : Sample Error Sources

Error Sources:		Reading					Bias	Bias%	
OMEGA pressure transducer	ΔP	x	±		V	±	0.0025	0.25	Vfs
Vernier barometer	p	752.8	±	0.5	mm Hg	±	0.000664	0.0664	
Wind Tunnel	p	x							

Table 5 : Sample Precision Uncertainty

	run1	run2	run3	Std Dev Excel	
U_WT	U m/s	U m/s	U m/s	**Std Dev**	**Unc ±**
10.19	6.42	6.41	5.13	0.61	0.30
10.25	7.54	7.53	6.70	0.40	0.20
10.23	8.28	8.26	7.76	0.24	0.12
10.31	8.89	8.80	8.44	0.19	0.10
10.24	9.25	9.16	8.97	0.11	0.06
10.25	9.56	9.39	9.25	0.13	0.06
10.04	9.58	9.60	9.36	0.11	0.05
10.01	9.66	9.84	9.64	0.09	0.05
10.19	9.86	9.84	9.78	0.03	0.02
10.21	9.96	9.93	9.85	0.05	0.02
10.10	9.96	10.01	10.01	0.02	0.01
10.09	9.88	9.86	9.93	0.03	0.02
10.10	9.65	9.73	9.83	0.07	0.04
10.15	9.36	9.43	9.65	0.12	0.06
10.10	8.87	8.80	9.01	0.09	0.05
9.96	8.12	8.29	8.57	0.18	0.09
9.82	7.20	7.36	7.95	0.32	0.16
9.84	6.11	6.71	7.33	0.50	0.25
9.92	4.80	4.87	6.08	0.59	0.29

8. REFERENCES

[1] A. C. Van den Kroonenberg, T. Spiess, M. Buschmann, T. Martin, P. S. Anderson, F. Beyrich and J. Bange, "Boundary layer measurements with the autonomous mini-UAV M2AV," in *Proceedings of DACH2007*, Hamburg, Germany, 2007.

[2] O. K. Rediniotis and G. Jones, "The compressible calibration of miniature multi-hole probes," *Journal of Fluids Engineering,* vol. 123, pp. 128-138, 2001.

[3] D. Telionis, Y. Yang and O. Rediniotis, "Recent developments in multi-hole probe (mhp) technology," in *20th International Congress of Mechanical Engineering*, 2009.

[4] Aeroprobe, "Conventional Multi-hole Probes," unpublished, Blacksburg.

[5] J. D. Jacob, D. Axisa and O. Steven, "Unmanned Aerial Systems for Atmospheric Research:," in *NCAR / EOL Community Workshop on Unmanned Aerial Systems for Atmospheric Research*, Boulder, 2017.

[6] Y. Nakayama, Introduction to fluid mechanics, Butterworth-Heinemann, 1998.

[7] S. Chue, "Pressure probes for fluid measurement," *Progress in aerospace sciences,* vol. 16, no. 2, pp. 147-223, 1975.

[8] D. W. Bryer and R. C. Pankhurst, "Pressure-probe methods for determining wind speed and flow direction," HM Stationery Office, 1971.

[9] M. Selig, R. Deters and G. Wiliamson, "Wind tunnel testing airfoils at low Reynolds numbers," in *49th AIAA Aerospace Sciences Meeting including the New Horizons Forum and Aerospace Exposition*, 2001, p. 875.

[10] A. Treaster and A. Yocum, "Calibration and Application of 5-Hole Probes," *ISA transactions,* vol. 18, no. 3, pp. 23-34, 1979.

[11] C. Lee and N. Wood, "Calibration and data reduction for a five-hole probe," *NASA STI/Recon Technical Report N,* vol. 86, p. 29157, 1986.

[12] T. J. Dudzinski and L. N. Krause, "Flow-direction measurement with fixed-position probes," *NASA Technical Memorandum 102200,* 1969.

[13] L. N. Krause and T. J. Dudzinski, "Flow Direction Measurement with Fixed Position Probes in Subsonic Flow over a Range of Reynolds Number," in *Proceedings for 15th International Aerospace Symposium*, Las Vegas, Nevada, 1969, pp. 217-223.

[14] J. Naughton, I. L. CATTAFESTA and G. Settles, "Miniature, fast-response five-hole conical probe for supersonic flowfield measurements," *AIAA journal,* vol. 31, no. 3, pp. 453-458, 1993.

[15] N. Sitaram and K. Srikanth, "Effect of chamfer angle on the calibration curves of five hole probes," *International Journal of Rotating Machinery,* vol. 2014, 2014.

[16] Díaz, K. Argüelles, J. F. Oro and E. B. Marigorta, "Cylindrical three-hole pressure probe calibration for large angular range," *Flow Measurement and Instrumentation,* vol. 20, no. 2, pp. 57-68, 2009.

[17] Díaz, K. Argüelles and e. al., "Head geometry effects on pneumatic three-hole pressure probes for wide angular range," *Flow Measurement and Instrumentation,* vol. 21, no. 3, pp. 330-339, 2010.

[18] P. Ligrani, B. Singer and L. Baun, "Miniature five-hole pressure probe for measurement of three mean velocity components in low-speed flows," *Journal of Physics E: Scientific Instruments,* vol. 22, no. 10, p. 868, 1989.

[19] T. Nakaya, M. Ebihara, Y. Hayashi, S. Suzuki, N. Kuwano, A. Hanzawa, T. Saitow, M. Usami and T. Iwata, "Truncated pyramid-shape multi-hole pitot probe and flight velocity detection system using said truncated pyramid-shape multi-hole pitot probe". USA Patent US Patent 5,423,209, 13 June 1995.

[20] R. Dominy and H. Hodson, "An investigation of factors influencing the calibration of 5-hole probes for 3-D flow measurements," in *ASME 1992 International Gas Turbine and Aeroengine Congress and Exposition*, American Society of Mechanical Engineers, 1992.

[21] J. Crawford, "Design and Calibration of Seven Hole Probes for Flow Measurement," Queen's University, Kingston, 2011.

[22] G. Zilliac, "Modelling, calibration, and error analysis of seven-hole pressure probes," *Experiments in Fluid,* vol. 14, no. 1, pp. 104-120, 1993.

[23] G. G. Zilliac, "Calibration of seven-hole pressure probes for use in fluid flows with large angularity," *NASA Technical Memorandum 102200,* 1989.

[24] S. Shaw-Ward, A. Titchmarsh and D. M. Birch, "Calibration and use of n-hole velocity probes," *AIAA Journal,* vol. 53, no. 2, pp. 336-346, 2014.

[25] A. Pisasale and N. Ahmed, "A novel method for extending the calibration range of five-hole probe for highly three-dimensional flows," *Flow Measurement and Instrumentation,* vol. 13, no. 1, pp. 23-30, 2002.

[26] J. D. Jacob, "Experimental investigation of the trailing vortex wake of rectangular airfoils," Diss. University of California, Berkeley, 1995.

[27] G. Morrison, M. Schobeiri and K. Pappu, "Five-hole pressure probe analysis technique," *Flow Measurement and Instrumentation,* vol. 9, no. 3, pp. 153-158, 1998.

[28] J. C. Gonsalez and E. A. Arrington, "Five-Hole Flow Angle Probe Calibration for the NASA Glenn Icing Research Tunnel," in *19th Advanced Measurement and Ground Testing Technology Conference, AIAA*, New Orleans, 1996.

[29] S.-H. Kim, Y.-J. Kang, R.-S. Myong, T.-H. Cho, Y.-M. Park and I.-H. Choi, "Calibration of a five-hole multi-function probe for helicopter air data sensors," *International Journal of Aeronautical and Space Sciences,* vol. 10, no. 2, pp. 43-51, 2009.

[30] B. A. Reichert and B. J. Wendt, "A new algorithm for five-hole probe calibration, data reduction, and uncertainty analysis," *NASA Techinical Memorandum 106458,* 1994.

[31] P. Ciolek, "Design and construction of a velocity probe calibration rig," Worcester Polytechnic Institute, 2013.

[32] W. Lewis, "Paper 8: Fixed-Direction Probes for Aerodynamic Measurements," in *Proceedings of the Institution of Mechanical Engineers, Conference Proceedings*, SAGE Publications, 1965, pp. 141-152.

[33] B. M. Witte, C. Schlagenhauf, J. Mullen, J. P. Helvey, M. A. Thamann and S. Bailey, "Fundamental Turbulence Measurement with Unmanned Aerial Vehicles," in *8th AIAA Atmospheric and Space Environments Conference*, 2016, p. 3584.

[34] A. Van den Kroonenberg, T. Martin, M. Buschmann, J. Bange and P. V{\"o}rsmann, "Measuring the wind vector using the autonomous mini aerial vehicle M2AV," *Journal of Atmospheric and Oceanic Technology,* vol. 25, no. 11, pp. 1969-1982, 2008.

[35] S. Metzger, W. Junkermann, K. Butterbach-Bahl, H. Schmid and T. Foken, "Measuring the 3-D wind vector with a weight-shift microlight aircraft," *Atmospheric Measurement Techniques,* vol. 4, no. 7, pp. 1421-1444, 2001.

[36] R. T. Palomaki, N. T. Rose, M. van den Bossche, T. J. Sherman and S. F. De Wekker, "ind estimation in the lower atmosphere using multi-rotor aircraft," *Journal of Atmospheric and Oceanic Technology,* 2017.

[37] L. Fingersh, M. Robinson, L. Fingersh and M. Robinson, "Wind tunnel calibration of 5-hole pressure probes for application to wind turbines," in *35th Aerospace Sciences Meeting and Exhibit*, 1998, p. 854.

[38] G. Brune, "Quantitative low-speed wake surveys," *Journal of Aircraft,* vol. 31, no. 2, pp. 249-255, 1994.

[39] D. Axford, "On the accuracy of wind measurements using an inertial platform in an aircraft, and an example of a measurement of the vertical mesostructure of the atmosphere," *Journal of Applied Meteorology,* vol. 7, no. 4, pp. 645-666, 1968.

[40] T. Nakaya, O. Okamoto, N. Kuwano, S. Suzuki, S. Sasa, H. Nakayasu and M. Sagisaka, "Air active control aircraft using three dimensional true airspeed detection system". USA Patent S Patent 5,797,105, 18 August 1998.

[41] S. Grimshaw and J. Taylor, "Fast settling millimetre-scale five-hole probes," in *ASME Turbo Expo*, 2016.

[42] S. Kline and A. McClintock, "Describing Uncertainties in Single-Sample Experiments," *ASME Mech.,* vol. 75, pp. 3-8, 1953.

[43] NXP Freescale Semiconductor, "Data Sheet: MPXV7002 Integrated Solicon Pressure Sensor On-Chip Signal Conditioned, Temperature Copensated and Calibrated," unpublished, 2005.

VITA

Solmoz Kathleen Azartash-Namin

Candidate for the Degree of

Master of Science

Thesis: EVALUATION OF LOW-COST MULTI-HOLE PROBES FOR ATMOSPHERIC BOUNDARY LAYER INVESTIGATION

Major Field: Mechanical and Aerospace Engineering

Biographical:

Education:

Completed the requirements for the degree of Bachelors of Science with a major in Mechanical and Aerospace Engineering at Oklahoma State University, Stillwater, Oklahoma in July 2017.

Experience:

Propulsion Engineering Intern: XCOR Aerospace, Mojave, CA

Graduate Teaching Assistant: Oklahoma State University, Mechanical & Aerospace Dept, Stillwater, OK

Graduate Research Assistant: Oklahoma State University, Mechanical & Aerospace Dept, Stillwater, OK

Professional Memberships:

AIAA, SWE